5-2017

Depositional Dynamics of the Upper Eagle Ford (Upper Cretaceous): Karnes and Gonzales Counties, South Texas

Josie Brunick
University of Arkansas, Fayetteville

Depositional Dynamics of the Upper Eagle Ford (Upper Cretaceous):
Karnes and Gonzales Counties, South Texas

A thesis submitted in partial fulfillment
of the requirements for the degree of
Master of Science in Geology

by

Josie Brunick
University of Arkansas
Bachelor of Science in Geology, 2015

May 2017
University of Arkansas

This thesis is approved for recommendation to the Graduate Council.

Dr. Walter Manger
Thesis Director

Dr. Thomas McGilvery
Committee Member

Dr. Adriana Potra
Committee Member

Abstract

The mixed siliciclastic/carbonate late Cretaceous Eagle Ford Formation is commonly divided into the lower Eagle Ford and the upper Eagle Ford. The lower Eagle Ford is arguably the most obvious organic rich interval highlighted with wireline log data; however, the upper Eagle Ford may have just as much potential for hydrocarbon production success as the lower Eagle Ford has had. A better understanding of the upper Eagle Ford will allow a more thorough and educated assessment into its full potential as an unconventional reservoir, and allow its sweet spots for oil or gas to be found and exploited.

This study is based on the description and interpretation of four cores of the upper Eagle Ford located within Karnes and Gonzales counties, Texas, thin sections, and key XRF data in an effort to better understand its sediment sources and depositional regime.

Seven lithofacies were identified in the upper Eagle Ford are as follows:

1) Bioturbated Wackestone/Packstone; 2) Deformed Wackestone/Packstone; 3) Wavy Laminated Wackestone/Packstone; 4) Massive Mudstone/Wackestone; 5) Coarsely to Finely Laminated Wackestone/Packstone; 6) Massive packstone/grainstone; 7) Volcanic Ash.

The highest Total Organic Carbon (TOC) percent relative to each core always occurred within the base of the upper Eagle Ford. In fact, the highest TOC percentage recorded was 4.5% within the base of the upper Eagle Ford in the most distally located core.

Thorium to Uranium ratios of the upper Eagle Ford were on average less than 1 indicating that the upper Eagle Ford contains very little terrigenous sourced material. Nickel, copper, vanadium, molybdenum, and uranium concentrations were also analyzed and correlated to relative organic matter influx and Paleoredox levels within the upper Eagle Ford in each core.

Acknowledgements

Much appreciation and gratitude goes out to the San Antonio division of EOG Resources (Eddie Valek and Nestor Phillips) for giving me this dataset for my thesis, and to my thesis committee (Dr. Walter Manger, Dr. Thomas McGilvery, and Dr. Adriana Potra) for their patience with working with me.

Dedication

To my husband, who no matter how stressed and irritable I was during my college career, was always willing to put up with my neglect and never lost faith in me.

Table of Contents

List of Figures

Introduction

The Eagle Ford Formation is an extensive unconventional reservoir that extends from east Texas, to the west Texas border, and likely into Mexico. In outcrop, the interval is known as the Boquillas Formation, west of the Pecos River in Texas near and in Big Bend National Park, and as the Eagle Ford Formation, east of this same river; however, it is generally called the Eagle Ford Formation in the subsurface (Frébourg et al., 2016). The Eagle Ford, named for the town of Eagle Ford, Texas, near Dallas, by R.T. Hill in 1887, is of particular interest because it produces prolific oil along its northern, up-dip extent and substantial natural gas in its southern, down-dip extent as can be seen in Figure 1. Energy companies have been particularly successful with producing oil and natural gas from this formation not only due to its estimated total organic content averaging as much as 7 percent in its richest interval, but also due to its brittleness related to its high carbonate content that allows hydraulic fracturing to be more successful (Treadgold et al., 2011a). In fact, in the geographic southern extent of the formation the carbonate percentage has been documented to be over 70 percent; However, the total carbonate percentage drops off significantly toward the Eagle Ford's northeastern extent, while the clay percentage steadily increases (Treadgold et al., 2011a).

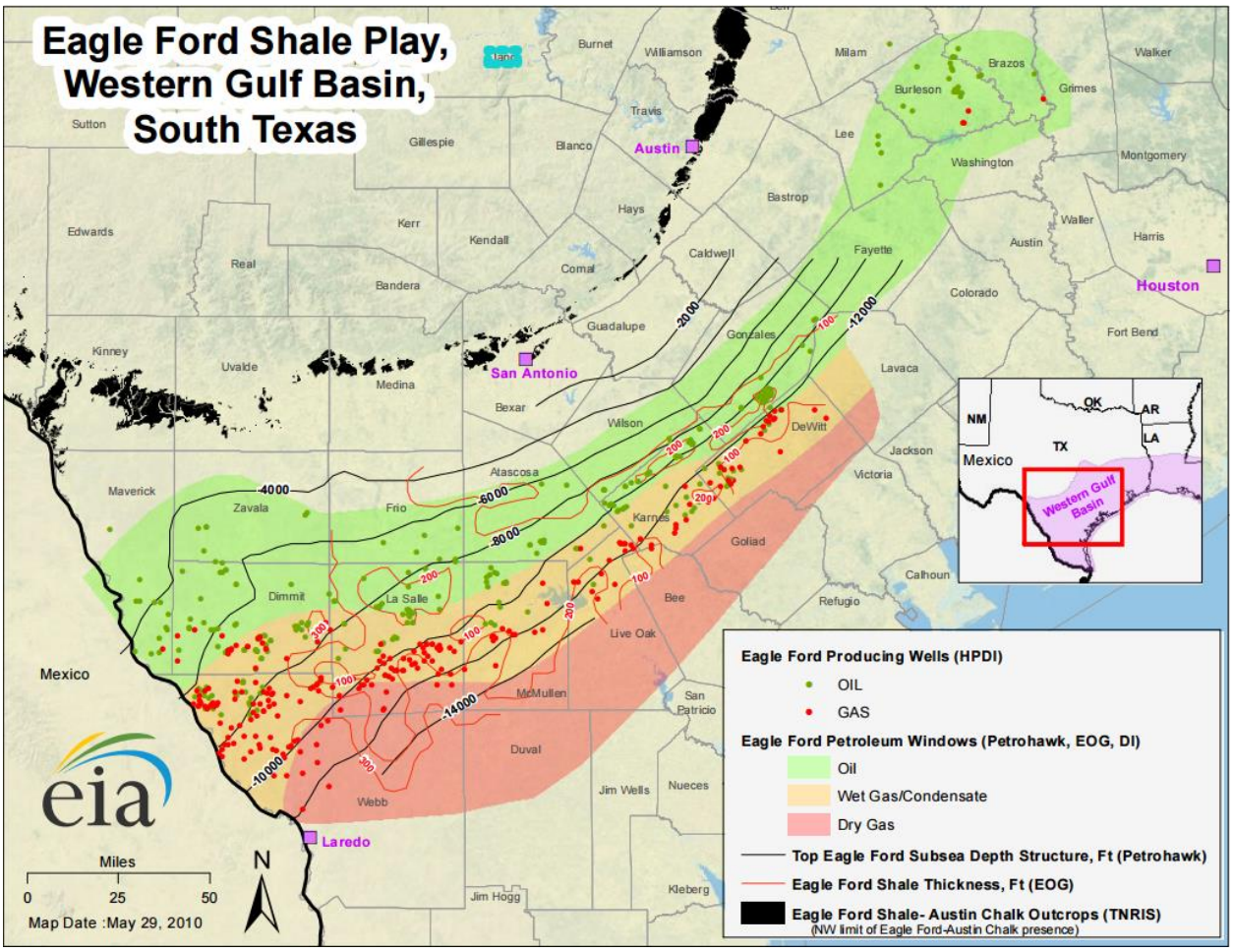

Figure 1: *EIA map of Eagle Ford Hydrocarbons*: Geographic location of the Eagle Ford outcrop (black). The dominant type of hydrocarbons produced from the Eagle Ford Formation (EIA, 2016).

This formation is stratigraphically located between the overlying Austin Chalk and the underlying Buda Limestone (Figure 2) (Treadgold et al., 2011b). The Eagle Ford-Buda contact is considered by most authors to be a regional unconformity. In east Texas, Eagle Ford deposition was heavily influenced by the Woodbine Delta, and shows an inter-fingering relationship with this delta's siliciclastic deposits. Moreover, some authors suggest that the subsurface formation commonly known as the Eagle Ford in east Texas is, in fact, not the Eagle Ford and is more accurately assigned to the Lower Woodbine Group (Organic Shale interval) that is laterally

equivalent to the Pepper Shale (Figure 2) (Adams and Carr, 2014). Moving toward west Texas, the Woodbine deltaic deposits pinch out, while the Eagle Ford/Austin Chalk contact has been identified in outcrop to be unconformable (Hentz and Ruppel, 2011; Hill, 1887b; Brown and Pierce, 1962).

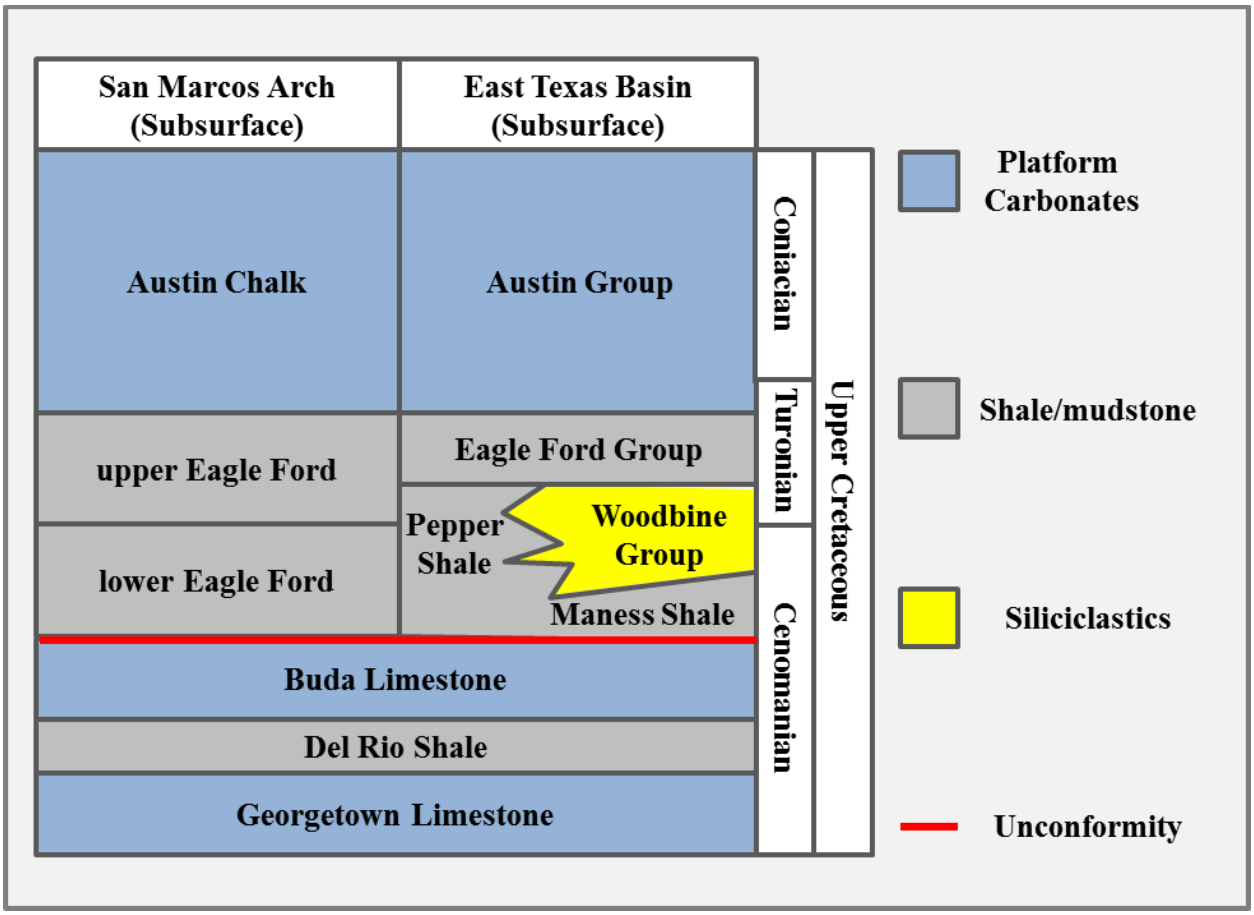

***Figure 2**: Simplified stratigraphic column* showing the subsurface position and age of the Eagle Ford Shale from East Texas to the San Marcos Arch area (Modified from both Hentz and Ruppel, 2011; Workman, 2013).

Geologic Background

The Eagle Ford Shale was deposited during the late Cretaceous period, specifically spanning the Cenomanian and Turonian Stages, approximately 93 million years ago (ma).

Zircons have been extracted and dated from the Eagle Ford/Boquillas outcrops along Highway 90 in Val Verde and Terrell Counties, Texas, that yielded a maximum age of 96 Ma near the base of this unit overlying the Buda Limestone, and a minimum age of 87 Ma near the top of this unit 10 feet below the Austin Chalk – Upper Boquillas/Eagle Ford contact (Fébourg et al., 2016). The Cenomanian and Turonian Stages were characterized by deposition during very low oceanic circulation, likely due to the non-glacial warm climate of the Cretaceous Period (Linnert et al., 2011). The lack of ocean circulation promoted bottom water anoxia and allowed organic-rich massive black shale units to be deposited (Linnert et al., 2011). During this time, what would become known as the Western Interior Seaway covered much of western North America, east of the Rocky Mountain Range (White et al., 2001). This seaway was fed from the Boreal Sea to the north, and the Tethys Sea to the south as can be seen in Figure 3 (Stanley, 2009). This seaway may or may not have been completely connected during the initial deposition of the lowermost portion of the lower Eagle Ford. Its maximum transgression is associated with the upper section of the lower Eagle Ford while the upper Eagle Ford is associated with a regressive phase of this seaway.

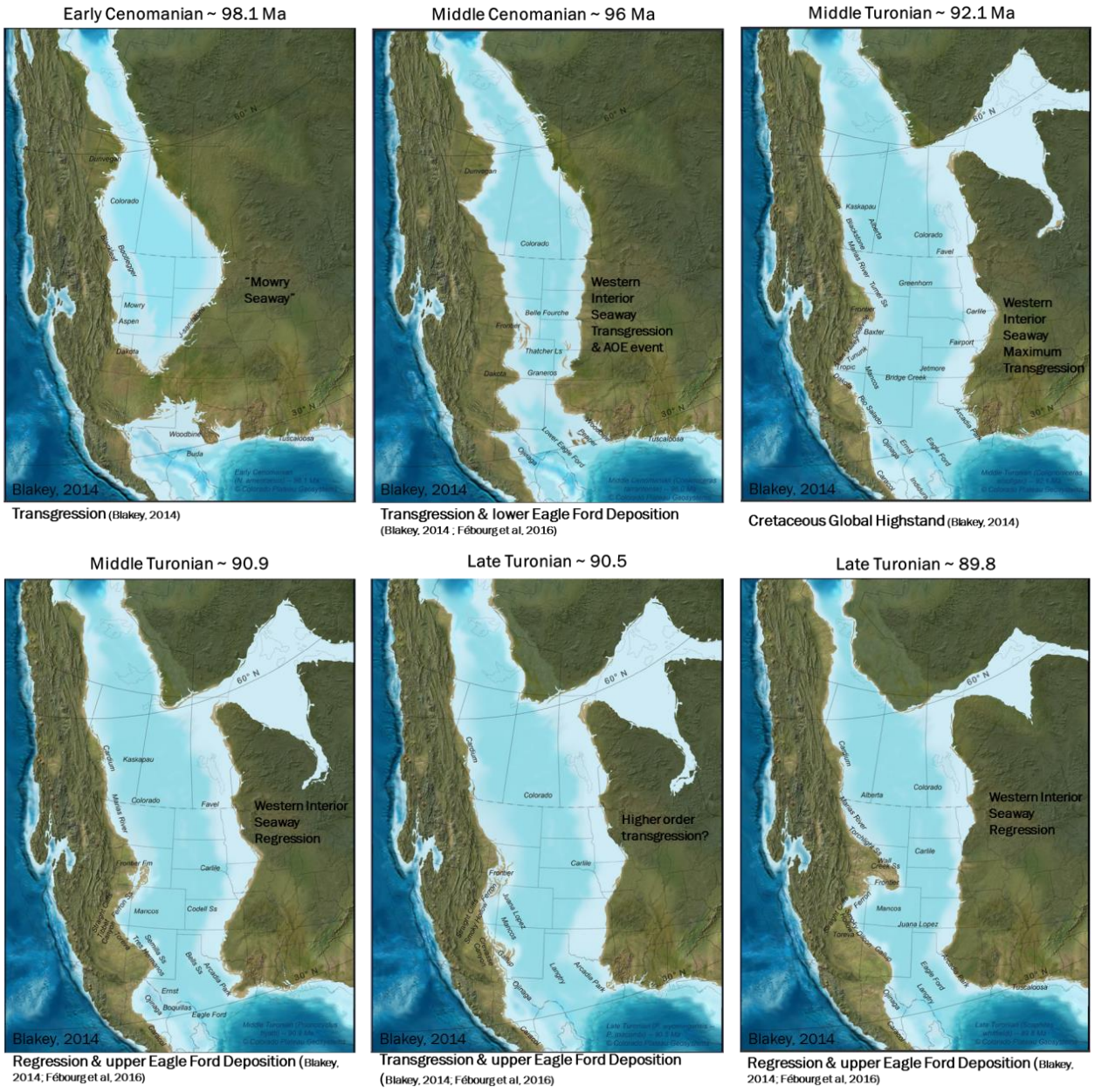

Figure 3: *Paleogeographic maps of the late Cretaceous* created by Ron Blakey (2014) depicting his interpretations of the Cenomanian-Turonian changes in relative sea level based on the current literature available during the time he created these maps.

Several tectonic events during and after Eagle Ford deposition are believed to have had a significant influence on the depositional dynamics of the Eagle Ford Formation (Figure 4) (Cardneaux, 2012). Some of the thickest deposits of the Eagle Ford are associated with paleo-troughs and along the margins of basins, including the East Texas Basin and the Maverick Basin

(Workman, 2013; Lehmann et al., 2000). This phenomenon can be tied to past tectonic events of the Mesozoic Era that formed paleo-geographic highs and lows that helped constrict water circulation and promote bottom water anoxia during the deposition of the Eagle Ford Shale (Alexander, 2014; Workman, 2013). The Llano Uplift is believed to have contributed to the development of a south-to-southeast plunging igneous and metamorphic rock dominated anticline called the San Marcos Arch (Cardneaux, 2012; Workman, 2013). This arch intersects the Eagle Ford Formation in its south-central area, and likely contributed to this unit becoming substantially thinner over the San Marcos Arch region (Cardneaux, 2012). In addition to this, the San Marcos Arch also appears to have inhibited the influx of clay-rich material (sourced at least in part from the Woodbine Delta located toward the northeast) from being incorporated into the richest organic intervals of the Eagle Ford Formation located to the southwest of the arch (Driskill et al., 2012).

To the west and south of the San Marcos Arch, is the well-known Maverick Basin (Figure 4). This basin is presumed to have been present since at least the Aptian Stage (Lower Cretaceous) because of the observed thickening in the Pearsall, McKnight, Georgetown, Del Rio, Buda, and Eagle Ford Formations (Driskill et al., 2012). Driskill et al. (2012) suggest that since the Maverick Basin had persisted for so long that its development is tied to crustal thinning linked to the rifting of the Gulf of Mexico. Furthermore, syndepositional faulting and loading of the ductile late Triassic and Jurassic Louann Salt within south-central Texas contributed to the formation of mini-basins/troughs and highs that helped constrain where the richest organic intervals within the Eagle Ford Formation were preserved (Cardneaux, 2012). One such area that experienced syndepositional faulting that led to thickening of the Eagle Ford deposits is known as the Karnes Trough. This trough is located within Karnes County to the Southwest of the San

Marcos Arch. The Edwards Platform margin, otherwise known as the Albian reef edge, is located southward of Maverick Basin and the San Marco Arch and spans from west to east Texas. It is representative of a paleo-geographic high during Eagle Ford deposition, which is indicated by observed thinning of the Eagle Ford deposits as they approach this margin (Cardneaux, 2012; Driskill et al., 2012; Workman, 2013). In far southwest Texas, just south of Maverick basin, however, the Eagle Ford Formation thickens once again after crossing the Edwards/Albian reef margin before thinning as it approaches an older reef margin known as the Sligo/Aptian reef margin (Driskill et al., 2012). A portion of this area has become known as the Hawkville Field. The location of these paleo-highs and basins that effected the deposition of the Eagle Ford Shale can be seen in Figure 4.

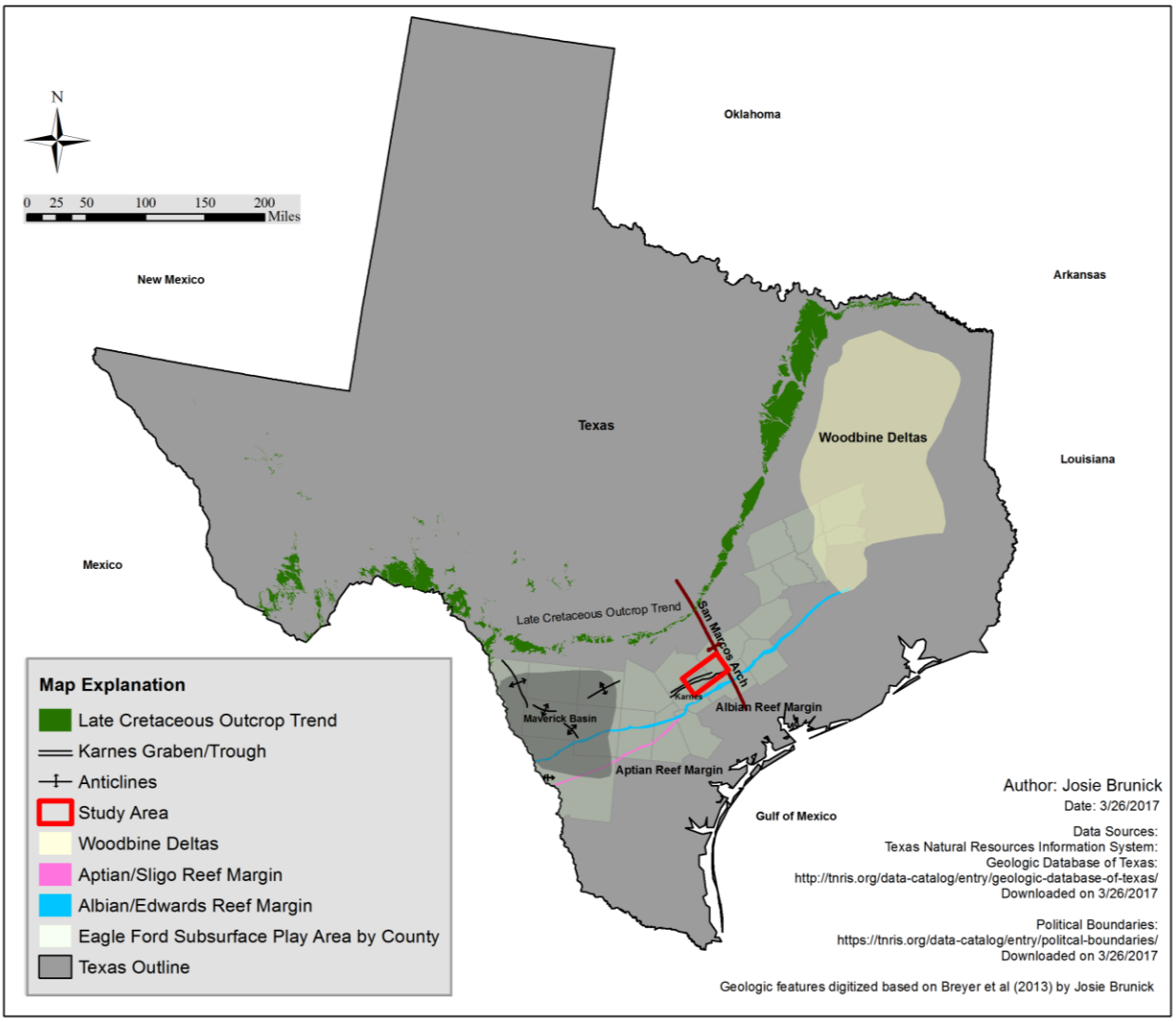

Figure 4: *Structural and Geologic Features* that influenced the deposition and development of the Eagle Ford Formation during the Late Cretaceous period (Digital data source: Texas Natural Resources Information System; Structural Features modified from Breyer et al, 2013).

Previous Investigations

Previous workers have studied the Eagle Ford Formation in detail throughout its depositional extent. Seth Workman (2013) studied the Eagle Ford Formation in south Texas. His study consisted of documenting and classifying the internal variability of the Eagle Ford facies in a sequence stratigraphic framework and tying those classifications to changes in reservoir quality

and wireline logs. His data consisted of four Eagle Ford cores, XRF/XRD data, and wireline logs. Workman (2013) divided the south Texas Eagle Ford into eight lithofacies. He documented an upward trend in: increasing grain size, decreasing TOC content, increase in bioturbation, transition from pelagic to traction modes of deposition, and changing lithology at a scale that he interpreted as a 2nd order regressive sequence. He also concluded that higher order sequences are preserved within the overall 2nd order sequence. The best reservoir quality was correlated with the higher frequency transgressive and early highstand cycles.

Ryan Harbor (2011) studied the Eagle Ford Formation to better understand the regional geological heterogeneity of unconventional reservoirs as indicated by variable well performance. One of his stated goals was to diagnose controls on the formation of facies within the Eagle Ford. He described the upper and lower Eagle Ford using 27 cores taken from 13 different counties across Texas (Maverick County to La Salle County to Caldwell County), and interpreted elemental chemistry and mineralogy, and tied his results back to wireline log signatures. He subdivided the Eagle Ford into nine different lithofacies that he concluded reflected a combination of sediment production processes, water column chemistry, and the effects of diagenesis. His facies suggest that the Eagle Ford was deposited in a low energy environment with episodic high energy currents, such as gravity-driven debris flows and turbidity currents. He further grouped these facies together to form three (instead of two) informal members within the Eagle Ford in south Texas. He recognized the lower Eagle Ford and upper Eagle Ford, but added a transitional unit located at the top of the upper Eagle Ford with the overlying Austin Chalk Formation. Harbor (2011) defined the transitional unit as characterized by "highly-cyclic (1) ripple-laminated, organic-rich wackestone (cycle base) and (2) burrowed, organic-lean lime

wackestones (cycle top)." He also concluded that the transitional Eagle Ford appears to be the distal equivalent to the foraminiferal lime wackestone of the Austin Chalk Formation.

There have been many other sedimentological studies conducted on the Eagle Ford. There was once some controversy over whether or not the Eagle Ford was deposited continuously as a transgressive cycle, a highstand cycle, or a full transgressive, highstand, and regressive sequence (Donovan and Staerker, 2010; Adams and Carr, 2010; Driskill et al., 2012; Cardneaux, 2012). This in part was due to the influence of higher order sequences on the stronger lower order sequence. Regardless, Driskill et al. (2012) concluded that the top of the lower Eagle Ford must have been deposited during a highstand due to their paleontological, sedimentological, and geochemical data indicating that Eagle Ford deposition occurred in what they believe to have been a low-energy neritic marine setting (100-200 meters depth) within a well stratified water column in a dysoxic to suboxic environment. Furthermore, Fébourg et al. (2016) believe that this unit was deposited during a second-order transgression that is capped by highstand deposits. Looking closer at wireline logs of the full Eagle Ford Shale interval reveals that it may not have been solely deposited during a transgression and highstand, but instead was influenced by a full transgressive, highstand, and regressive cycle. The Eagle Ford in the subsurface is commonly divided into a lower and upper interval. The lower interval lies unconformably on the Buda Limestone, and consists of well-laminated shales that contain high concentrations of organic material. The upper Eagle Ford interval consists predominately of calcareous shales, fractured limestones, and bentonite clays, and is more representative of a near-shore environment than the lower Eagle Ford (Martin et al., 2011). Martin et al. (2011) proposed that due to the obvious changes in the Eagle Ford log signature, the lower Eagle Ford represents a transgressive interval that grades into a highstand interval and finally into the upper Eagle Ford

regressive interval. Interestingly, some authors have also pointed out that within the Maverick Basin, the lower Eagle Ford and upper Eagle Ford boundaries are marked by an upward increase in density and carbonate content with a thin, but measurable clay-rich section lying at the lower to upper Eagle Ford boundary as indicated by density and Elemental Capture Spectroscopy curves (Driskill et al., 2012). Overall, the large-scale vertical variability and change of the Eagle Ford is in part due to the influence of high-frequency sea level changes; however, looking closer at the middle Eagle Ford interval reveals what Fébourg et al. (2016) describes as a vertically alternating globigerinid, argillaceous wackestone, volcanic ash interval, and pelagic grainstone unit successions. Fébourg et al. (2016) concluded that this succession may indicate that much of the small scale vertical variability is more heavily influenced by changes in the faunal productivity related to the presence or absence of iron caused by the deposition of iron-rich volcanic ash-bearing sediments.

In addition to the vertical variability of the Eagle Ford, it also contains marked lateral variability with recognizable bedforms. It is possible that the overall lateral sedimentological variability within the Eagle Ford Formation is due to the effect of bottom water currents that occur in outer-shelf marine settings below normal wave base (Fébourg et al., 2016; Trabucho-Alexandre, 2015). Although clay-size particles were once believed to only accumulate in low energy settings, particularly deep marine environments, recent data suggest that not only is the deep marine ocean floor subject to considerable bottom currents, but clay-size sediments can be deposited and accumulate in relatively high energy environments allowing bedforms and small unconformities to be produced (Trachucho-Alexandre, 2015; Fébourg et al., 2016). Studying Hjulstrøm's (1976) diagram reveals that clay-size particles may flocculate and act as a larger grain size, thereby requiring more energy to erode and transport. Given the documentation of

bedforms within fine-grained deposits, this phenomenon may be more important in the initial deposition of shales than once thought. Fébourg et al. (2016) also recorded that the middle section of the Eagle Ford Formation contains isolated discontinuous sedimentary bed forms that include hydraulic dunes, mega-ripples, and sand sheets along with truncated stratigraphic features. These workers concluded that for the middle Eagle Ford section within the Maverick Basin, these features had to have been formed by bottom water currents below storm wave base that transported and reworked previously deposited material.

Statement of the Problem

The Eagle Ford Formation is commonly divided into the lower Eagle Ford and the upper Eagle Ford. The lower Eagle Ford is recognized as the more organic rich interval commonly targeted by energy companies, and has therefore, stolen much of the attention away from the upper Eagle Ford. Many theses have been written about the lower Eagle Ford, or about the full Eagle Ford interval (averaging the upper and lower Eagle Ford together). Although descriptions of upper Eagle Ford core have been done, very few studies have focused exclusively on this informal unit. The lower and the upper Eagle Ford represent two different depositional regimes, and consequently have many different characteristics. Averaging these two units together introduces significant error. The lower Eagle Ford is arguably the most obvious organic rich interval highlighted with wireline log data; however, the upper Eagle Ford may have just as much potential for hydrocarbon production success as the lower Eagle Ford has had. Since the decline in oil prices in 2015, many companies have been looking more seriously at the upper Eagle Ford as an economical unconventional reservoir, since it is higher in the section and may allow lower associated drilling costs (Hiller, 2015). This thesis describes and interprets core, thin sections, and XRF/XRD data of the upper Eagle Ford in an effort to better understand its

sediment sources and depositional regime, in contrast to that known about the lower Eagle Ford. The intended goal of this thesis is to identify and document different facies, and depositional dynamics within the upper Eagle Ford. A better understanding of the upper Eagle Ford will allow a more thorough and educated assessment of its full potential as an unconventional reservoir, and allow its sweet spots for oil or gas to be found and exploited.

Data and Methods

EOG Resources in San Antonio provided access to four conventional cores located in Karnes and Gonzales counties in south Texas (Figure 5). These cores cover the full Eagle Ford interval including portions of the underlying Buda Formation and overlying Austin Chalk. The cores have been numbered 1 to 4 with Core 1 being the most eastward and Core 4 being the most westward. Cores 1 and 4 occupy the most northern positions relative to cores 2 and 3. Core 2 is the most southerly located core, while Core 3 is located slightly north of Core 2 within the Karnes Trough. These four cores are located relatively close to each other with the furthest distance separating them less than 40 miles.

The upper Eagle Ford portion of these cores was described, and the different lithofacies and lithologies identified within were interpreted according to different environmental conditions and depositional processes that could have led to their development; thereby providing a detailed description as to the different depositional processes that led to the development of the upper Eagle Ford. These core descriptions were recorded to scale digitally in PowerPoint. To better quantify the lithofacies assemblages between cores, histograms and/or pie charts were created to graphically show their abundances and distribution between each core.

Thin section photomicrographs were supplied by EOG Resources. There were taken in plain polarized light from intervals throughout the Eagle Ford Formation. Unfortunately, the

method of thin section preparation was not provided. 139 of these photomicrographs were used and incorporated into the core description formatted in PowerPoint. 39 of these photomicrographs were from Core 4, 17 from Core 3, 49 from Core 2, and 34 from Core 1. These thin sections were described according to the Dunham (1962) classification method (Figure 6). Describing these thin sections aided in understanding the depositional and diagenetic processes controlling some of the dominant and reoccurring lithologies documented in the upper Eagle Ford. For example, noting positions of fossil fragments provided clues into the degree of bottom water currents that may have reworked upper Eagle Ford sediment. The thin section analysis also provided clues as to whether or not the upper Eagle Ford is genetically related to the Austin Chalk by noting fossil assemblages that are present or are not present in both the Austin Chalk and upper Eagle Ford.

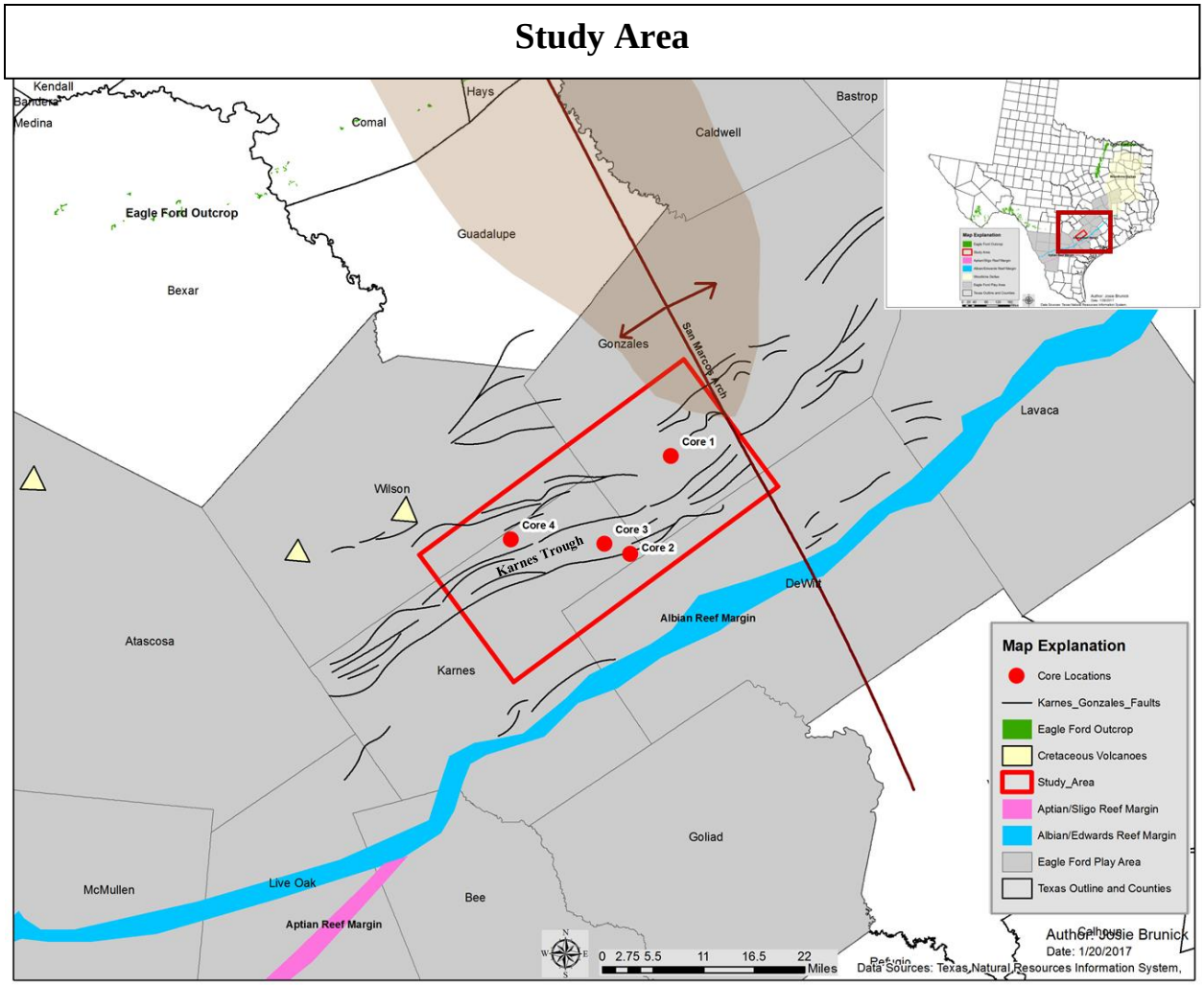

Figure 5: *Study area map* created in ArcGIS for Desktop by Josie Brunick showing the location of the four cores along with Ewing (1987) identified Cretaceous volcanism represented by yellow triangles and the Karnes Trough (bold black lines). Also shown are the Edwards (blue) and Sligo (pink) reef margins, the approximate location of San Marcos Arch (brown polygon), and the southernmost end of the Woodbine Delta digitized from Breyer et al. (2013).

In addition, previously gathered X-ray florescence (XRF) and X-ray Diffraction (XRD) data were provided for all four cores, again through EOG Resources. Little information was provided as to the error margins or methods of extraction for these measurements except that a hand held device was used. These data were used to help assess the degree of bottom water anoxia or oxygenation that the upper Eagle Ford experienced.

In summary, describing the core and thin sections of the upper Eagle Ford was the primary focus of this study, and has aided in answering questions of the sediment sources and depositional dynamics/processes of this interval. The XRF/XRD data will allow some of the environmental conditions, such as levels of anoxia, to be better identified.

Data Limitations

The conclusions drawn in reference to the depositional processes and sediment sources of the upper Eagle Ford are limited by the spatial distribution and low number of cores described in this study. In other words, the conclusion drawn from the analysis of these four cores can only represent processes that were occurring locally, and may not be representative of the upper Eagle Ford as a whole across its depositional extent.

Only photomicrographs of the thin sections in plain polarized light were provided. This significantly limited the identification of fossils and grain types due to the lack of being able to view the thin sections in cross-polarized light and rotate the microscope stage to view the extinction and birefringence character of the grains and matrix. Furthermore, the thin section sampling was fairly random throughout the Eagle Ford, and as a consequence, many defined lithologies from each core did not have a thin section to reference.

<table>
<tr><th colspan="6">Dunham Classification of Carbonate Rocks According to Depositional Texture</th></tr>
<tr><td colspan="5">Depositional Texture Recognizable</td><td>Depositional Texture not Recognizable</td></tr>
<tr><td colspan="4">Original Components Not Bound Together During Deposition</td><td rowspan="3">Components bound together during deposition</td><td rowspan="3">Woodbine Delta

Crystalline Carbonate</td></tr>
<tr><td colspan="3">Contains Carbonate Mud (clay and fine silt size)</td><td rowspan="2">Lacks mud and is grain-supported

Grainstone</td></tr>
<tr><td colspan="2">Mud-supported</td><td rowspan="2">Grain-supported

Packstone</td></tr>
<tr><td>Less than 10% Grains

Mudstone</td><td>More than 10% Grains

Wackestone</td><td></td><td></td><td>Boundstone</td><td></td></tr>
</table>

Figure 6: *Dunham (1962) classification of carbonate rocks* according to depositional textures. Modelled after Dunham (1962).

Lithofacies Descriptions

Seven major lithofacies groups of the upper Eagle Ford in South Texas were identified by describing four cores that contained a combined upper Eagle Ford thickness of 371 feet. These lithofacies were primarily identified according to their sedimentary structures, lithology, and color providing valuable clues into the depositional processes that were occurring. Observations of these lithofacies identified by the core description were augmented by the study of 139 thin sections. Dunham classification method was used with regard to the total percentage of grains and whether or not the section was matrix or grain supported (Dunham, 1962). The following seven major lithofacies groups were defined to characterize the upper Eagle Ford in South Texas:

1. Bioturbated Wackestone/Packstone
2. Deformed Wackestone/Packstone
3. Wavy Laminated Wackestone/Packstone
4. Massive Mudstone/Wackestone
5. Coarsely to Finely Laminated Wackestone/Packstone
6. Massive Packstone/Grainstone
7. Volcanic Ash

These seven lithofacies can be further subdivided into a total of 13 lithologies based predominantly on how dark/light the section is and on the presence of recognizable bedforms. This was done to better document the changing lithologies within one lithofacies. Three general lithologies were recognized. These were limestone, shale, and ash. The limestone and shale lithologies were primarily differentiated according to their relative color (light vs. dark). If the section was medium to light gray, it was categorized as a limestone. If the section was very dark to medium gray it was characterized as shale. Difficulty arose

when the section was medium gray and therefore, either limestone or shale was subjectively assigned based on the darkness of the underlying and overlying lithologies of the section in question.

Further distinction was assigned to each section based on the recognizable bedforms. The recurring bedforms that were recognized are as follows: Bioturbated, Deformed, Coarsely Laminated, Finely Laminated, Wavy Laminated, and Massive. A “bioturbated” distinction was used when the laminae were highly disrupted with very little preserved parallel laminations. A “deformed” distinction was used when laminations exhibited convolute bedding, which was interpreted to be the result of soft sediment deformation. These sections contain disrupted and deformed laminae that remain fairly parallel to each other. A “coarsely laminated” distinction was used to denote obvious and fairly horizontally parallel laterally continuous laminae. A “finely laminated” distinction was used to denote barely perceivable fairly horizontally parallel and laterally continuous laminae. A “Wavy Laminated” modifier was used to indicate laminae were nearly cross-stratified and/or wavy, and commonly thickened and thinned horizontally. A “Massive” distinction was used to denote that there were no perceivable laminations apparent. These lithologies with their modifiers are listed below:

1. Bioturbated Limestone
2. Bioturbated Shale
3. Deformed Limestone
4. Deformed Shale
5. Coarsely Laminated Limestone
6. Coarsely Laminated Shale

7. Finely Laminated Limestone
8. Finely Laminated Shale
9. Wavy Laminated Limestone
10. Wavy Laminated Shale
11. Massive Limestone
12. Massive Shale
13. Volcanic Ash

The following paragraphs provide a detailed description of each lithofacies with their included lithologies.

Bioturbated Wackestone/Packstone

This lithofacies ranges in color from very dark gray to light gray depending on the total percentage of carbonate, clay and/or organics, and includes the Bioturbated Limestone and Bioturbated Shale lithologies (Figure 7). It is dominated by highly disrupted bedding with little to no preservation of laminations. Cryptically developed to well-developed burrows that range in size from a few millimeters to a few centimeters in cross-section also define this lithofacies. The abundance of this lithofacies increases upward within the upper Eagle Ford.

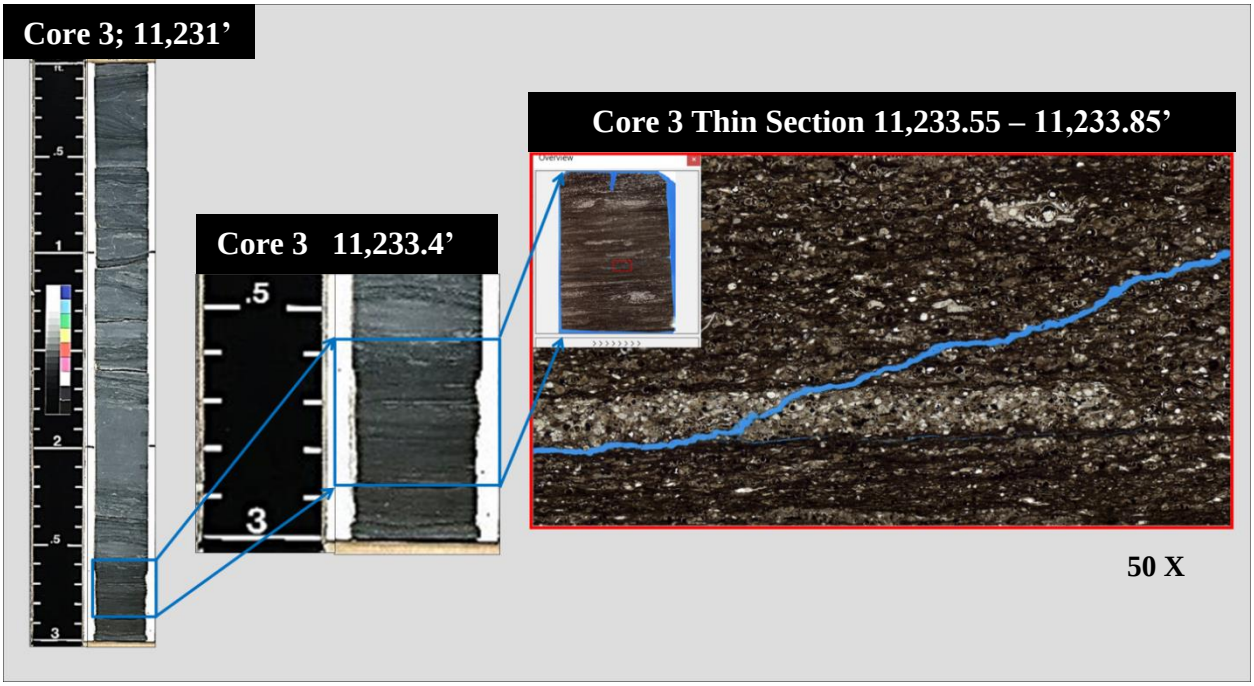

Figure 7: *Bioturbated Wackestone/Packstone* facies core photo and thin section photomicrograph displaying a Bioturbated Shale lithology from Core 3 near 11, 233.5 feet.

The primary constituents within the Bioturbated Wackestone/Packstone include planktonic foraminifera and silt/clay/organic particles. This lithofacies is interpreted to represent a relatively low energy environment below effective wave-base within slightly more oxygenated waters that allowed for the existence of burrowing organisms. The Bioturbated Wackestone/Packstone lithofacies is the most abundant in Cores 4 and 3, and the least abundant in Core 1 (Figure 8).

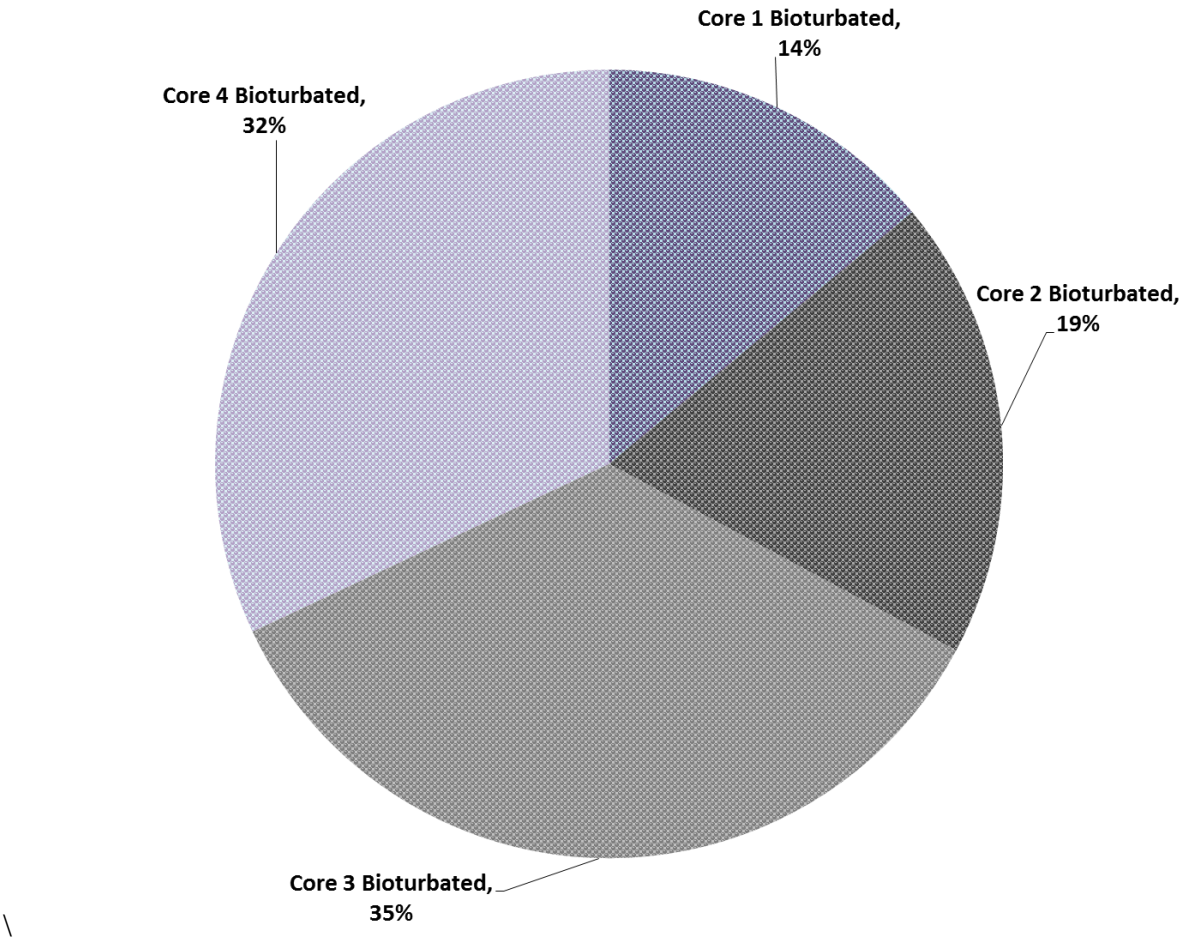

Figure 8*: Normalized distribution of the Bioturbated Wackestone/Packstone* lithofacies between all four cores. Normalization was completed by first calculating the percentage of the specified lithofacies within each individual core. Next, those individual core percentages were normalized to 100% by dividing each individual core lithofacies percentage by the sum of the specified lithofacies percentages from all cores.

Deformed Wackestone/Packstone

This lithofacies ranges in color from very dark gray to light gray depending on the total percentages of carbonate, clay and/or organic material, and includes the Deformed Limestone and Deformed Shale lithologies (Figure 9). It is dominated by the presence of highly deformed

laminae some of which appear to have been "rolled" over top of one another. These "jelly rolls" can be indicative of soft sediment deformation attributed to slow down-slope creep. The occurrence of this lithofacies also increases upward within the upper Eagle Ford.

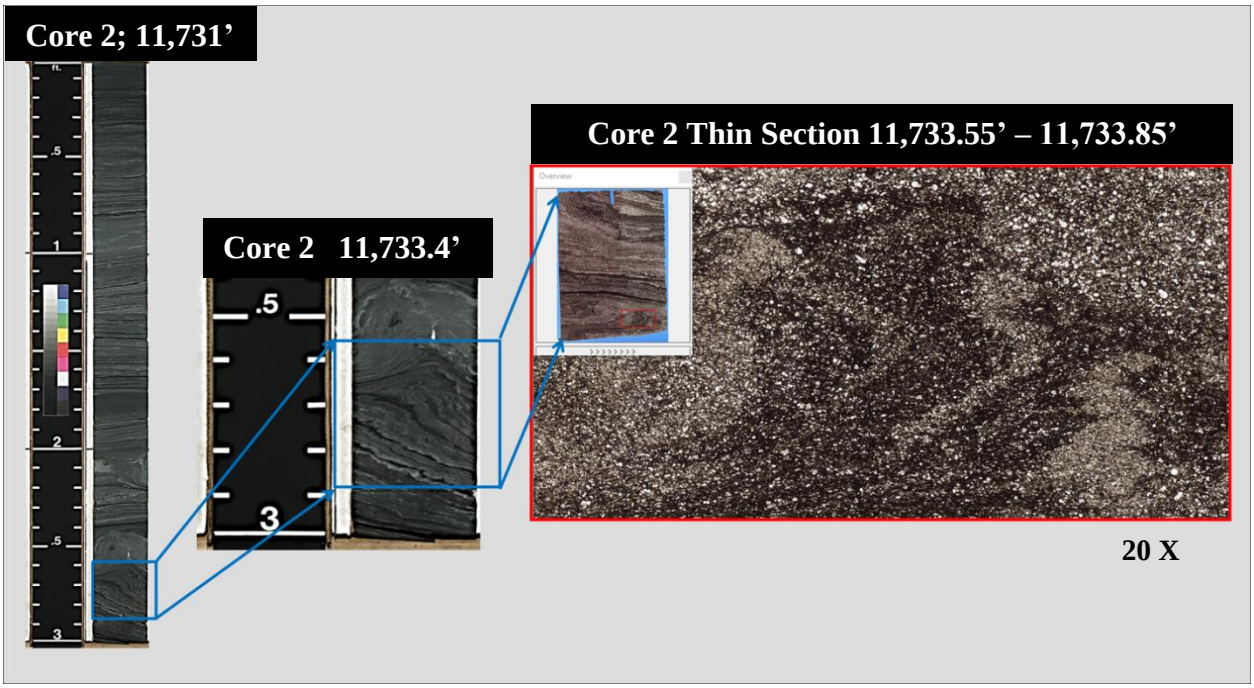

Figure 9: *Deformed Wackestone/Packstone* facies core photo and thin section photomicrograph from Core 2 near 11, 733.5 feet.

The primary constituents within the Deformed Wackestone/Packstone include planktonic foraminifera, silt/clay/organic particles, ostracods, and sparse bivalve shells. This lithofacies is interpreted to represent soft sediment deformation that developed due to differential compaction and down-slope sediment creep due to a gradual buildup of gradient during upper Eagle Ford deposition. This lithofacies is by far the most abundant in core 2, and is the least abundant in core 1 (Figure 10).

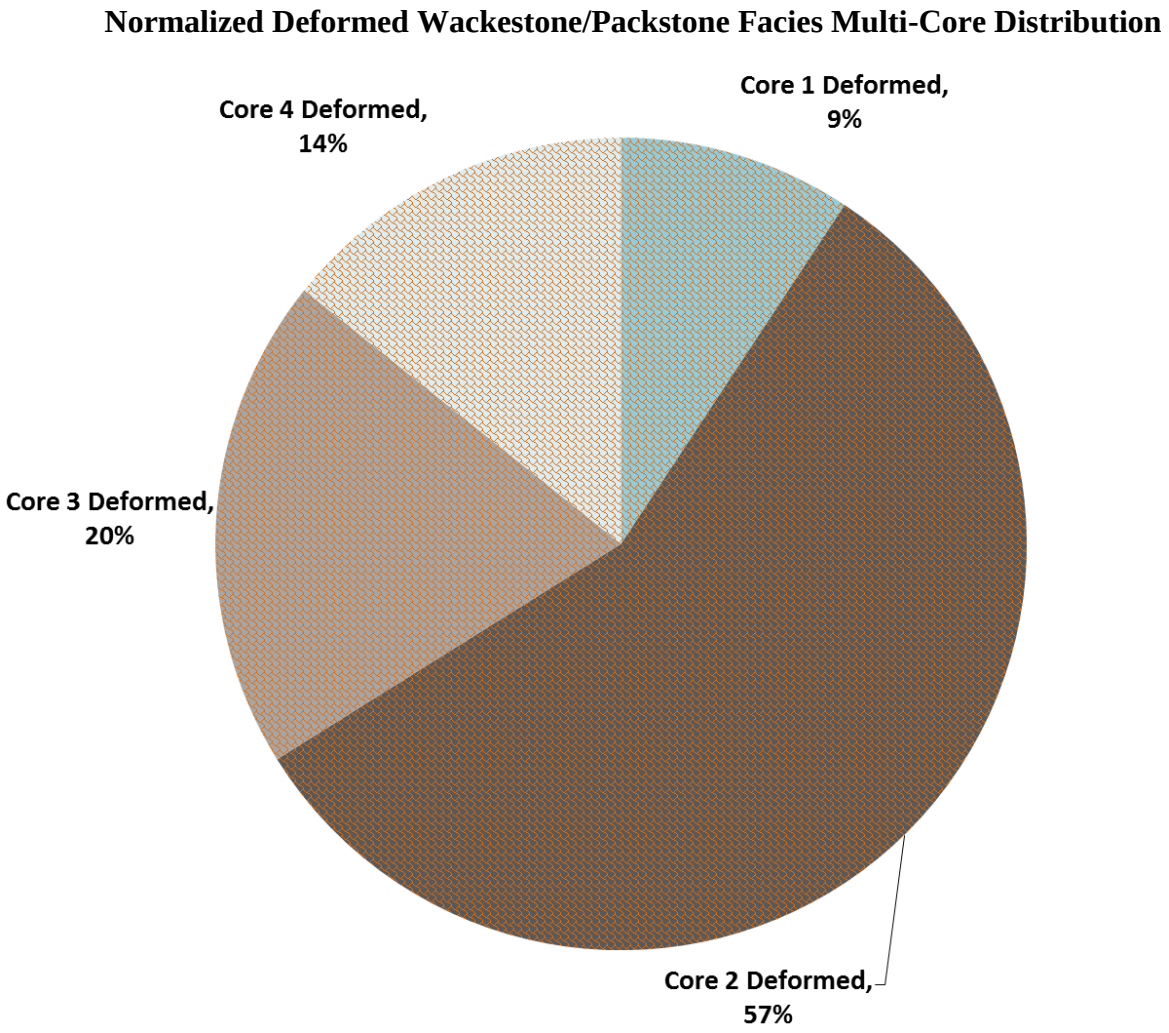

Figure 10: *Normalized distribution of the Deformed Wackestone/Packstone* facies between all four cores. This facies is the most abundant in Core 2, which is the most distally located core.

Wavy Laminated Wackestone/Packstone

This lithofacies ranges in color from very dark gray to light gray depending on the total carbonate and clay/silt/organic content (Figure 11). The Wavy Laminated Wackestone/Packstone lithofacies is defined by thickening and thinning laminae that are relatively continuous, but slightly disrupted. This lithofacies includes the Wavy Laminated Limestone and the Wavy Laminated Shale lithologies. The Wavy Laminated Wackestone/Packstone lithofacies increases

upward within the upper Eagle Ford, but is the most abundant in both proximal cores (Cores 1 and 4 Figure 5; Figure 12).

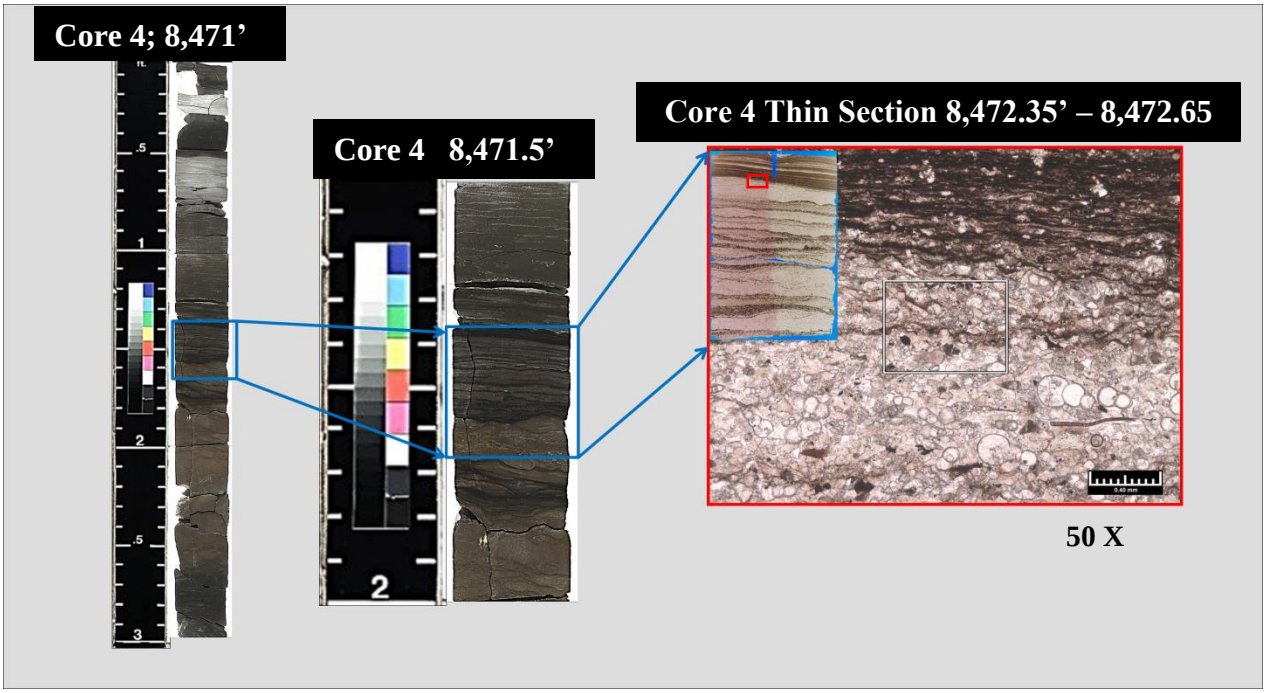

Figure 11: *Wavy Laminated Wackestone/Packstone* facies core photo and thin section photomicrograph from Core 4 near 8,472.35 feet.

The primary constituents within the Wavy Laminated Wackestone/Packstone are planktonic foraminifera, silt/clay/organic particles, ostracod fragments, and sparse bivalve fragments. Many of the bivalve fragments are commonly found in hydro-dynamically stable positions indicating that there has been at least minor bottom water current reworking of sediment. This lithofacies is interpreted to represent either a slightly higher energy environment that is near wave-base, and therefore, is more frequently affected by storm-wave base, or an environment subjected to sustained bottom water-currents.

Normalized Wavy Laminated Wackestone/Packstone Facies Multi-Core Distribution

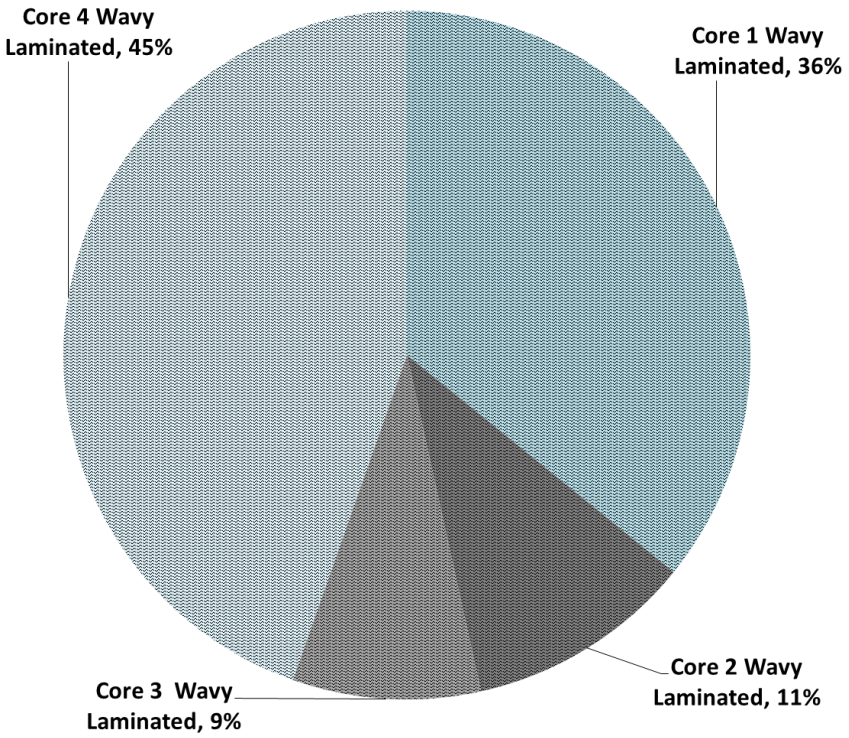

Figure 12: *Normalized distribution of the Wavy Laminated Wackestone/Packstone* facies between all four cores. This facies is the most abundant in Core 4, which is one of the most proximally located cores.

Massive Mudstone/Wackestone

The Massive Mudstone/Wackestone lithofacies ranges in color from very dark gray to medium gray depending on the total carbonate and clay/silt/organic content (Figure 13). With the exception of Volcanic Ash, this is the least abundant lithofacies within the study area. It includes the Massive Shale lithology, and is defined by a near homogeneous appearance with some sections containing dispersed clasts in random orientations.

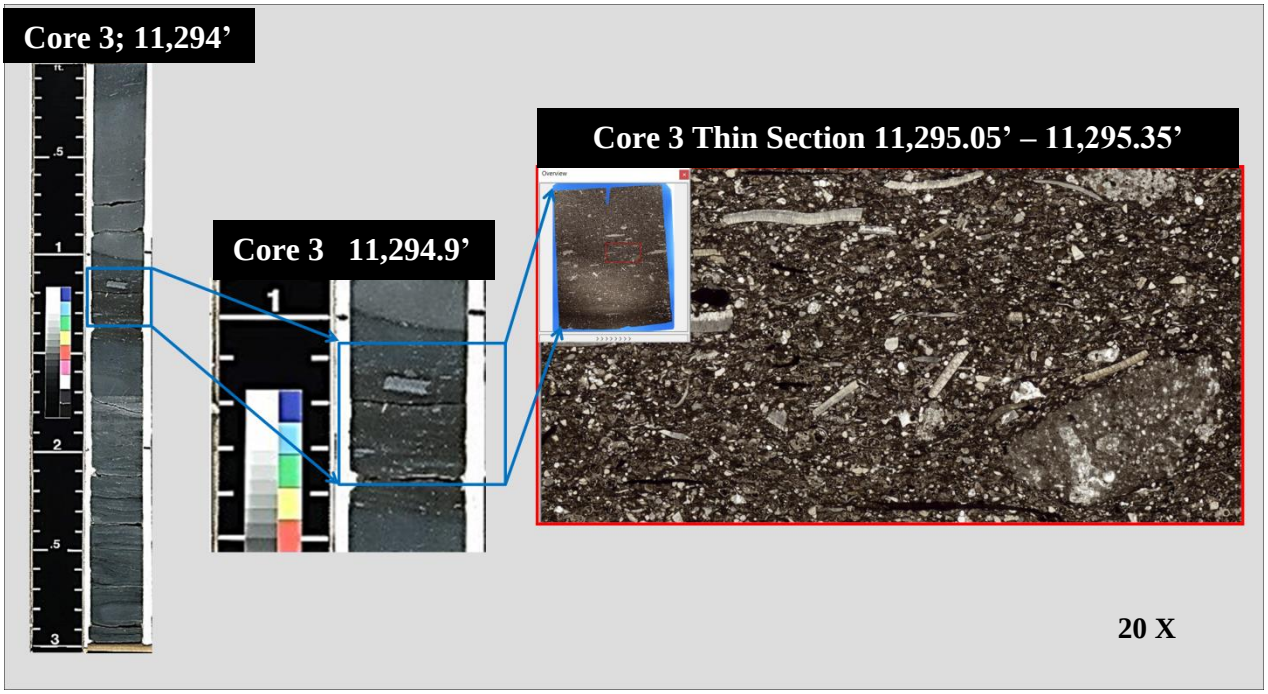

Figure 13: *Massive Mudstone/Wackestone* facies core photo and thin section photomicrograph from Core 3 near 11,295.05 feet.

The Primary constituents of the Massive Mudstone/Wackestone lithofacies is clay/silt/organic particles, frequent to sparse clasts and bone fragments, dispersed planktonic foraminifera, frequent to sparse bivalve and ostracod fragments, and diagenetic calcite crystals. Some of these deposits appear to be the end of waning low-density mud-rich debris flows. These are the massive mudstone/wackestone sections that contain dispersed clasts. Other massive units appear to be nearly homogeneous and are composed predominantly of very fine grained clay, silt, and/or organic particles. This latter type of Massive Mudstone/Wackestone could have been homogenized by bioturbation, but any traces of burrows are not recognizable or preserved. Within each core, the thickest sections of the homogeneous Massive Mudstone/Wackestone lithofacies are commonly found above substantial Volcanic Ash deposits. This lithofacies is the most abundant in core 4, and is the least abundant in core 1 (Figure 14).

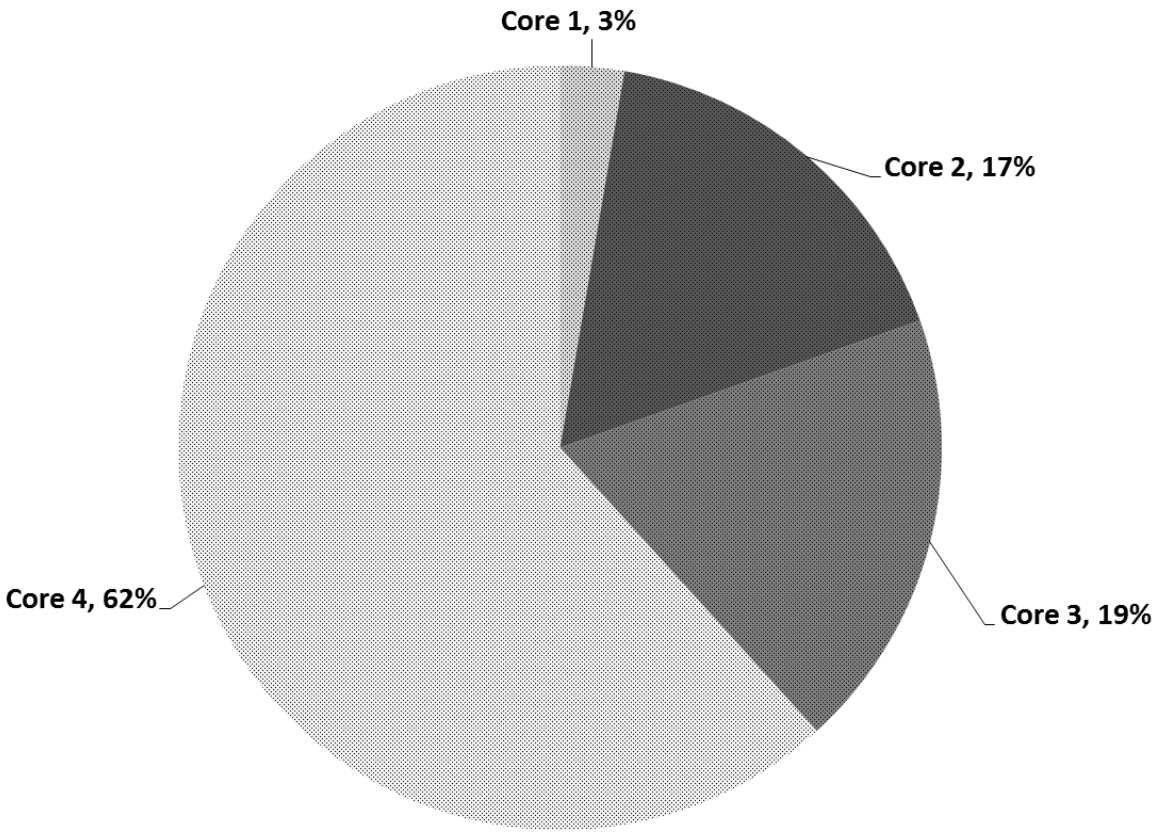

Figure 14: *Normalized distribution of the Massive Mudstone/Wackestone* facies between all four cores. This facies is the most abundant in Core 4, which is one of the most proximally located cores and the core located closest to the western province of the Cretaceous volcanic activity as defined by Ewing (1987).

Coarsely to Finely Laminated Wackestone/Packstone

This lithofacies ranges in color from very dark gray to light gray depending on the relative abundances of carbonate, clay and/or organic material, and includes the Coarsely Laminated Limestone, Finely Laminate Limestone, Coarsely Laminated Shale, and the Finely Laminated Shale lithologies (Figure 15). This is the most abundant lithofacies within the study

area. It can be subdivided into Coarsely Laminated Wackestone/Packstone and Finely Laminated Wackestone/Packstone with the defining feature being how obvious the laminations are. A Finely Laminated Wackestone/Packstone is defined as barely visible, but still apparent laminations, each averaging between 0.5 millimeters to 2 millimeters thick. Conversely, the Coarsely Laminated Wackestone/Packstone is defined as containing clearly visible, obvious laminations also averaging between 0.5 millimeters to 2 millimeters thick. The laminations, whether fine or coarse, are laterally continuous, parallel, and alternating light and dark. The lighter laminae are primarily composed of concentrated planktonic foraminifera, while the darker laminae are composed of clay, silt, and/or organic particles. The primary difference in how obvious the laminae appear is due to the relative concentrations of foraminifera and/or the degree of diagenetic calcite crystallization between the foraminifera-rich laminae. The coarser laminations have a higher concentration of foraminifera and/or calcite crystallization, while the fine laminations contain a lower concentration of foraminifera and/or calcite crystallization. In addition to the planktonic foraminifera, bivalve and ostracods fragments are sparsely incorporated into some sections.

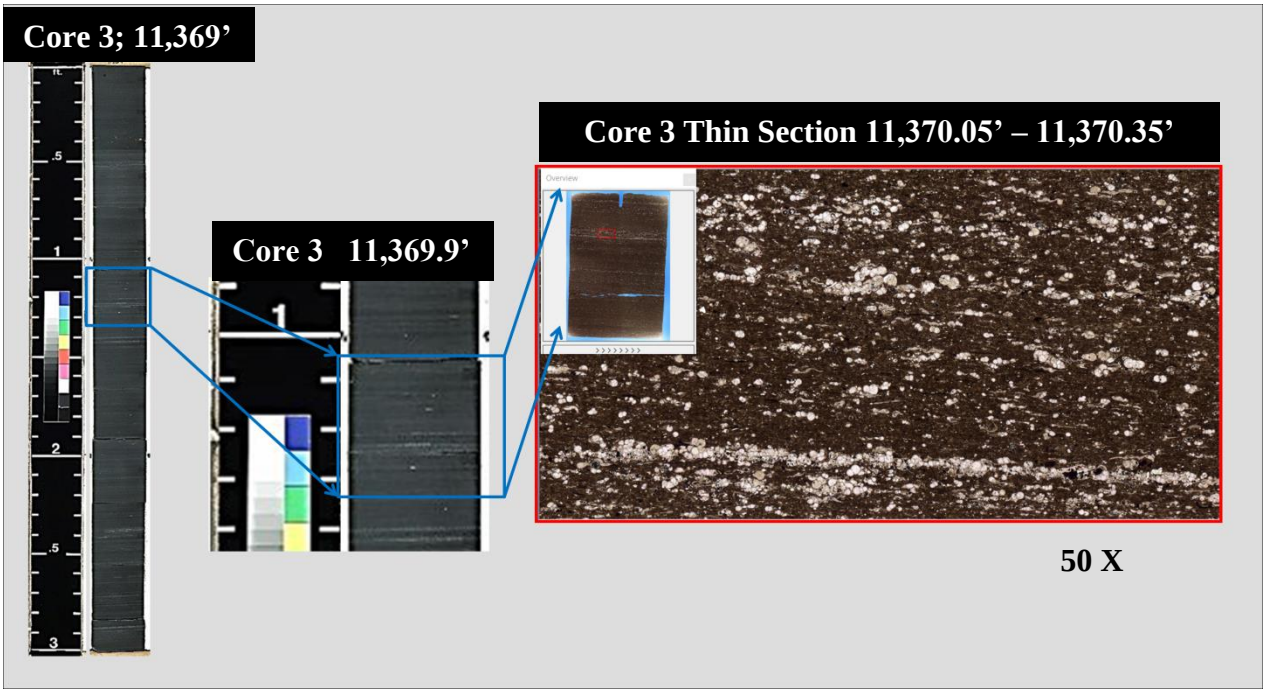

Figure 15: *Coarsely to Finely Laminated Wackestone/Packstone* facies core photo and thin section photomicrograph from Core 3 near 11,370.05 feet.

Primary constituent of this lithofacies is again planktonic foraminifera, clay/silt/organics and sparse bivalve and bone fragments, and ostracod fragments. This is the most abundant lithofacies of the upper Eagle Ford overall. It is interpreted to represent a very low energy marine environment below wave-base that may have been influence infrequently by waning low density debris flows. The laminations are reminiscent of seasonal varves and are likely caused by mass die-offs of foraminifera related to various cyclic climate changes and the organism's life and death cycle. This is similar to what has been documented in the Black Sea (Arthur et al., 1994). This lithofacies is the least abundant in Core 4, but occurs in near equal proportions in Cores 1, 2, and 3 (Figure 16).

Normalized Coarsely to Finely Laminated Wackestone/Packstone Facies Multi-Core Distribution

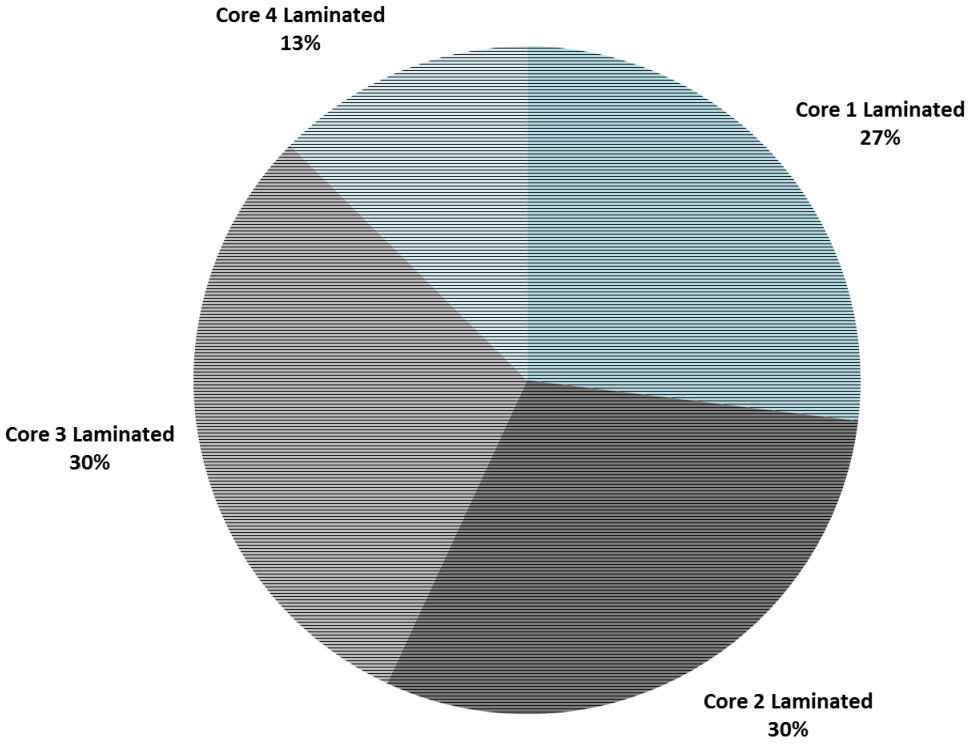

Figure 16: *Normalized distribution of the Coarsely to Finely Laminated Wackestone/Packstone* facies between all four cores. This facies is the most abundant in Cores 2 and 3, which are the most distally located cores.

Massive Packstone/Grainstone

This lithofacies is characterized by a medium to light gray color and a homogeneous texture and appearance (Figure 17). The Massive Packstone/Grainstone lithofacies includes the Massive Limestone lithology. The bases of these sections are commonly scoured. Diagenetic calcite crystallization has been documented the most in this lithofacies, and sometimes forms what appear to be concretions.

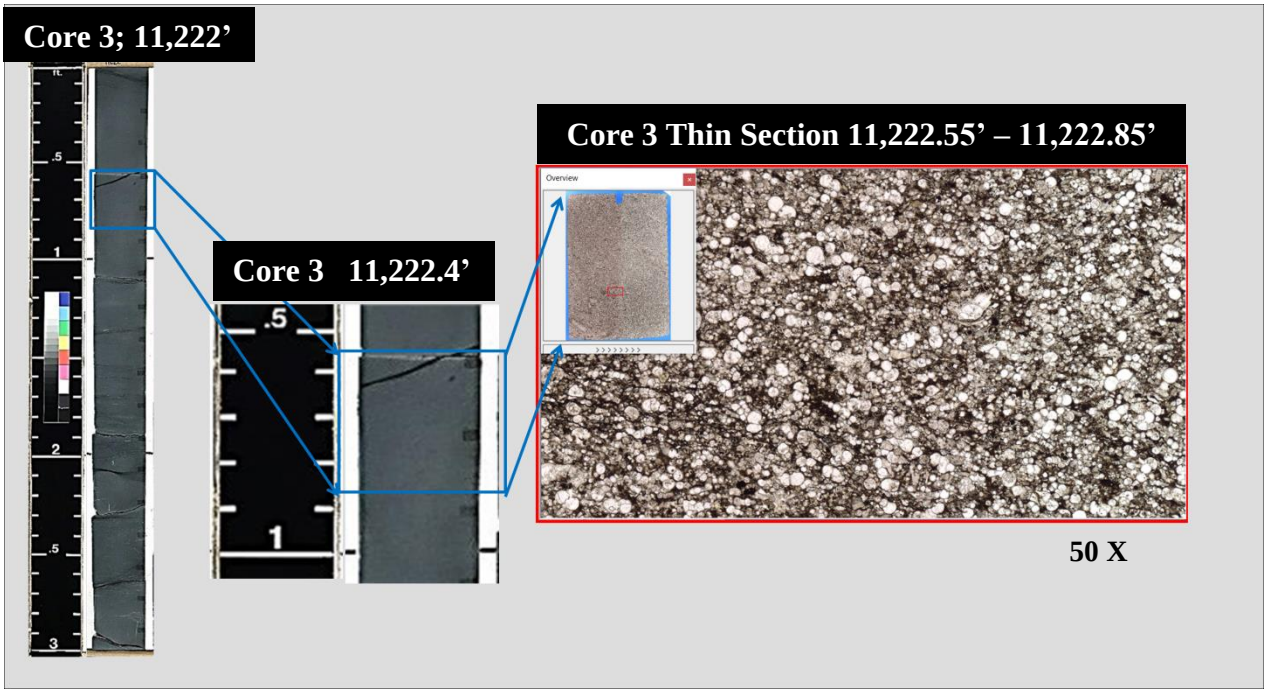

Figure 17: *Massive Packstone/Grainstone* facies core photo and thin section photomicrograph from Core 3 near 11,222.55 feet showing significant diagenetic calcite crystallization.

This lithofacies is interpreted to represent a combination of turbidity current events that experienced varying degrees of recrystallization, and stratigraphically confined horizons of concretionary formation that may be related to the anaerobic bacterial decay of organic material. Most of the concretions appear to have formed just below the sediment-water interface, while the sediment was still relatively soft. This is indicated by a slight deforming of the lamination above and below these recrystallized sections. This lithofacies is most abundant in Cores 3 and 2, and least abundant in Core 4 (Figure 18).

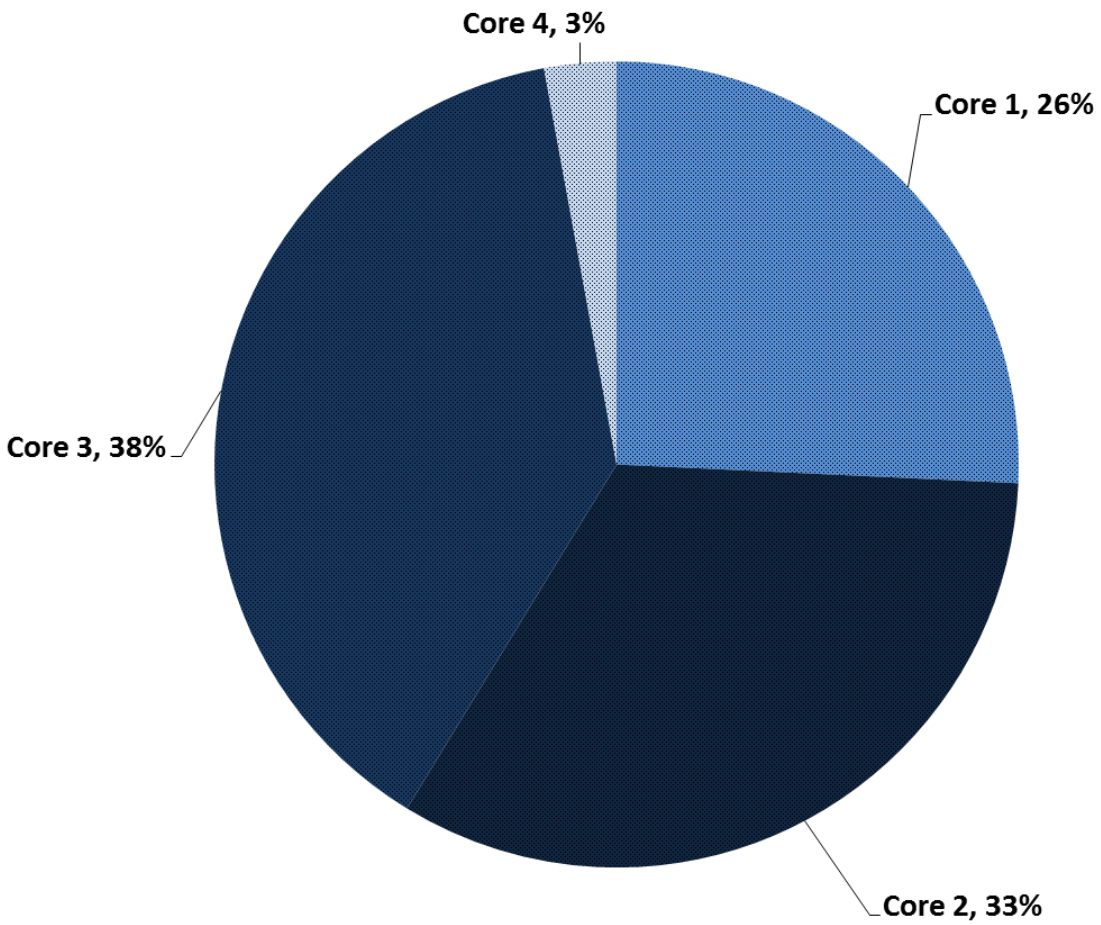

Figure 18: *Normalized distribution of the Massive Packstone/Grainstone* facies between all four cores. This facies is the most abundant in Cores 2 and 3, and the least abundant in core 4.

Volcanic Ash

Volcanic Ash beds are common in both the lower and upper Eagle Ford. The Volcanic Ash lithofacies is by far the least abundant in the study area. Due to the varied depositional processes and deformation occurring during upper Eagle Ford deposition many of the ash beds are somewhat obscured and not as apparent as they are within the lower Eagle Ford. Most ash

beds are a very dark greenish-brown color with a smooth tight texture. A few of the ash beds are light brown in color with a very rough splintery texture (Figure 19). Most of these sections have a sharp basal contact and a rapidly gradational to gradational upper contact.

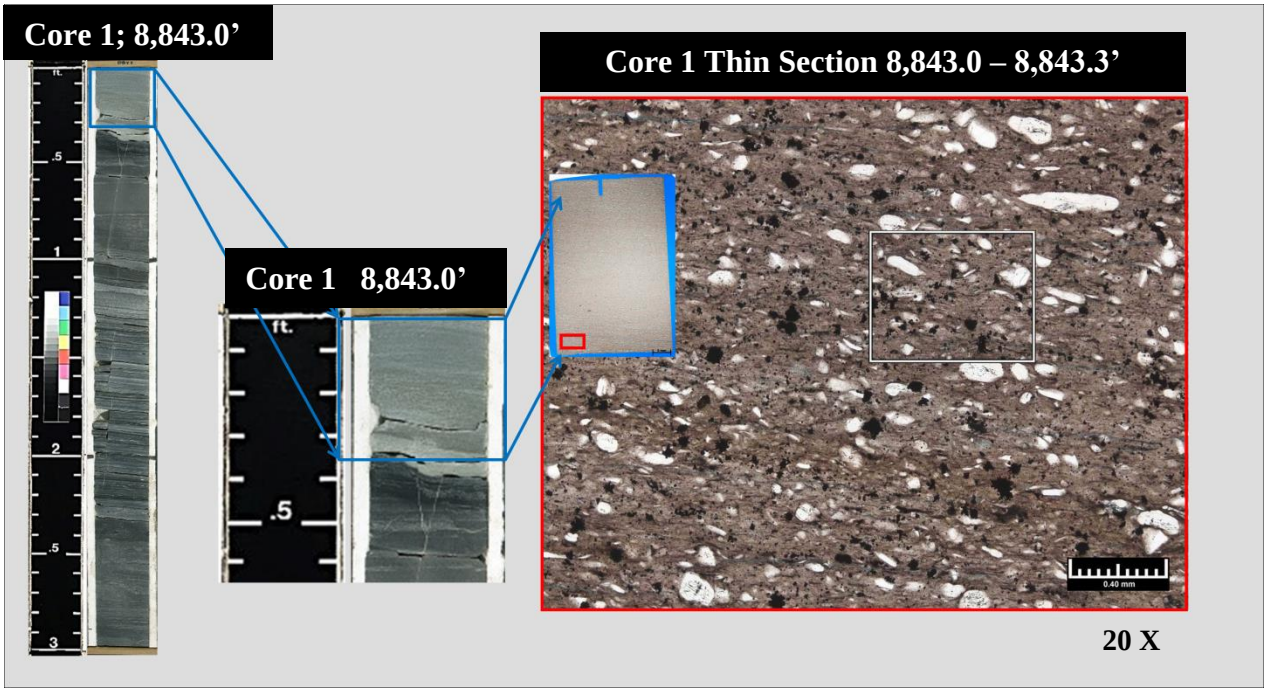

Figure 19: *Volcanic Ash* facies core photo and thin section photomicrograph from Core 1 near 8,843.0 feet.

Many of these deposits appear to be ash formed as fallout from subaerial volcanic eruptions; however, there is a substantial Ash deposit in Core 1 that exhibits a highly-scoured base indicating that the ash deposit originated from a subaqueous eruption, or perhaps a subaerial eruption that triggered a subaqueous mass wasting event leaving an irregular scar on which the resultant ash fallout was deposited. The deposited ash was concentrated enough to retain its light gray color. Interestingly, the thickest homogeneous, massive mudstone/wackestone lithofacies in all four cores is located directly above an unusually thick ash deposit. This relationship indicates that this correlative ash deposit that was overlain by the homogeneous mudstone/wackestone

lithofacies was created by a volcanic eruption that significantly changed the environmental conditions and/or water chemistry near these cores. This lithofacies is the least abundant in Core 2, but occurs in near equal abundances in Cores 4, 1, and 3 (Figure 20).

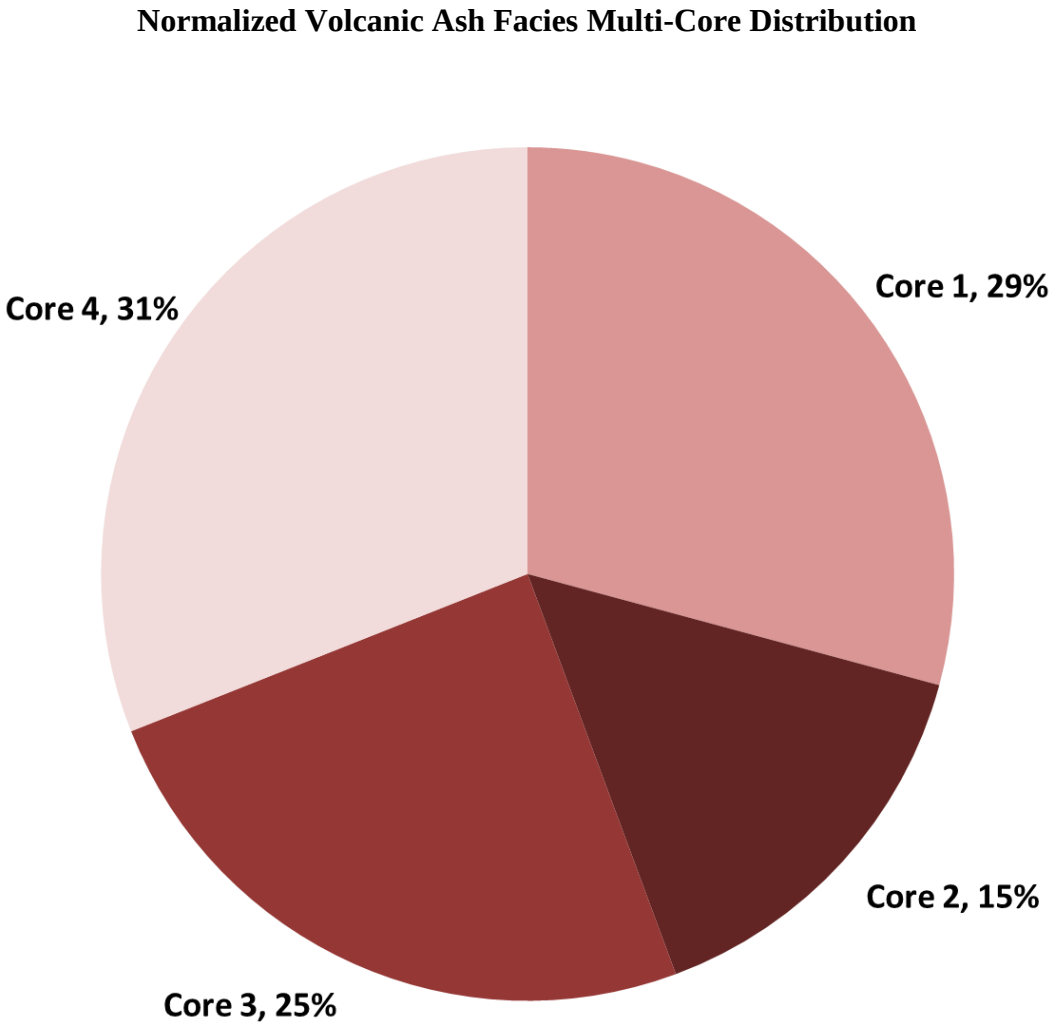

Figure 20: *Normalized distribution of the Volcanic Ash* lithofacies between all four cores. This lithofacies is slightly more abundant within core 4, which is the core proposed to be located closest to the western Cretaceous volcanic province.

Depositional Processes Evaluation

Finely to Coarsely Laminated Wackestone/Packstone: Suspension Settling

Different depositional processes produce unique sets of features. These features can be used to interpret the possible depositional environments and processes that lead to that particular sedimentary deposit. One of the most common sedimentary structures is plane bedding, which is defined as simple horizontal bedding (Prothero and Schwab, 2014). If these planes are less than 1 centimeter thick, they are considered to be laminations (Prothero and Schwab, 2014). This type of plane bedding is abundant in both the lower and upper Eagle Ford Formation. Although the presence of plane bedding/laminations in sedimentary rocks can be formed in many different environments, processes, and flow regimes it can still provide clues into some of the depositional processes that were occurring. For instance, the type and shape of the grains/fossils that compose each plane/lamination provide evidence of where the sediment originated, and how it got to its present position. Plane bedding can be representative of cyclic climatic changes both on a large or small time frame if, it appears to be repetitive and alternating (much like varves). Plane bedding in the form of laminations present in fine grained deposits, such as the Eagle Ford, are traditionally thought to result from slow and consistent deposition (Prothero and Schwab, 2014).

In the case of the Eagle Ford Formation, these laminations are alternating lighter colored planktonic foraminifera-rich laminae, and darker colored clay-rich laminae. The high degree of symmetry between each foraminiferal lamination, and the dominance of planktonic foraminifera creating these light colored laminae indicates that these are possibly related to the life and death cycle of planktonic foraminifera and could loosely be thought of as marine “varves” related to climatic/environmental changes during the Cretaceous period that influenced the productivity of foraminifera.

According to Berger (1971), foraminifera are sensitive to varying climatic conditions. In fact, in temperate latitudes, a rapid increase in the abundance of certain species of living foraminifera, commonly known as a "spring bloom," can be triggered by an increase in sunlight and nutrient availability in the surface waters (Berger, 1971). This rapid increase in population likewise leads to a concentration of foraminifera tests settling through the water column (Berger, 1971). The preservation potential of these tests depends on a variety of factors. A few of these factors include the settling velocity, the size of the test, the weight of the test, the shape of the test, the wall thickness of the test, the chemical composition and temperature of the seawater, as well as the depth at which the tests are deposited (Kucera, 2007). According to Kucera (2007), the slower the settling velocity of the test through the water column the higher the likelihood of complete dissolution preventing it from being deposited on the ocean floor. In addition, Kucera (2007) noted that larger tests have a higher settling velocity than smaller foraminiferal tests and therefore, are disproportionately preserved in the stratigraphic record. This comparison of relative settling velocity applies to empty tests (Kucera, 2007). If the test contains a higher amount of residual cytoplasm that allows an increase in density, it will increase the settling velocity for that test (Kurcera, 2007). In this manner, it is plausible to postulate that concentrations of smaller foraminifera preserved in the stratigraphic record may be related to mass die-off caused by a detrimental climatic shift that led to unfavorable surface water conditions in which the organism could not survive. This is in contrast to the larger foraminiferal tests that are typically associated with mature organisms, their reproductive processes, and "spring blooms" (Berger, 1971; Kucera, 2007).

The preservation potential of calcium carbonate tests is strongly related to the depth at which they are deposited. Dissolution of foraminiferal tests is dependent on the saturation levels

of calcium carbonate in seawater with the lower the saturation of calcium carbonate in seawater correlated with increased dissolution rates of foraminifera tests (Berger, 1970). Deeper waters are typically less saturated in calcium carbonate (Berger, 1970). The best preservation potential for foraminiferal tests is located above the lysocline which is typically located several hundred meters above the calcite compensation depth (Berger, 1970; Kucera, 2007). The lysocline depth is representative of the depth at which the calcium carbonate dissolution rate rapidly increases and reaches a maximum (Prothero and Schwab, 2014). In other words, any foraminifera that are deposited near this depth are poorly preserved (Berger, 1970). Additionally, the decomposition of organic matter can create an acidic environment not conducive to the preservation of tests composed of calcium carbonate (Kucera, 2007). The presence of organic content within the upper Eagle Ford and the abundance of fairly well preserved foraminifera suggest that the upper Eagle Ford was deposited in a fairly shallow water depth above the lysocline in an oxygen poor environment that inhibited the loss of deposited organic matter.

Wavy Laminated Wackestone/Packstone: Bottom Water Currents

Marine black shale depositional systems are traditionally thought of as very low energy anoxic environments that have little to no influence of bottom water currents. However, the occurrence of the Wavy Laminated Wackestone/Packstone lithofacies within the upper Eagle Ford suggest that this mixed siliciclastic/carbonate black shale was influenced by bottom water currents (Figure 21). Interference ripples are commonly associated with a bidirectional flow regime where, in the case of lenticular bedding formation, small lenses of sand-sized grains are caught within minute depressions of a muddy (silt and clay) substrate (Prothero and Schwab, 2014). If this sand to mud ratio is near 50:50, then this bedform is more accurately termed wavy bedding. In the case of the upper Eagle Ford, the previously deposited foraminifera acted as the

sand-sized grains, and were reworked forming what could be interpreted as either millimeter-scale starved ripples and/or lenticular/wavy bedding (Prothero and Schwab, 2014). This could indicate that the bottom water currents that were affecting the upper Eagle Ford were influenced by or were at least in part a function of tidal flow in the more proximal locations. High angle relationships were also noted among the upper Eagle Ford laminae indicating the formation of cross-stratification and migrating ripples. Consistent with an overall shallowing sequence, these sections were typically found stratigraphically higher in the upper Eagle Ford, and were the most common in Core 4, which was the most westward proximally located core (Figures 5 and 12). These sedimentary bedforms indicate that bottom water currents played a role in upper Eagle Ford deposition.

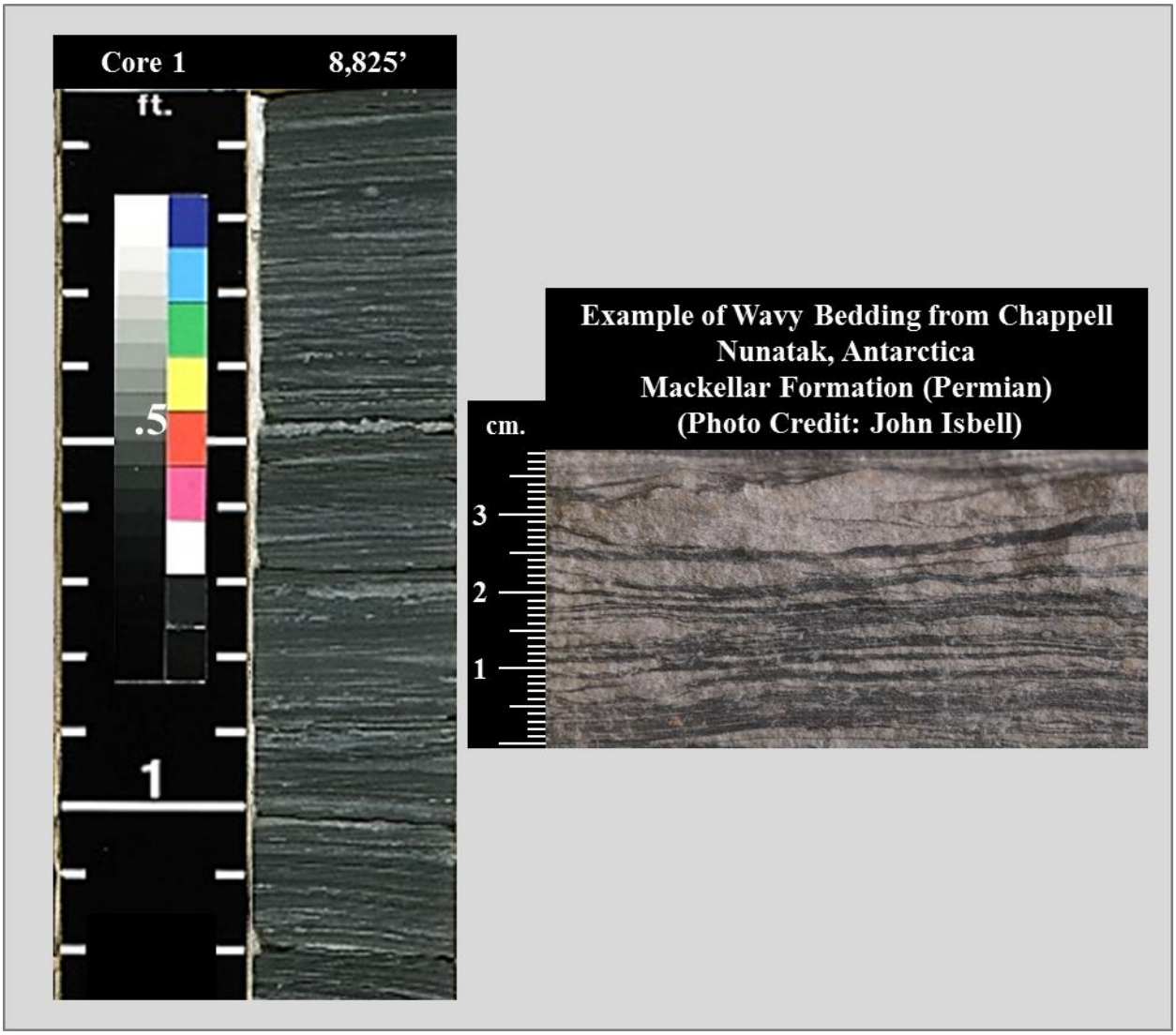

Figure 21: *Traditional Wavy Bedding vs. Eagle Ford Wavy Laminated Wackestone/Packstone*: Comparison of sedimentary bedforms observed within Core 1 near 8,825' and classified as the Wavy Laminated Wackestone/Packstone facies to an example of traditional wavy bedding from Chappell Nunatak, Antarctica. Photo Credit: John Isbell (used with permission).

Deformed Wackestone/Packstone: Post-Deposition Soft-Sediment Deformation Processes

Several post-depositional processes in the form of soft-sediment deformation occurred in the upper Eagle Ford. There are numerous sedimentary structures that indicate soft-sediment deformation. The deformation features most commonly seen in the upper Eagle Ford near Karnes

Trough are convoluted lamination. These laminations are warped to the extent of forming near perfect “S” shapes commonly called or known as “Jelly Rolls.” This type of soft-sediment deformation is not associated or indicative of rapid deposition. Instead, these convoluted laminations are most associated with very slow and gradual down-slope sediment creep under the influence of gravity (Prothero and Schwab, 2014). These structures are the most abundant in the upper section of Core 2 with Core 3 being a close second. This could indicate that these two locations experienced a gradual build-up of slope gradient increase caused by elevated upper Eagle Ford sedimentation rates that resulted in local downslope sediment creep. On the other hand, and more likely given the location of these cores, movement of the Karnes Trough fault system could have provided a mechanism for gradual down-slope creep. Determining the original depositional facies of this section is complicated by post depositional deformation. However, it is likely these sections were originally either of the finely to Coarsely Laminated Wackestone/Packstone lithofacies, or possibly of the Wavy Laminated Wackestone/Packstone lithofacies.

Karnes Trough is a graben feature positioned between north and south bounding normal faults. The full Eagle Ford section in Core 3 is over 86 feet thicker than the most distally located core (Core 2), and over 200 feet thicker than the most proximally located cores (Core 1 and 4). This indicates that Karnes Trough was actively subsiding during Eagle Ford deposition. This gradually allowed more accommodation space, and led to a thicker section of the Eagle Ford Formation within this graben. Strictly comparing the upper Eagle Ford thicknesses suggests that this trough was active during upper Eagle Ford deposition. The upper Eagle Ford section in Core 3 is over 78 feet thicker than the most distally located core (Core 2). This is approximately 91% of the observed thickening of the full Eagle Ford section in Core 3 in comparison to Core 2.

Furthermore, the upper Eagle Ford in Core 3 is over 130' feet thicker than the two most proximally located cores (Core 1 and 4). This accounts for approximately 65% of the observed full Eagle Ford thickening between Core 3 and Cores 1 and 4. These observations could indicate any number of scenarios. One scenario is that the Karnes Trough subsided at a near constant rate throughout Eagle Ford deposition, but was able to accommodate a higher influx of sediment represented by a higher rate of sedimentation during upper Eagle Ford deposition. On the other hand, the increased thickening of the upper Eagle Ford could indicate that Karnes Trough was subsiding at increased rates during upper Eagle Ford deposition allowing it to accommodate more upper Eagle Ford sediment. This latter possibility could be in conjunction with increased upper Eagle Ford sedimentation rates as well.

The core that contains the thickest sections of the Deformed Wackestone/Packstone lithofacies, Core 2, is located on the south footwall bounding block of the Karnes Trough. A phenomena known as footwall uplift could explain the increased occurrence of soft-sediment deformation in the upper Eagle Ford in this core. Footwall uplift is thought to occur as a result of hangingwall subsidence. In other words, as the hangingwall actively subsides, the footwall block is not only partially displaced by the hangingwall, but also experiences unloading related to the movement of the hangingwall block down the fault plane. This allows the footwall block to be permanently uplifted by isostasy (Jackson and McKenzie, 1983). In fact, Jackson and McKenzie (1983) estimated that footwall uplift can be approximately 0.1 times the hangingwall subsidence rate within normal fault systems. If this was affecting the Karnes Trough faults, the gradual uplift of the southern footwall block could have slowly increased the slope gradient beneath still soft upper Eagle Ford sediments allowing these sediments to slowly deform by down-slope creep.

Bioturbated Wackestone/Packstone: Higher Oxygenation and Thriving Organisms

Trace fossils in the form of burrows are indicative of (at minimum) slightly oxygenated waters and conditions that allow bottom dwelling organisms to live. Not surprisingly, this lithofacies becomes more abundant in the upper section of the upper Eagle Ford in all four cores suggestive of an upward shallowing sequence. Interestingly, many event beds deposited in the more distally located cores seem to show a positive correlation with the occurrence of at least minor bioturbation. Modern day studies of Tertiary deposits near Baja California suggest that gravity driven mass wasting events can transport organisms with short lived flushes of oxygenated water to environments where these organisms, referred to as "Doomed Pioneers," would normally not live (Föllmi and Grimm, 1990). The oxygen rich water that was brought along with the organism can allow the organism to live for a short period of time with some organisms, such as *Callianassa* shrimps, surviving up to 5 to 7 days of anoxia (Föllmi and Grimm, 1990). This type of shrimp is associated with creating *Thalassinoides* and *Gyrolithes* burrows that Föllmi and Grimm (1990) documented preferentially within small event beds that ranged in thickness from 1-20 cm (and the immediately underlying sediments). These event beds and areas of bioturbation were sandwiched between laminated fine grained deposits that showed no other signs of bioturbation (Föllmi and Grimm, 1990).

Massive Mudstone/Wackestone: Mass Wasting Events

As mentioned before, there are two broad types of Massive Mudstone/Wackestone deposits: (1) homogeneous fine grained clay, silt, and/or organic sections (Figure 22), and (2) sections that contain dispersed clasts and numerous larger shell fragments (Figure 23). The sections that contain dispersed clasts are interpreted as mud-rich event beds; however, the homogeneous fine grained sections could represent highly bioturbated sections, deposits of event

bed in more distal environments, and/or a reduction of the primary production of planktonic foraminifera. The most extensive homogeneous fine grained section occurs in Core 4 with many other similar sections appearing above major volcanic ash deposits. The correlation between these deposits and volcanic ash deposits may suggest that some of the volcanic eruptions altered the environmental conditions in such a way to reduce the productivity of planktonic foraminifera. Core 4 is the location that contains some of the best developed wavy laminations indicative of ripple formation suggesting that this area may have been subject to higher oxygenation levels within the water column. If this massive homogeneous fine grained section in Core 4 is from intense bioturbation, then it is also indicative of a much higher degree of oxygenation at this location. This deposit could also be representative of a low-density gravity flow. If radiographic analysis were to be used to examine these homogeneous sections as outlined by Hamblin (1962), small scale sedimentary structures, including micro-burrows and/or cross-stratification, may be revealed. Using radiographic analysis Hamblin (1962) was able to demonstrate that within several samples of seemingly homogenous sandstones, interpreted to have been deposited by similar means, had exhibited major differences in their sedimentary structures and were not representative of the same depositional processes. Radiographic analysis could be applied to fine grained rocks, such as the Eagle Ford, to help distinguish homogeneous sections caused by bioturbation from apparent homogeneous sections that in reality contain microscopic sedimentary structures such as micro-cross-stratification or parallel micro-laminae (Hamblin, 1962).

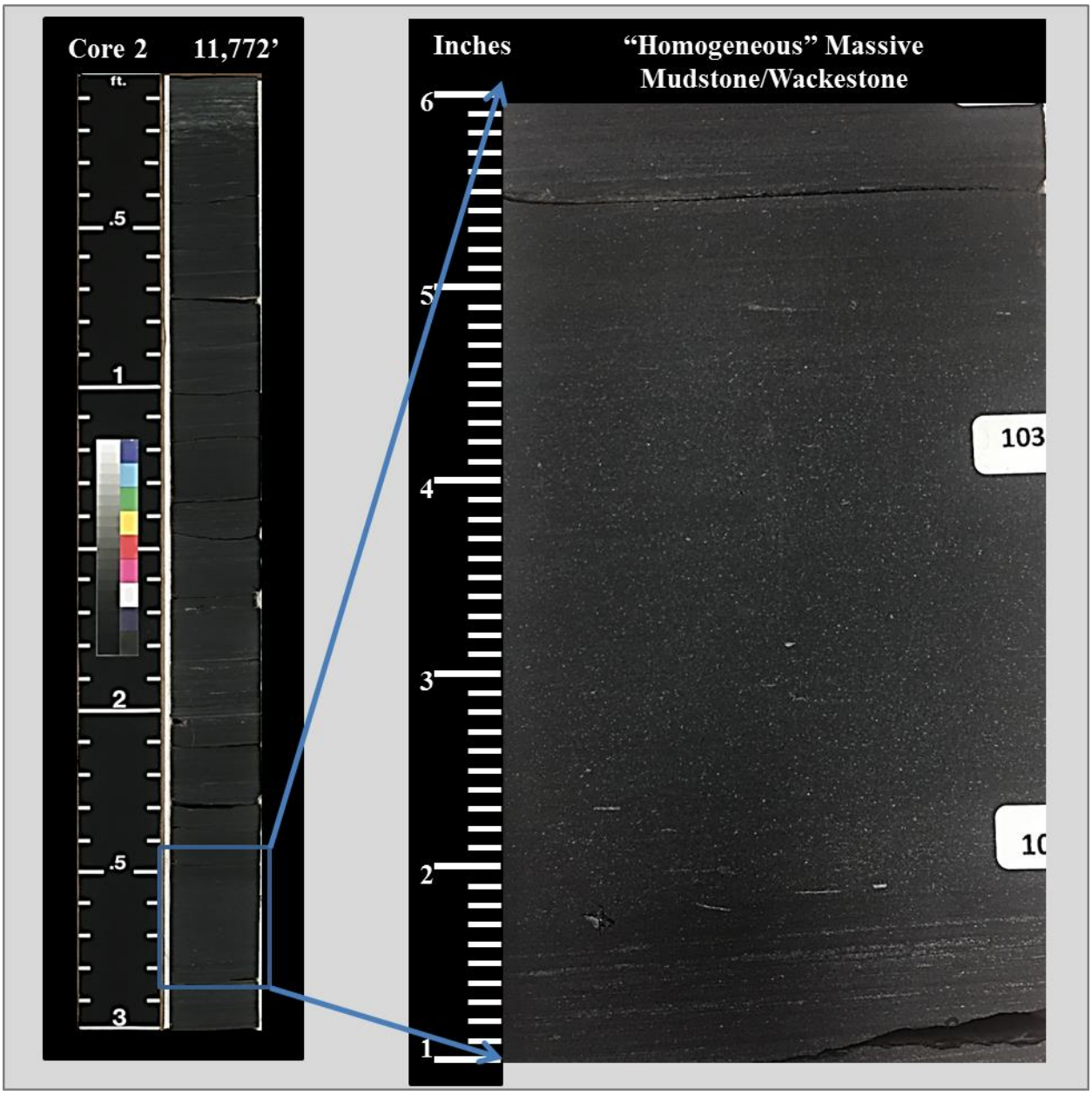

Figure 22: *"Homogeneous" Massive Mudstone/Wackestone* deposit in Core 2 near 11,774.5 feet. This likely represents the fine grained deposits of a low density gravity flow.

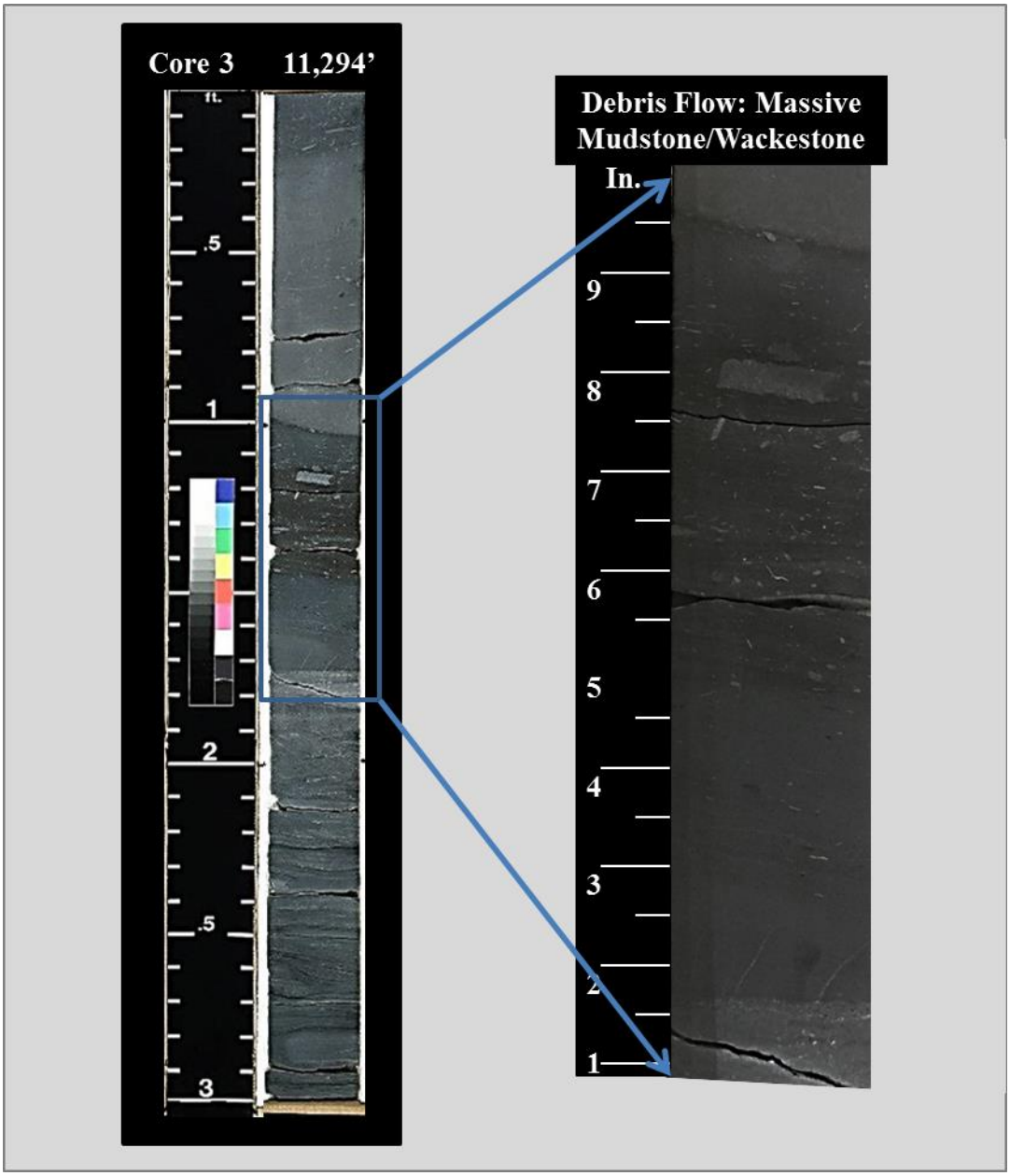

Figure 23: *"Heterogeneous" Massive Mudstone/Wackestone* deposit in Core 3 near 11,295.5 feet with inverse grading and large clasts indicating this is a deposit from a debris flow.

Massive Packstone/Grainstone: Turbidites and Diagenetic Recrystallization

The Massive Packstone/Grainstone sections represent deposits of waning turbidity currents that experienced varying degrees of diagenetic recrystallization. The sections that

contain little to no diagenetic recrystallization typically retain cryptic laminations some of which clearly show the typical Bouma horizons T_{a-e} associated with turbidites (Figure 24). When laminations were clearly visible, these sections were classified as Finely Laminated Wackestone/Packstone in an effort to distinguish between sections that experienced a high degree of diagenetic alternation that caused their original depositional texture to be lost (Figure 25), and those sections that retained their original depositional fabric. This distinction is drawn because of the otherwise high degree of similarity in thickness and overall macroscopic texture and color between the Finely Laminated Wackestone/Packstone and the Massive Packstone/Grainstone lithofacies.

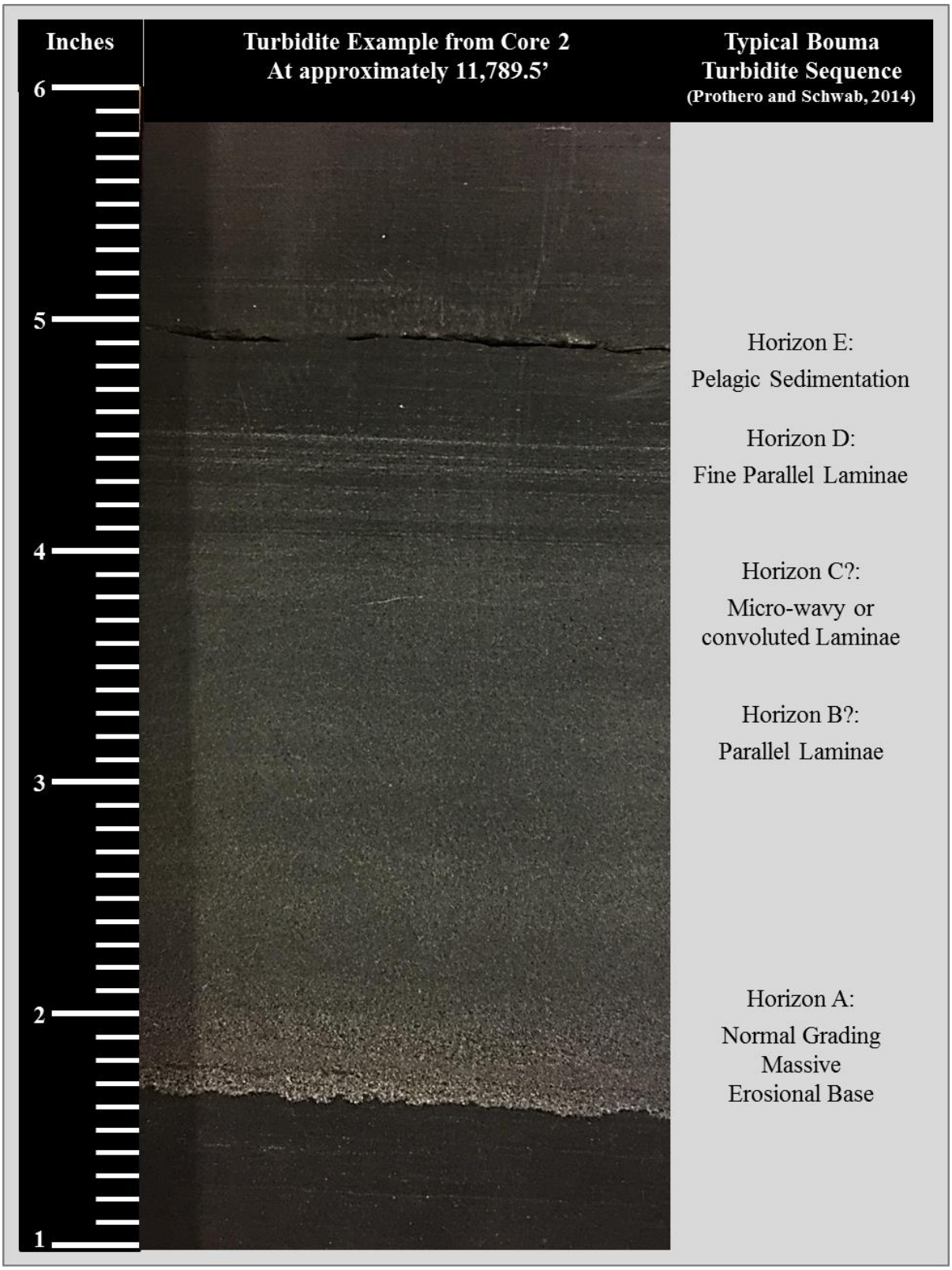

Figure 24: *Turbidite Deposit* found in Core 2 near 11,789.5 feet. The erosional base and massive structure with normal grading (horizon A), and the very fine parallel laminae toward the top of

this deposit (typically associated with horizon D) are clearly visible. In this case, the coarser lighter grained material is foraminifera with dispersed tiny dark colored bone fragments. Turbidite horizon sequence referenced from Prothero and Schwab, 2014.

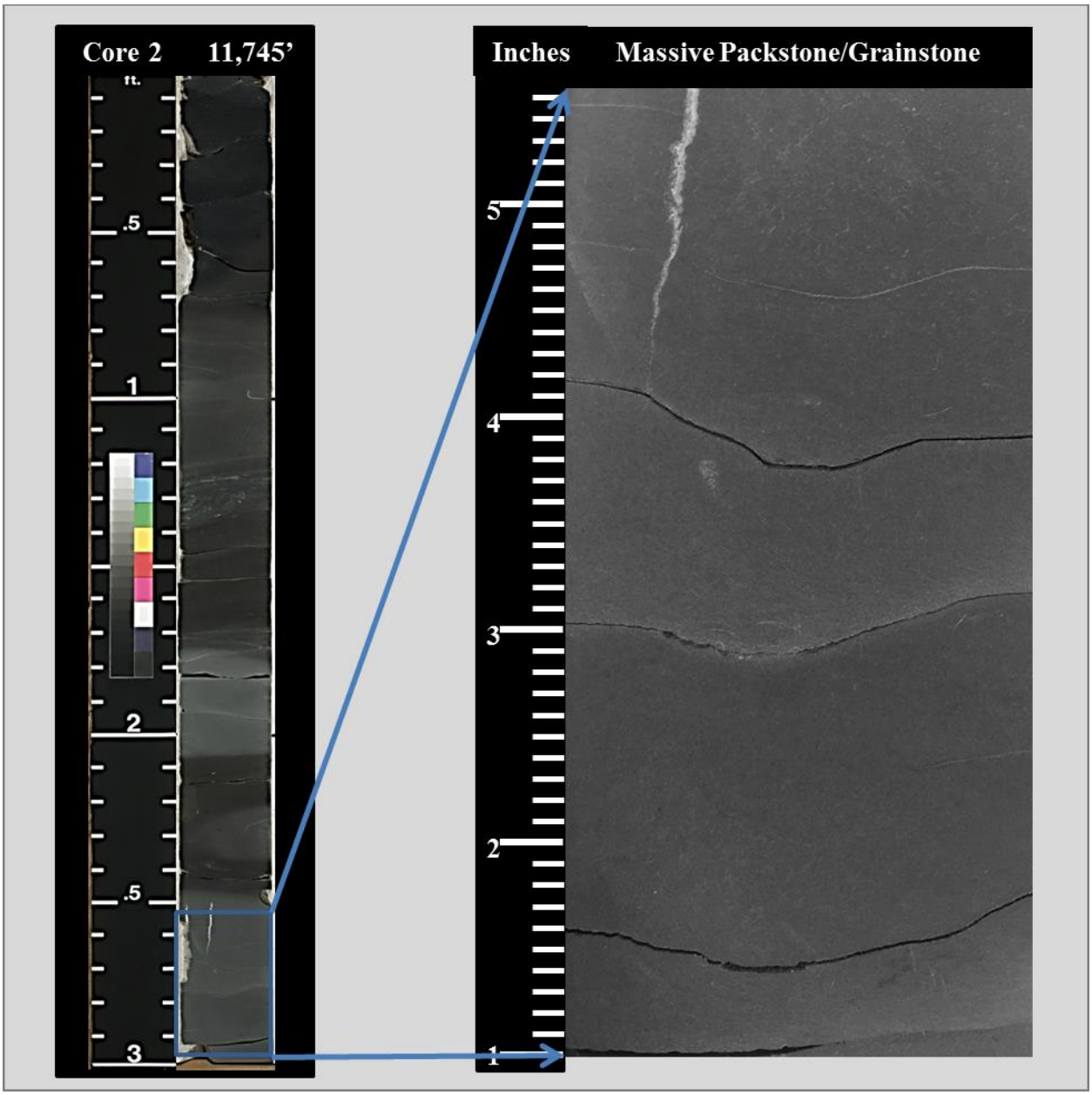

Figure 25: *Massive Packstone/Grainstone* lithofacies found in Core 2 near 11,747.5 feet. The high degree of recrystallization has caused much of the original depositional fabric to be lost.

Some of the sections classified as the Massive Packstone/Grainstone lithofacies appear to be the formation of concretions below the water-sediment interface, while the sediment was still

soft. This is indicated by convex-up-warped laminae tracing the top of these sections, and convex-down-warped laminae tracing along the bottom of these sections. However, lateral continuity of these apparent "concretions" could not be assessed due to the width of the cores, but were common in all four cores. It is unclear why these sections vary in their degree of diagenetic crystallization; however, concretionary formation and diagenetic calcite crystallization within black shales is not uncommon.

Carbonate concretionary growth requires supersaturation of carbonate that can be derived by methanogensis and methane oxidation related to microbial activity within near-surface anaerobic sediments (Raiswell, 1987; Raiswell and Fisher, 2000; Siegel et al., 1987; Irwin et al., 1977; Wignall, 1994). This conclusion is primarily based on carbon isotope analysis of carbonate concretions (Raiswell and Fisher, 2000; Irwin et al., 1977). Raiswell (1988) proposed that these concretions could form as shallow as 1 meter below the sediment-water interface. Carbonate concretions have been documented to occur in a variety of sizes, even reaching several meters in diameter (Lash and Blood, 2004). Locks and Ruppel (2007) documented carbonate concretions ranging in size from 1 inch to 1 foot occurring in the Mississippian Barnett Shale of the Fort Worth Basin. These microspar and pseudospar rich concretions are believed to have formed prior to significant compaction within the Barnett Shale due to the internal preservation of uncompacted bedding (Locks and Ruppel (2007). Additionally, Lash and Blood (2004) documented laterally persistent horizons of carbonate concretions up to 2.7 meters in diameter in the upper Devonian Rhinestreet black shale of western New York. Concretionary development in the Rhinestreet black shale is suggested to have been directly related to the upward diffusion of methane (CH_4) and dissolved carbonate from the zone of biogenic methanogensis into the zone of anaerobic methane oxidation located near the base of sulfate reduction while depositional and

subsidence rates were slow (Lash and Blood, 2004; Raiswell, 1988). This interaction allowed carbonate precipitation to occur near the base of the sulfate reduction zone (Raiswell, 1987; Lash and Blood, 2004). Furthermore, Lash and Blood (2004) concluded that the slower the sedimentation/subsidence rate, the longer the zone of sulfate reduction and anaerobic methane oxidation would remain at a set distance between the sediment-water interface and the zone of biogenic methanogensis, thereby allowing carbonate concretionary growth to occur along a stratigraphic horizon. Raiswell (1988) postulated that (partially) depending on the length of time that the methane oxidation zone remains constant, carbonate concretions could eventually merge into one-another forming a thin but laterally continuous diagenetic limestone interval. Lash and Blood (2004) also drew the conclusion that the initiation of each concretion was related to the existence of permeable pathways/fractures between the zone of biogenic methanogensis and the zone of sulfate reduction. This conclusion is in contrast to another proposed concretionary development hypothesis that the apparent random lateral distribution of concretions is tied to local concentrations of organic matter (Raiswell 1976; Coleman and Raiswell, 1993; Coleman and Raiswell, 1995). One of the major issues with Raiswell (1976) hypothesis of concretionary formation related to localized concentrations of organic matter is that visual/textural evidence of the proposed organic matter would be expected to be present; however in the case of the Rhinestreet black shale, no preserved organic textural evidence was present (Raiswell and Fisher, 2000; Lash and Blood, 2004).

A detailed carbon isotope analysis would need to be conducted on the limestone intervals of the upper Eagle Ford in order to better isolate their processes of formation. It is possible that these intervals represent a variety of formational processes including turbidity currents, rapid changes in sea level related to the Milankovitch cycles, rapid changes in water oxygenation

levels, and/or the interactions between the upward diffusion of methane and dissolved carbonate with the zone of sulfate reduction.

Geochemistry

Introduction

Chemical variations within shale laminae can provide insights into changes of the environment of deposition, and can possibly give indication of diagenetic processes that have occurred; however, to fully comprehend what chemical variations within strata indicate, an understanding is needed of the processes that may influence particular elements and how these elements interact with each other. Of particular importance, is identifying similar elements that behave alike in nearly all environments with notable exceptions. Comparing various elemental ratios can potentially provide further fine tuning of variations of environments and diagenetic history for any given sedimentary formation (Tribovillard et al., 2006). These ratios may also give insights into periods of non-deposition in marine environments with the hypothesis that the longer a surface is exposed to sea water rich in dissolved metals, the greater the ability (and time) for metals to precipitate and be incorporated into the marine sediments (Adams and Weaver, 1958) underlying oxygen depleted waters (Emerson and Huested, 1991). For example, if for a given sedimentary formation the thorium and uranium concentrations were found to be low, but relatively high concentrations of an element less easily oxidized that is also associated with organic matter is found, such as molybdenum (Mo) (Emerson and Huested, 1991), then this could indicate deposition with organic matter in an anoxic environment followed by some short duration oxidation event that was greater than or equal to the oxidation required for uranium, but less than the oxidation required for molybdenum.

A detailed analysis of the distribution of elements preserved within the upper Eagle Ford is beyond the scope of this study; however, a generalized analysis of particular trace and heavy metals preserved within the upper Eagle Ford will be briefly reviewed so that tentative conclusions can be drawn about the environment of deposition, levels or variations of water column anoxia, and total organic carbon preservation potential.

Thorium to Uranium Ratio

The element thorium is generally associated with detrital material whereas uranium is largely of authigenic origin within sedimentary successions (Luning and Kolonic, 2003). Therefore, taking the ratio of the thorium (Th) concentration to the uranium (U) concentration in sedimentary rocks can give an indication of the degree of oxygenation that the source material experienced during or after the time of deposition, and can therefore lead to a determination of whether the depositional environment was partially sourced by terrigenous material (Adams and Weaver, 1958). In regard to marine shale deposits, Adams and Weaver (1958) concluded that the lower the thorium to uranium ratio, the more distal the environment of deposition. Values less than 7 generally represent marine deposits and values greater than 7 generally represent oxidized continental material. Some authors have taken this relationship further to estimate the total organic content (TOC) that is potentially preserved within the strata (Wignall, 1994; Luning and Kolonic, 2003). The separation between thorium and uranium is primarily because of the difference in sensitivities of these elements to oxygenation, which causes differences in their mobility in aqueous systems (Klinkhammer and Palmer, 1991). This separation can be further enlarged by differences in materials that allow fixation of uranium and not thorium and vice versa (Adams and Weaver, 1958).

In addition, the morphology of the shelf is closely tied to the amount of uranium that may be preserved within organic matter (Wignall, 1994). The uranium concentration within sediments is directly related to the uranium concentration of the source material, the duration and intensity of bottom water anoxia, and the reducing ability of the sediments at the sediment-water interface, and it is indirectly related to the sedimentation rate (Wignall, 1994; Klinkhammer and Palmer, 1991). The increase in sedimentation rate causes a few changes. For one, even if a higher percentage of organic material were to be deposited from a higher sedimentation rate, the higher sedimentation rate could also be introducing a higher degree of mixing within the water column which could introduce oxygenated waters into once anoxic areas, and thereby remobilizing any uranium complexed within the sediments (Klinkhammer and Palmer, 1991). In fact, it only takes two to three minutes of exposure to the oxygenated water to cause the uranium to be remobilized, while leaving the organic material (Klinkhammer and Palmer, 1991). Secondly, the amount of uranium capable of being complexed within organic rich sediment is directly related to the amount of time that sediment is at the sediment-water interface (Komlos et al., 2008). Increasing the sedimentation rate (even with a higher percentage of organic material) will decrease the ability of the sediments to immobilize and complex with uranium (Wignall, 1994; Klinkhammer and Palmer, 1991; Komlos et al., 2008). Therefore, there is a high likelihood of having organic rich deposits preserved within the stratigraphic record that are relatively lean in their uranium concentration, or contain no apparent pattern to the uranium enrichment. Considering how easily the continental shelf is influenced by the variations of sea level, a predictable pattern of preservation of uranium within organic material is even less likely within these relatively shallow deposits. The areas of the shelf that have the highest potential to preserve the initial uranium concentration would be low lying mini-basins within the shelf's morphology

that would hinder circulation of oxygenated waters and have a tendency to develop stratified water columns. As stated in Wignall's *Black Shale*, Hallam and Bradshaw (1979) postulated the same relationship and recognized "…the importance of an irregular bottom water topography in the preservation of black (organic-rich) shales" (1994). They developed a conceptual basin morphology model showing that these mini-basins would have a tendency to trap fine-grained sediment and stagnant water allowing the conservation of organic material. Wignall (1994) redrew Hallam and Bradshaw's Irregular Bottom-Water Topography Model (page 97 in his book *Black Shales)* and termed it the Puddle Model in order to emphasize the importance of small depressions in stagnating water and collecting organic material. A modified version of Wignall's (1994) drawing is included below (Figure 26).

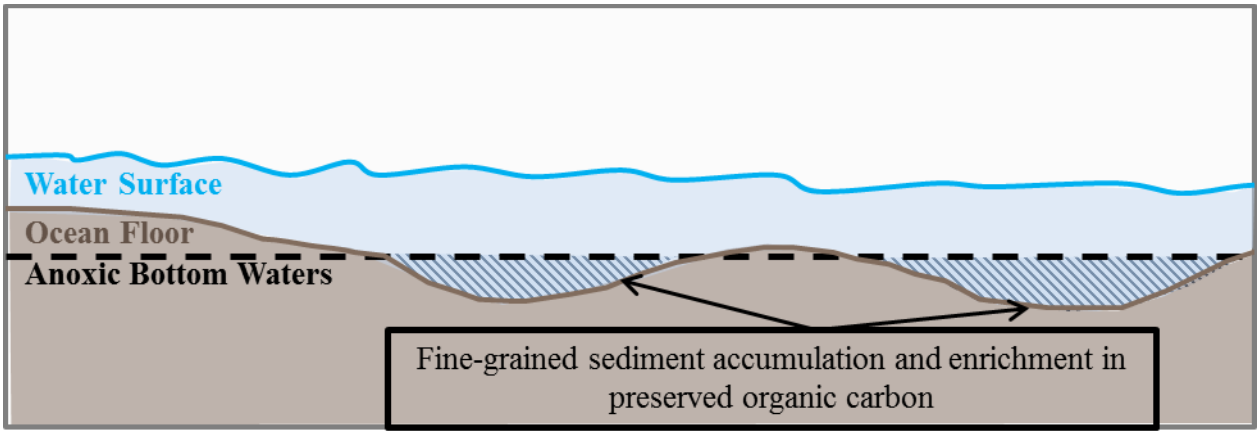

Figure 26: *Modified Wignall's Puddle Model*: Diagram depicting how shelf morphology can influence the preservation of organic-rich sediments (Modified from Wignall, 1994).

This model attempts to illustrate that marine shale intervals likely exhibit a heterogeneous character in relation to their organic richness and elemental distributions. Because these depressions would hypothetically hinder water circulation they would promote anoxic waters (Hallam and Bradshaw, 1979), and allow smaller grain sizes to settle out of the water column. These finer grains would include organic material that would ultimately cause these depressions

to contain a higher percentage of organic material and/or enrichments in certain redox sensitive elements (Huc, 1988). Because uranium reduction and immobilization is directly related to the reducing ability of the sediments and the degree of anoxia of the water (Klinkhammer and Palmer, 1991), these depressions would have a greater ability to reduce uranium ions. Consequently, the "Puddle Model" implies a heterogeneous initial distribution of uranium enriched deposits that coincide with these mini-basins. That being said, a drop in sea level or a strong storm event would likely cause these small depressions to be influenced by oxygenated waters at some point in time. If this caused a two-three minute flush of oxygenated waters the once immobilized uranium would be remobilized and moved elsewhere in the system (Klinkhammer and Palmer, 1991).

Of course, the variables discussed above are not the only factors that influence the relative abundances of uranium and thorium preserved in sedimentary rocks. Diagenetic processes also strongly influence the preserved abundance of these elements (Komlos et al., 2008). Herein is the most obvious problem of only using the ratio of uranium to thorium to determine depositional environments. Uranium has been shown to be oxidized and remobilized very quickly from short duration oxidation events in aquatic environments (Komlos et al.., 2008); therefore, a present day low uranium concentration does not indicate for certain that (1) organic matter is absent, or (2) that the uranium concentration at the time of deposition was not significantly higher. One method to reduce the uncertainty in characterizing the environment of deposition and the quantity of TOC present solely based on the thorium to uranium ratio is to compare it with ratios of other heavy metals or trace metals.

Thorium to Uranium Ratio Method

All thorium and uranium data were filtered to only include values above 0 and less than 25. This range was selected base on conclusions drawn by Adams and Weaver (1958) that thorium to uranium ratios can range from less than 0.02 to more than 21. The thorium to uranium ratio was calculated in excel by dividing the thorium measurements (in ppm) by the uranium measurements (in ppm). Statistics (mean, median, maximum, minimum, and standard deviation) were only calculated over the upper Eagle Ford interval as defined within each core description. Depth verses the thorium to uranium ratios were graphed to visually display the data.

Thorium to Uranium Ratio Results

It is remarkable how similar the four cores are when comparing the thorium to uranium ratio graphs and statistics of the upper Eagle Ford (Figures 27-30). This is not surprising given their close proximity. The upper Eagle Ford in all four cores contains an average thorium to uranium ratio of far less than 7 indicating that the source material is primarily marine and enriched in uranium relative to thorium (Adams and Weaver, 1958). Core 3 could be thought of as being located within a “mini” basin (Karnes Trough), and therefore, relative to Cores 1, 2, and 4, should theoretically contain the highest chance of preservation of organic material and enrichment of uranium relative to thorium; however, this does not appear to be the case. Although Core 3 may still contain a higher abundance of preserved organics, it does not appear to be more enriched in uranium relative to the other cores. This discrepancy could indicate that the upper Eagle Ford within Karnes Trough was prone to the influence of a higher frequency of periodic gravity flow events that caused short lived oxidative flushes of water that enabled the leaching of any adsorbed uranium. Unfortunately, the Thorium to Uranium ratio relationship as

described by Adams and Weaver (1958) does not seem to provide any other insights in a core to core comparison for this study.

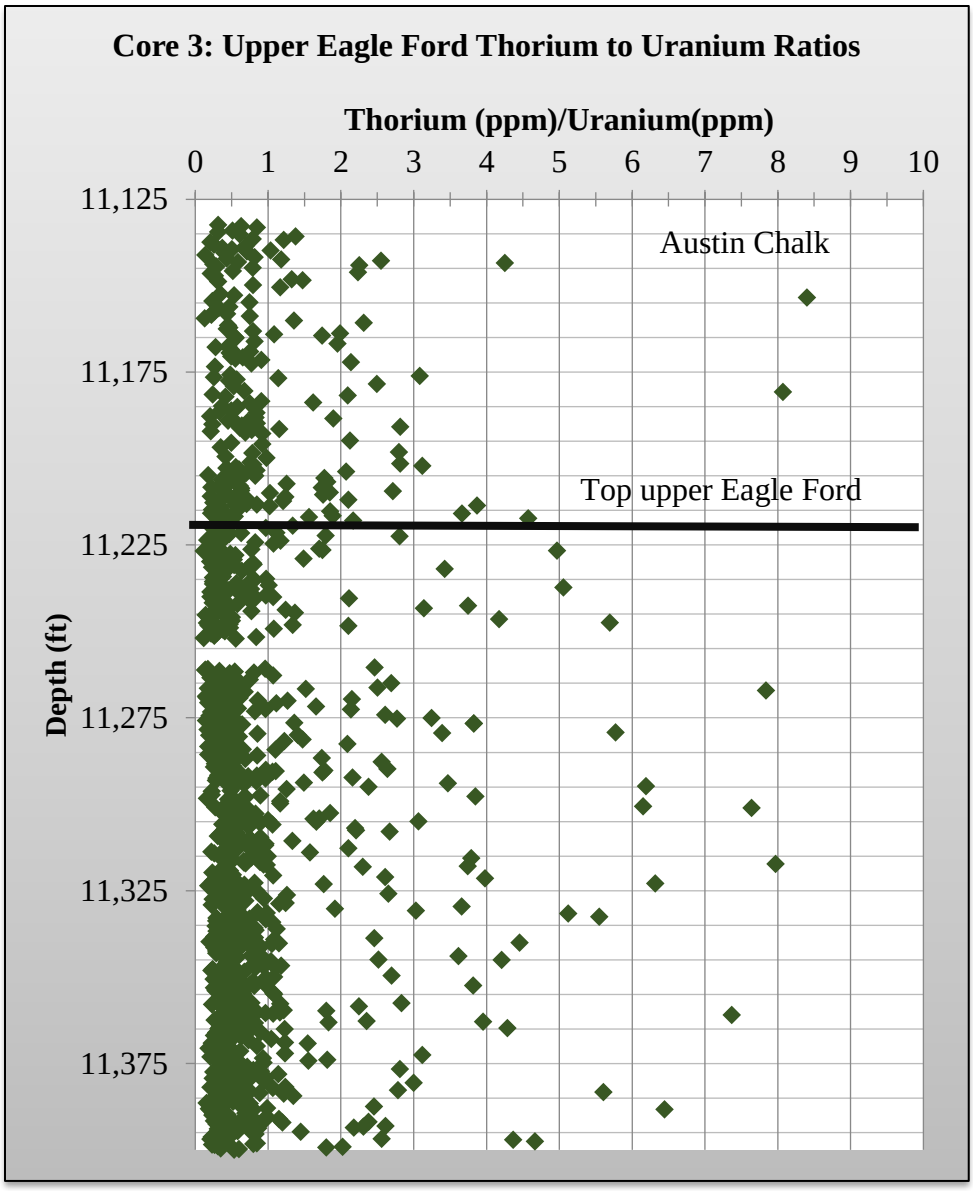

Core 3 upper Eagle Ford Th/U Statistic	Value
Mean	**0.95**
Geometric Mean	**0.6**
Median	**0.52**
Max	**15.72**
Min	**0.12**
Number of Data Points	**821**
Standard Deviation	**1.76**

***Figure 27**: Core 3 XRF Thorium to Uranium Ratio graph and table*

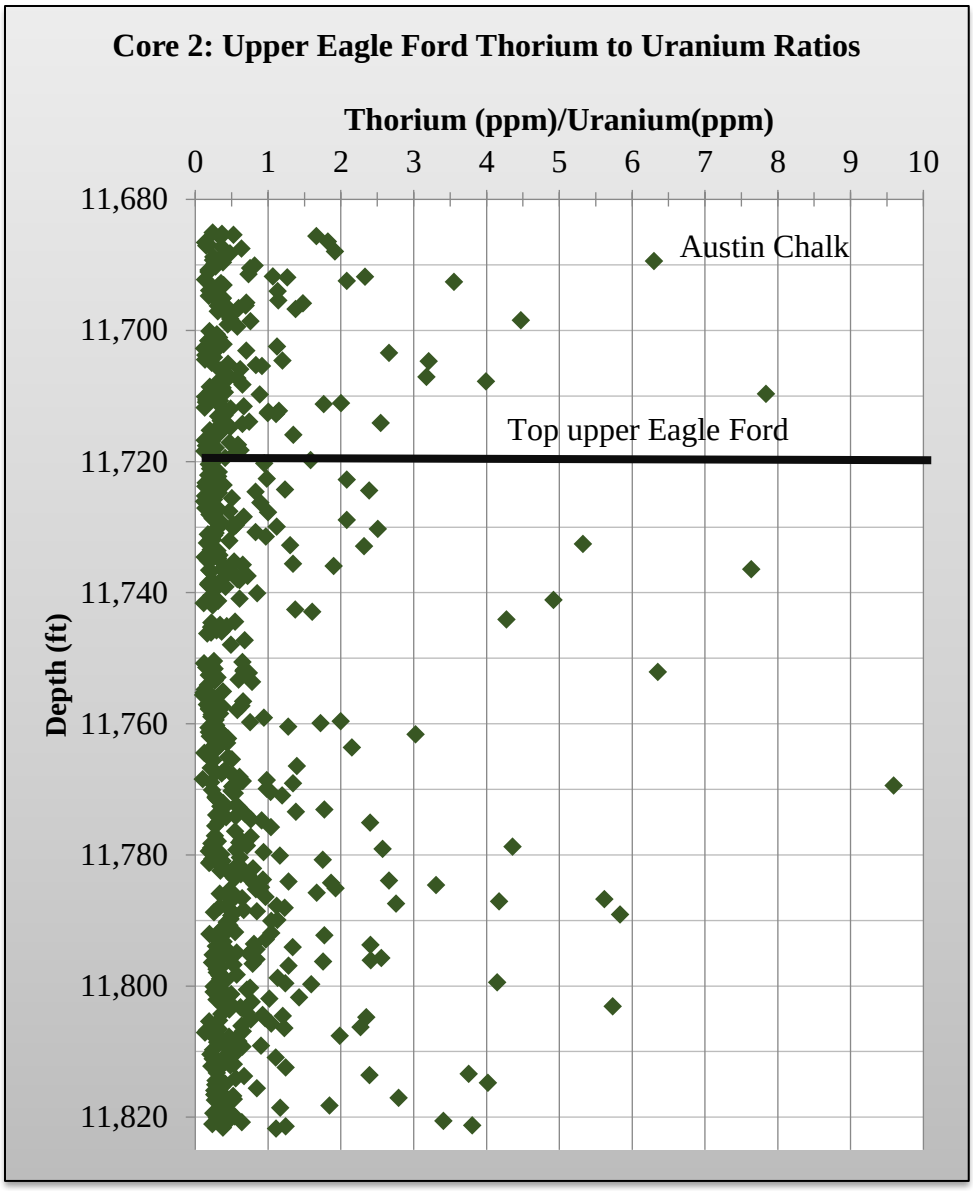

Core 2 Upper Eagle Ford Th/U Statistic	Value
Mean	**0.87**
Geometric Mean	**0.51**
Median	**0.44**
Max	**20.20**
Min	**0.11**
Number of Data Points	**451**
Standard Deviation	**1.64**

***Figure 28**: Core 2 XRF Thorium to Uranium Ratio graph and table*

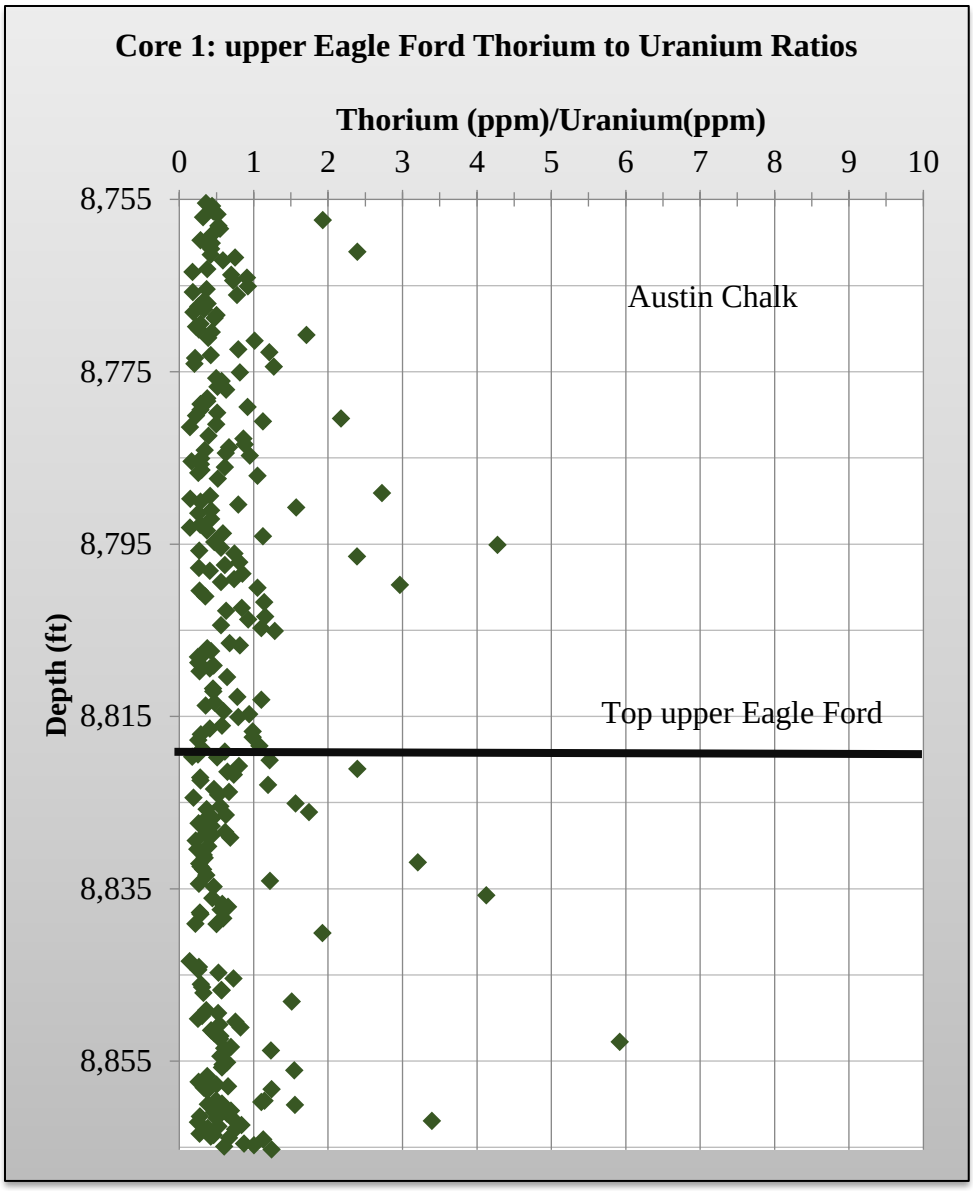

Core 1 upper Eagle Ford Th/U Statistic	Value
Mean	**0.71**
Geometric Mean	**0.55**
Median	**0.52**
Max	**5.92**
Min	**0.14**
Number of Data Points	**127**
Standard Deviation	**1.6**

***Figure 29**: Core 1 XRF Thorium to Uranium Ratio graph and table*

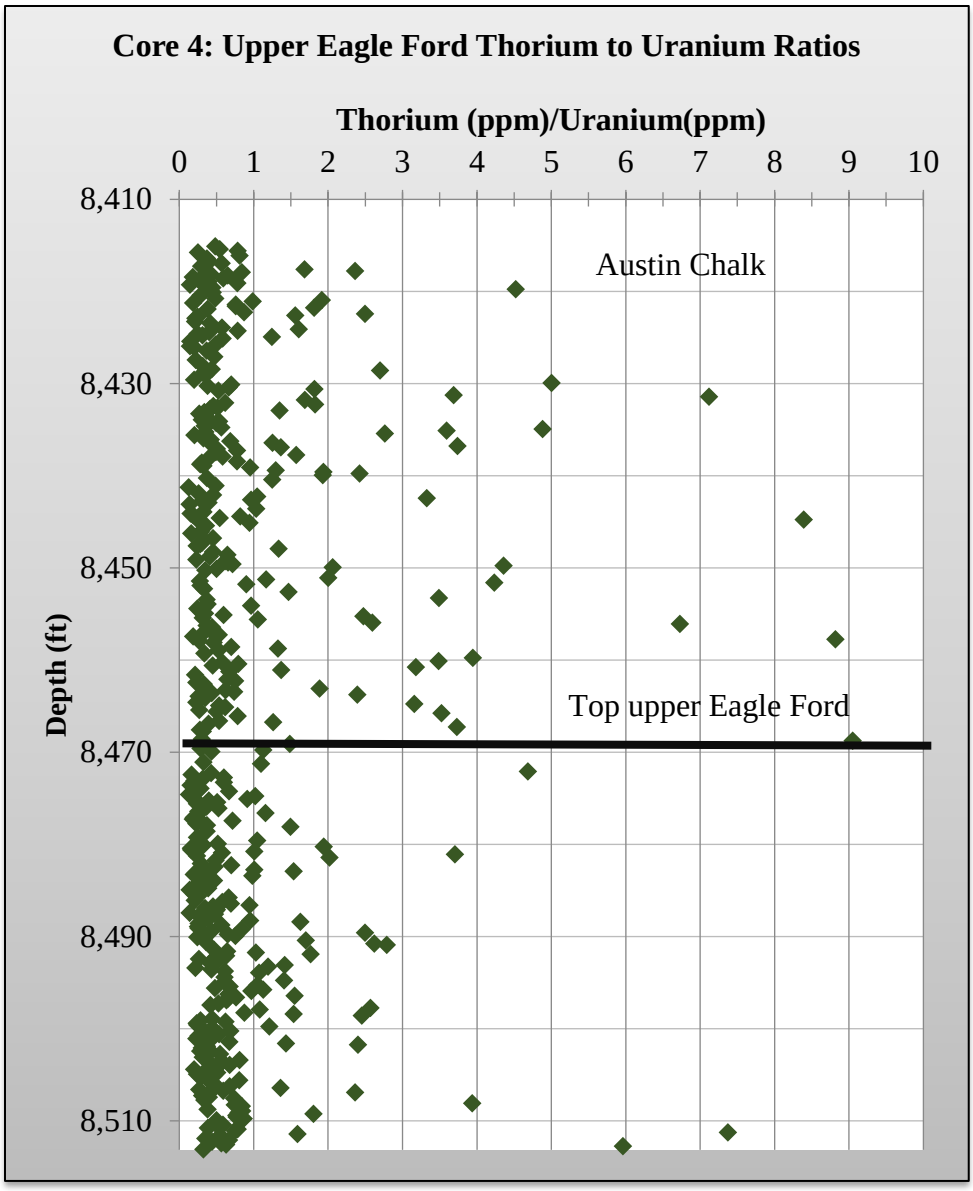

Core 4 Upper Eagle Ford Th/U Statistic	Value
Mean	**0.9**
Geometric Mean	**0.56**
Median	**0.5**
Max	**17.71**
Min	**0.13**
Number of Data Points	**218**
Standard Deviation	**2.96**

***Figure 30**: Core 4 XRF Thorium to Uranium Ratio graph and table*

Nickel and Copper Enrichments as Organic Matter Flux Indicators

Because of the affinity of nickel and copper to adsorb onto organic molecules within the water column, they can cautiously be used as proxies to the relative amounts of organic matter flux experienced at the time of deposition (Tribovillard et al., 2006). The logic behind this conclusion is that the dominant delivery method to the sediment-water interface of nickel and copper is through the adsorption onto organic particles within the water column (Tribovillard et al., 2006). In other words, without organics within the water column, it is hypothesized that sediments cannot become enriched in nickel or copper. However, sulfate-reducing conditions must be present at the time of deposition in order for this enrichment to be preserved (Tribovillard et al., 2006). Nevertheless, Tribovillard et al. (2006) states that because iron-sulfide minerals can retain nickel and copper once they have become fixated, enrichments in nickel and copper do not necessarily indicate that the organic matter originally present was not later degraded or removed.

Nickel and Copper Analysis Results

Comparing plots of the nickel and copper abundances in the upper Eagle Ford in Cores 1 and 4, reveals that the lowermost and uppermost portion of the upper Eagle Ford may have experienced a higher influx of organic material while experiencing at minimum sulfate reducing conditions relative to the middle portion (Figures 31-32). This is more clearly evident in Core 1 than in Core 4. Cores 2 and 3 appear to have three of these higher organic particle “pulses”: one at the base of the upper Eagle Ford, one near the middle, and a smaller pulse at the top (Figures 33-34). Again, this does not mean that organic matter has been preserved in those intervals, but that those internals may have experienced a higher rate of organic material sedimentation under sulfate reducing conditions.

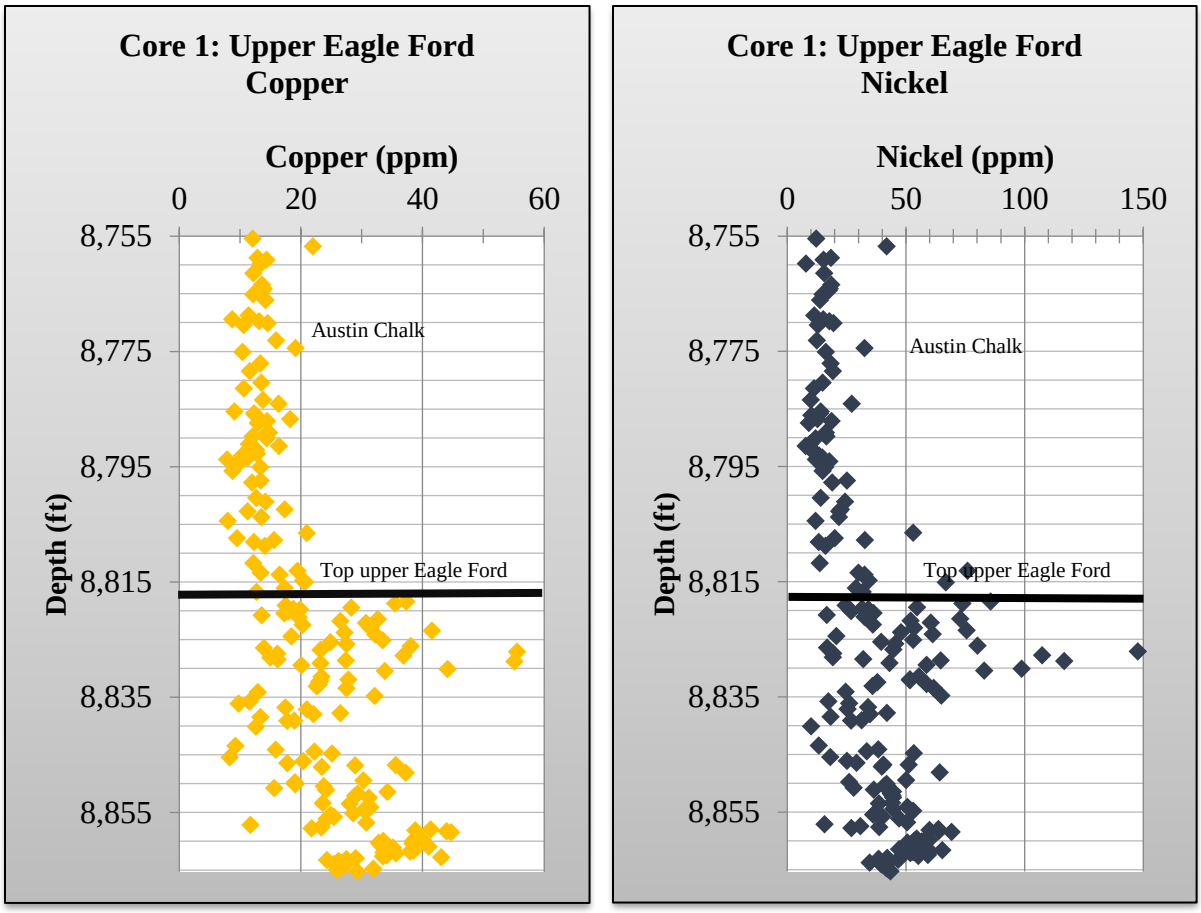

Figure 31: *Core 1 XRF Copper and Nickel Graphs:* Upper Eagle Ford top as identified in the core 1 description indicated by a bold black line. Within the upper Eagle Ford there are two sections that are more enriched in copper and nickel. These are located at the base of the upper Eagle Ford and at the top, with the top interval containing slightly higher values relative to the base.

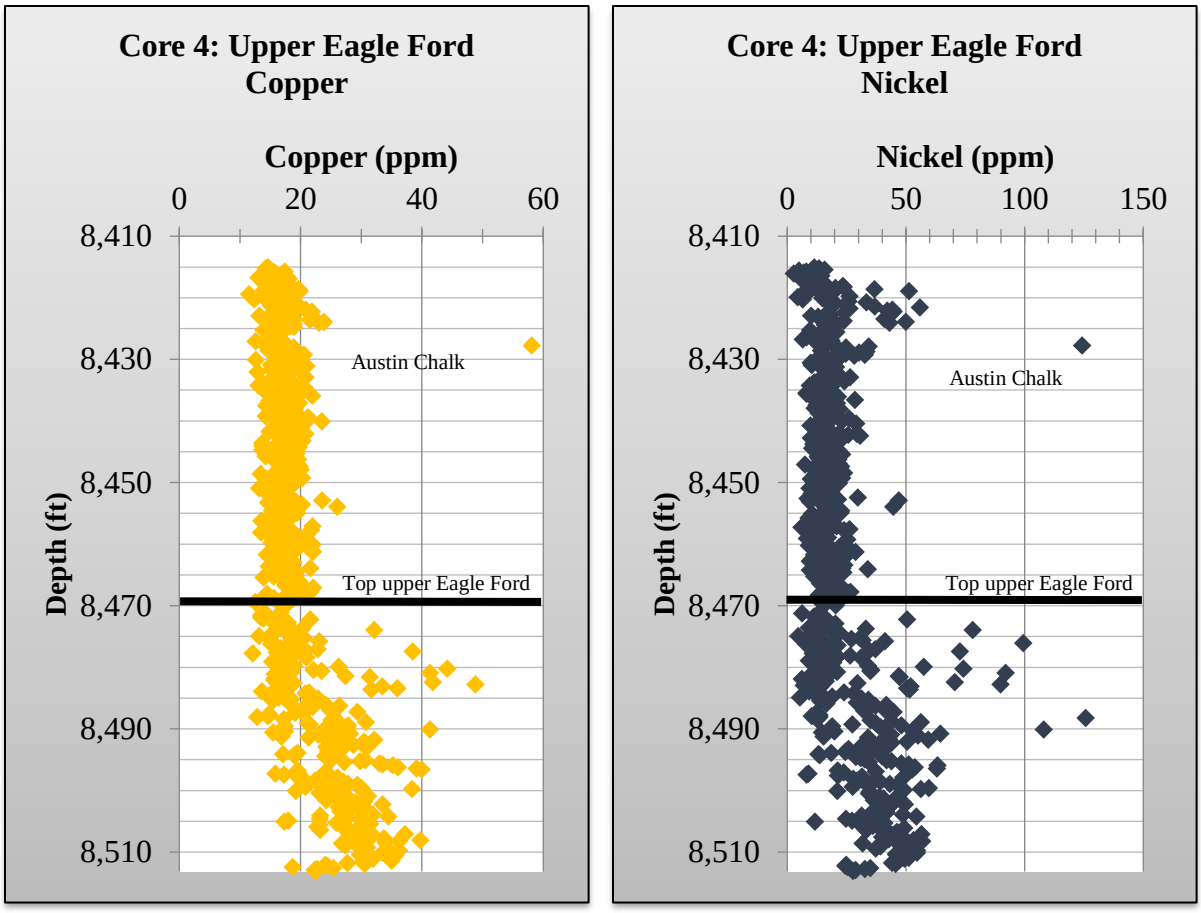

Figure 32: *Core 4 XRF Copper and Nickel Graphs:* Upper Eagle Ford top as identified in the core 4 description indicated by a bold black line. Within the upper Eagle Ford there appear to be two sections that are more enriched in copper and nickel; however the middle section that separates these two enrichments appear to be condensed relative to what is seen in Core 1. These two slight enrichments are located near the base of the upper Eagle Ford and near the top of the upper Eagle Ford.

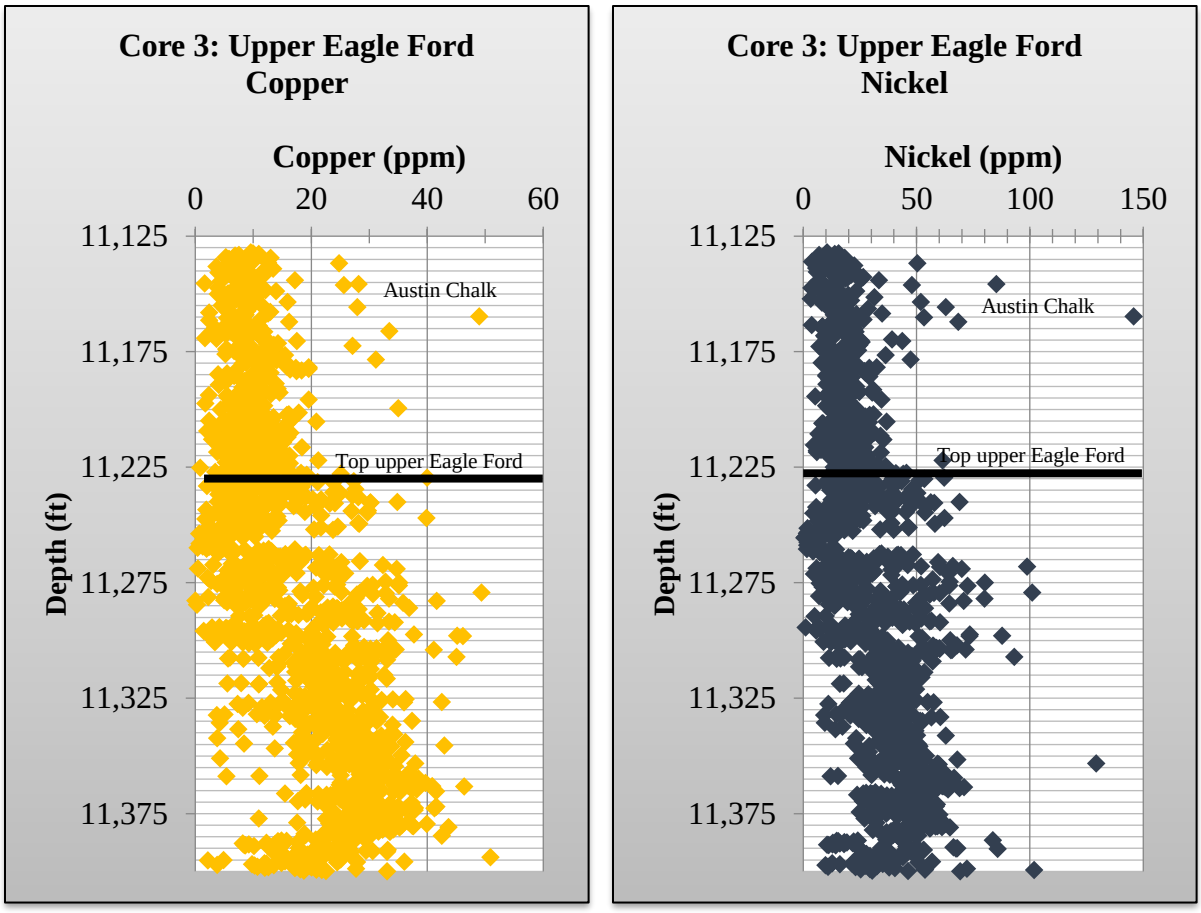

Figure 33: *Core 3 XRF Copper and Nickel Graphs:* Upper Eagle Ford top as identified in the core 3 description indicated by a bold black line. Within the upper Eagle Ford in this core there three sections that are slightly more enriched in copper and nickel. These are located at the base of the upper Eagle Ford, near the middle of the upper Eagle Ford, and at the top of the upper Eagle Ford. The middle and base sections nearly merge into each other. There is an overall upward decrease in the copper and nickel enrichment.

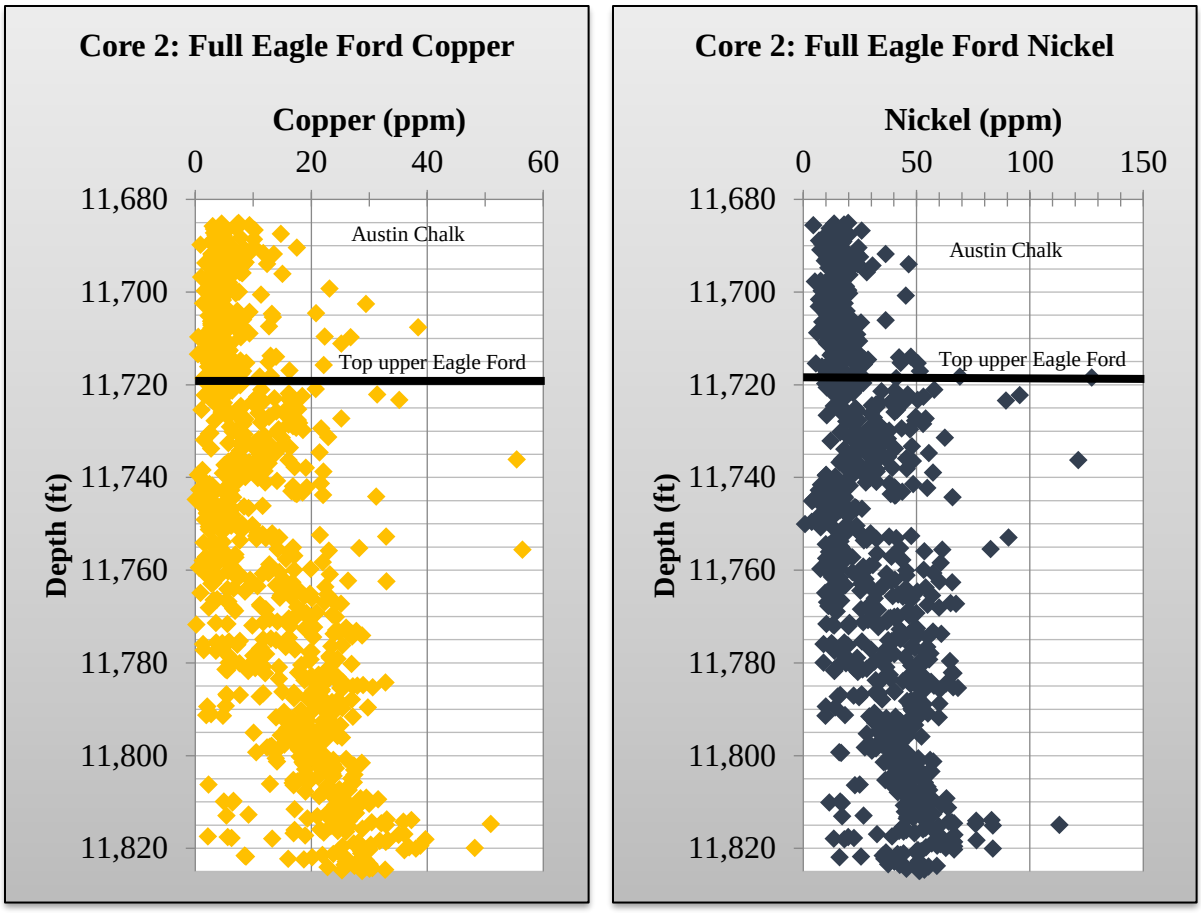

Figure 34: *Core 2 XRF Copper and Nickel Graphs:* Upper Eagle Ford top as identified in the core 2 description indicated by a bold black line. Within the upper Eagle Ford in this core there are three sections that are slightly more enriched in copper and nickel. These are located at the base of the upper Eagle Ford, near the middle of the upper Eagle Ford, and at the top of the upper Eagle Ford, with the base interval containing slightly higher values relative to the other two "pulses."

Molybdenum, Vanadium, and Uranium Enrichments as Paleoredox Conditions

Enrichments of molybdenum, vanadium, and uranium combined can indicate an anoxic environment at the time of deposition (Tribovillard et al., 2006; Emerson and Huested, 1991). Trace elements respond differently to different redox levels with some preferentially accumulating in suboxic environments, others accumulating in anoxic environments, and still others preferentially accumulating in euxinic environments (hydrogen sulfide-rich anoxic

conditions) (Tribovillard et al., 2006). For example, molybdenum enrichments are associated with euxinic organic rich environments (Helz et al., 2011; Tribovillard et al., 2004). Vanadium and uranium enrichments can occur in association with suboxic conditions, and do not necessarily require hydrogen sulfide-rich conditions as molybdenum does (Tribovillard et al., 2006). Furthermore, molybdenum enrichments are believed to be resistant to removal by short lived oxygenated flushes of water or other diagenetic processes whereas uranium is easily removed, and vanadium is less resistant to removal than molybdenum but more resistant to removal than uranium (Tribovillard et al., 2004; Klinkhammer and Palmer, 1991; Tribovillard et al., 2006). Therefore, comparison of the relative enrichments of these elements can provide clues into the oxic, suboxic, vs. euxinic conditions experienced within the depostional environment. For example, an enrichment of molybdenum and vanadium without much enrichment of uranium could indicate that euxinic conditions were present at the time of depostion, but subsequent reoxidation processes remobilized uranium near the sediment-water interface (Tribovillard, 2006; Kilnkhammer and Palmer, 1991). Furthermore, an enrichment in vanadium and uranium with little to no enrichment in molybdenum could indicate that suboxic to anoxic conditions were present during depostion, but euxinic conditions were not met (Tribovillard et al., 2006).

Molybdenum, Vanadium, and Uranium Analysis Results

Comparing the uranium, vanadium, and molybdenum abundances of the upper Eagle Ford found within the study area reveals that the molybdenum values range from slightly less than 10 ppm up to near 70 ppm with less scatter occurring in the lowermost upper Eagle Ford. The uranium values are highly scattered, but range from near 0 up to near 30 ppm, and the vanadium values range from near 5 ppm to 200 ppm (Figures 35-38). The vertically changing concentrations of these elements within the upper Eagle Ford in all four cores indicates that

changing levels of water oxygenation were experienced, which could be a reflection of changes in relative sea level.

In the lowermost portion of the upper Eagle Ford in Core 1 (Figure 35), vanadium and uranium concentrations appear to both be slightly enriched with only a minor enrichment of molybdenum. This could suggest that the lowermost upper Eagle Ford experienced an anoxic to slightly euxinic environment. This section is also correlative to slightly higher nickel and copper concentrations (presented in the previous section) indicating that there was also a higher influx of organic material during that time. The middle section of the upper Eagle Ford near 8,840' in Core 1 contains a slight enrichment of vanadium with lower concentrations of uranium and molybdenum (as well as nickel and copper). This could indicate that this section experienced a slightly more oxidative environment under low sulfuric conditions in comparison to the lowermost section (Tribovillard, 2006). Conversely, it could also be a reflection of lower organic sedimentation. The highest molybdenum enrichment within this core is located near 8,825', but with a high degree of scatter. This indicates that this section may have experienced the most euxinic conditions, or at least experienced variable hydrogen-sulfide fluxes at the time of deposition that allowed the fixation of molybdenum. Interestingly, this is correlative to the highest concentrations of nickel and copper as presented in the previous section suggesting that some of the highest influxes of organic material occurred within this section.

Overall, there appears to be little correlation between changes in the uranium concentration and changes in the vanadium concentration. This is interpreted to mean that there were diagenetic processes occurring that influenced the preserved concentrations of uranium (more so than vanadium). In other words, the present day concentrations of uranium are not an

accurate reflection of redox conditions at the time of deposition. This is true for all of the cores in this study.

The total organic carbon (TOC) percentage graph reveals that the highest TOC content (~3.75%) occurs in the lowermost upper Eagle Ford. This is correlative to the “less scattered” higher molybdenum concentration within this core as well as the higher vanadium and uranium concentrations. This section is also correlative to the Finely to Coarsely Laminated Wackestone/Packstone lithofacies within the core description, and is the lithofacies most similar to that seen within the lower Eagle Ford.

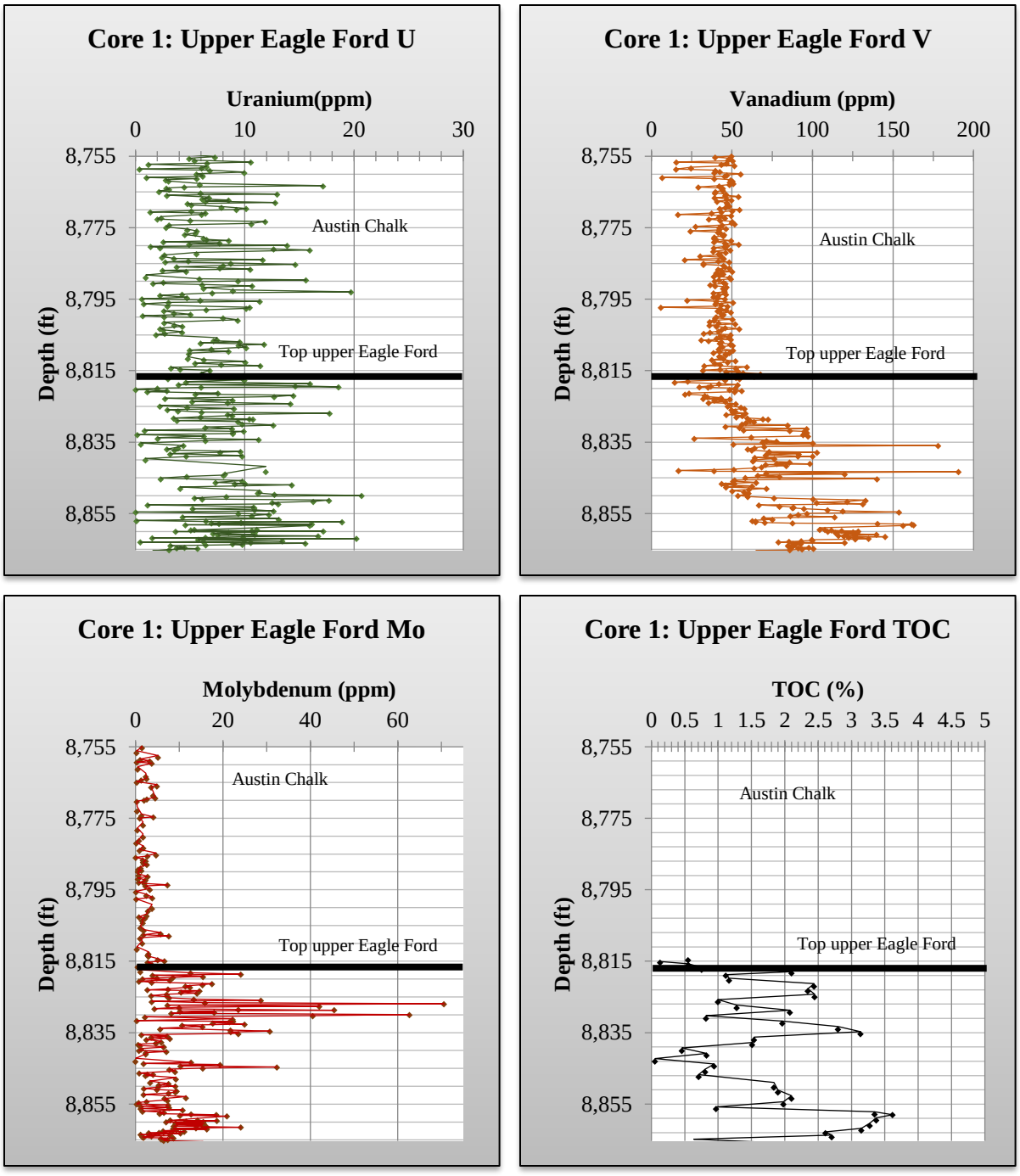

Figure 35: *Core 1 XRF Uranium, Vanadium, Molybdenum, and TOC Graphs* with a two period running average trendline. Upper Eagle Ford top as identified in the core 1 description indicated by a bold black line. Within the upper Eagle Ford the section that contains the highest vanadium enrichment is the lowermost portion of the upper Eagle Ford. The highest enrichments of molybdenum occur in the uppermost section of the upper Eagle Ford; however the lowermost portion of molybdenum contains less scatter at higher values. The highest enrichments of uranium and TOC occur in the lowermost and uppermost portion of the upper Eagle Ford.

Core 4 shows a similar enrichment pattern as Core 1 (Figure 36). The exception between the similarities is found within the lowermost portion of the upper Eagle Ford. Core 4 contains lower concentrations of vanadium, uranium, and molybdenum in this lower section than Core 1. The lowermost section within Core 4 does contain slightly higher concentrations of nickel and copper. These data indicates that the lowermost portion of the upper Eagle Ford in the most westward proximal locations experienced a slightly higher organic matter influx, but under higher oxygenation levels. The middle portion of the upper Eagle Ford in Core 4 near 8,490' contains slightly higher concentrations of vanadium and molybdenum with upward decreasing uranium concentrations. This is suggestive of slightly more euxinic conditions at the time of deposition that experienced periodic oxidative events that led to the leaching and redistribution of uranium.

The TOC percentage reveals that Core 4's highest TOC content at approximately 3.0% occurs in the uppermost section and the lowermost section of the upper Eagle Ford; however, the lowermost section contains consistently higher percentages of TOC relative to the uppermost portion with an overall upward trend in decreasing TOC values. The higher TOC percentages seem to be better correlative to average increases in the uranium concentrations than either molybdenum or vanadium. The lowermost section of the upper Eagle Ford is correlative to the Finely to Coarsely Laminated Wackestone/Packstone lithofacies and to the lower end members of the Wavy Laminated Wackestone/Packstone lithofacies.

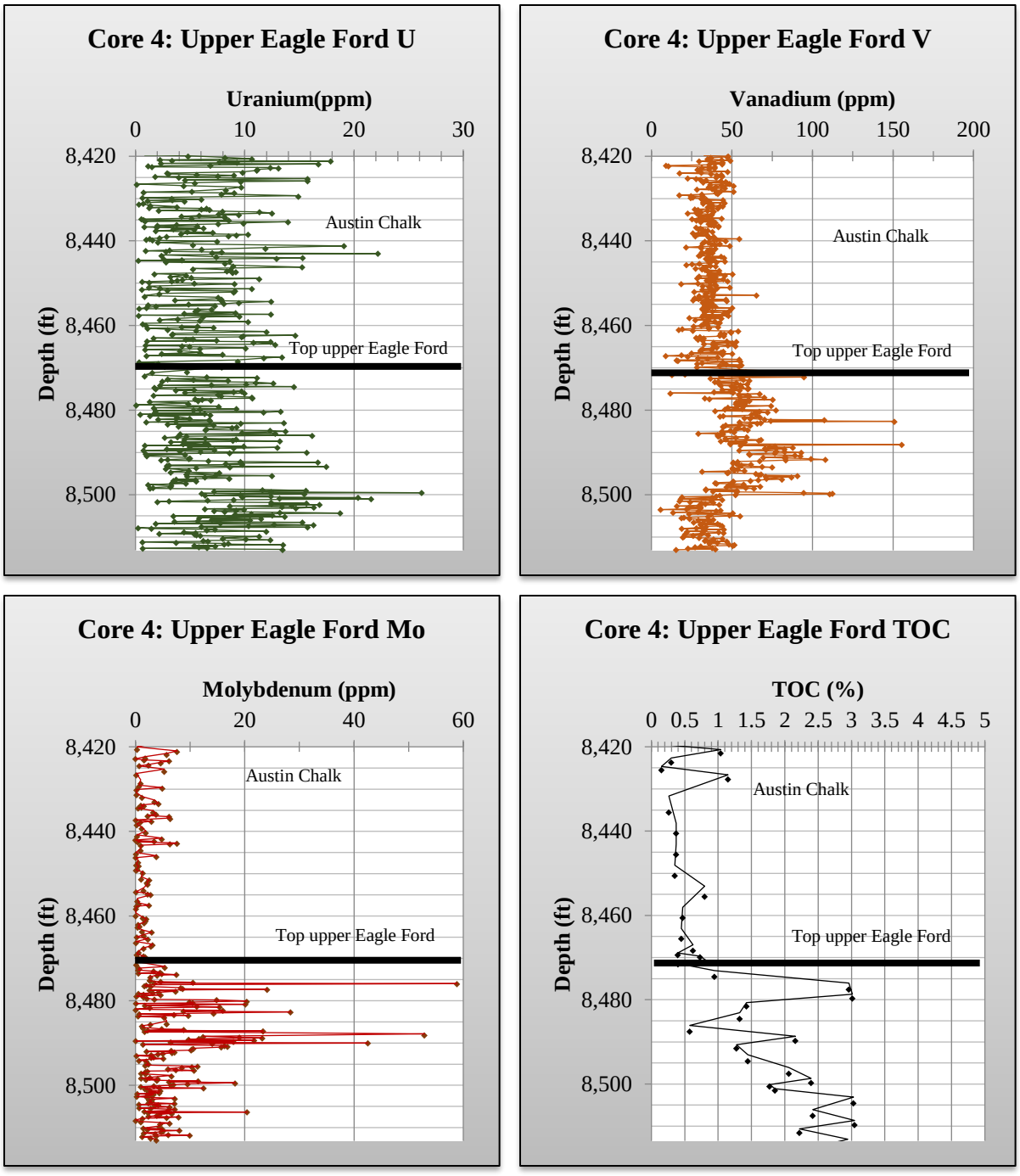

Figure 36: *Core2 XRF Uranium, Vanadium, Molybdenum, and TOC Graphs* with a two period running average trendline. Upper Eagle Ford top as identified in the core 2 description indicated by a bold black line. Within the upper Eagle Ford in this core the section that contains the highest vanadium enrichment is located within the central portion of the upper Eagle Ford. The highest enrichments of molybdenum occur in the uppermost section of the upper Eagle Ford. The highest and most consistent enrichments of uranium and TOC occur within the lowermost portion of the upper Eagle Ford.

Core 3 contains highly scattered uranium concentrations that show an overall upward decrease (Figure 37). This is indicative of an environment that experience several flushes of oxidative events in an overall upward shallowing sequence. There are three enrichment "pulses" of vanadium located near 11,375', 11,315', and 11,265'. Molybdenum enrichments occur within two primary "pulses" located near 11,375' and 11,265'. The combination of both molybdenum and vanadium enrichments occurring near 11,375' and 11,265 suggest that those two intervals experienced anoxic to near euxinic conditions. The middle section of the upper Eagle Ford experienced vanadium enrichment, but not as much molybdenum enrichment suggesting that conditions may be better described as suboxic to anoxic vs. euxinic within the middle Eagle Ford located in Karnes Trough. Similar to what is seen in the vanadium graph, the highest nickel and copper concentrations occur in three pulses located near the bottom, middle, and upper portions of the upper Eagle Ford. This suggests that enrichments in vanadium may be tied to higher organic input near these intervals; however this does not mean that the original organic content was preserved.

The TOC percentage reveals that Core 3's highest TOC content at approximately 4.5% occurs in the lowermost section of the upper Eagle Ford. There is an overall upward trend in decreasing TOC values. This lowermost section within Core 3 that contains higher TOC percentages, and slightly higher vanadium, uranium, and molybdenum concentrations is correlative to the Finely to Coarsely Laminated Wackestone/Packstone lithofacies. The relationship between increases in copper and nickel concentrations and increases in the TOC content is not as clearly apparent in Core 3 as it is in the most proximal cores. This is in part caused by the differences in the number of data points graphed between the TOC values and the

nickel and copper values. Filtering the copper and nickel data to only include those points that contain a TOC value reveals that a positive correlation still exits.

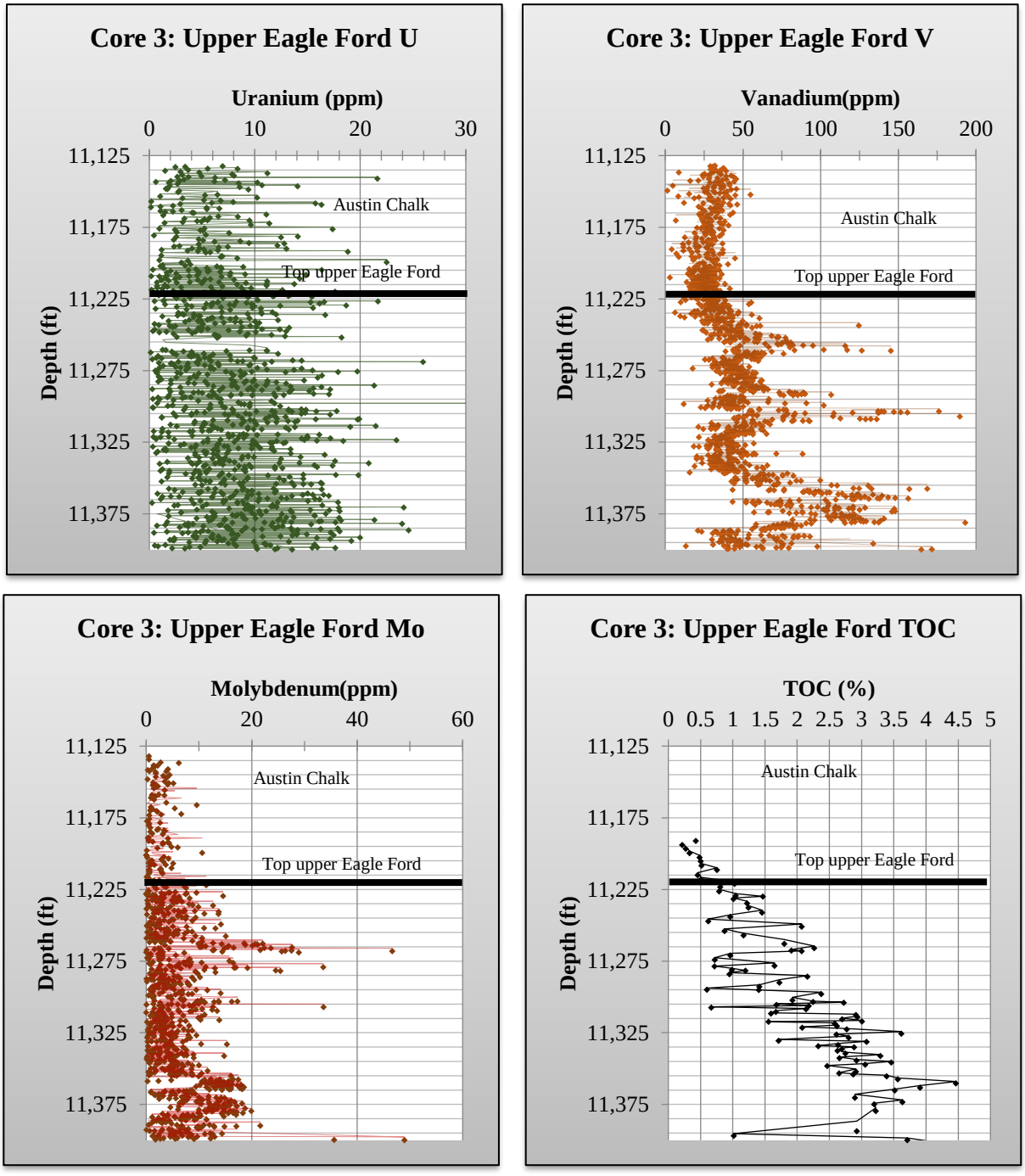

Figure 37: *Core3 XRF Uranium, Vanadium, Molybdenum, and TOC Graphs* with a two period running average trendline. Upper Eagle Ford top as identified in the core 3 description indicated by a bold black line. Within the upper Eagle Ford in this core the section that contains the highest vanadium enrichment is located within the lowermost portion of the upper Eagle Ford.

The highest enrichments of molybdenum occur in the uppermost and lowermost section of the upper Eagle Ford with the lowermost section containing slightly less scatter. The uranium concentrations appear relatively random, but the lowermost portion of the upper Eagle Ford appears to have slightly higher values. The TOC percentages show an upward decreasing trend with the highest value occurring at 4.5% within the lowermost section.

Core 2 displays very similar patterns to Core 3 (Figure 38). It two has 3 separately occurring vanadium enrichments intervals, and an overall scattering of uranium concentration. Molybdenum enrichments intervals do not appear as obvious as they were in Core 3, but lower, middle, and top intervals of very slight molybdenum enrichment may be correlative with the lower, middle, and top vanadium enrichments. Likewise, there are 3 very slight increases in nickel and copper in correlative intervals. This is suggestive that upper Eagle Ford deposition in more distal areas experienced three pulses of increased organic-rich sedimentation that was accompanied by anoxic to euxinic conditions. The increase in the abundance of organic matter and subsequent degradation which would have ensued may have been what triggered anoxia (Tribovillard et al., 2006).

Core 2's highest TOC content at approximately 4.75% occurs in the lowermost section of the upper Eagle Ford. This is the highest TOC percentage recorded between all four cores. TOC percentages within this core also display an overall upward decreasing trend. This lowermost section within Core 2 is correlative to the Finely to Coarsely Laminated Wackestone/Packstone lithofacies. Much like that found in Core 3, the relationship between increases in copper and nickel concentrations and increases in the TOC content is not as clearly apparent as it is in the most proximal cores; however, filtering the copper and nickel data to only include those points that contain a TOC value reveals that a positive correlation does still exits.

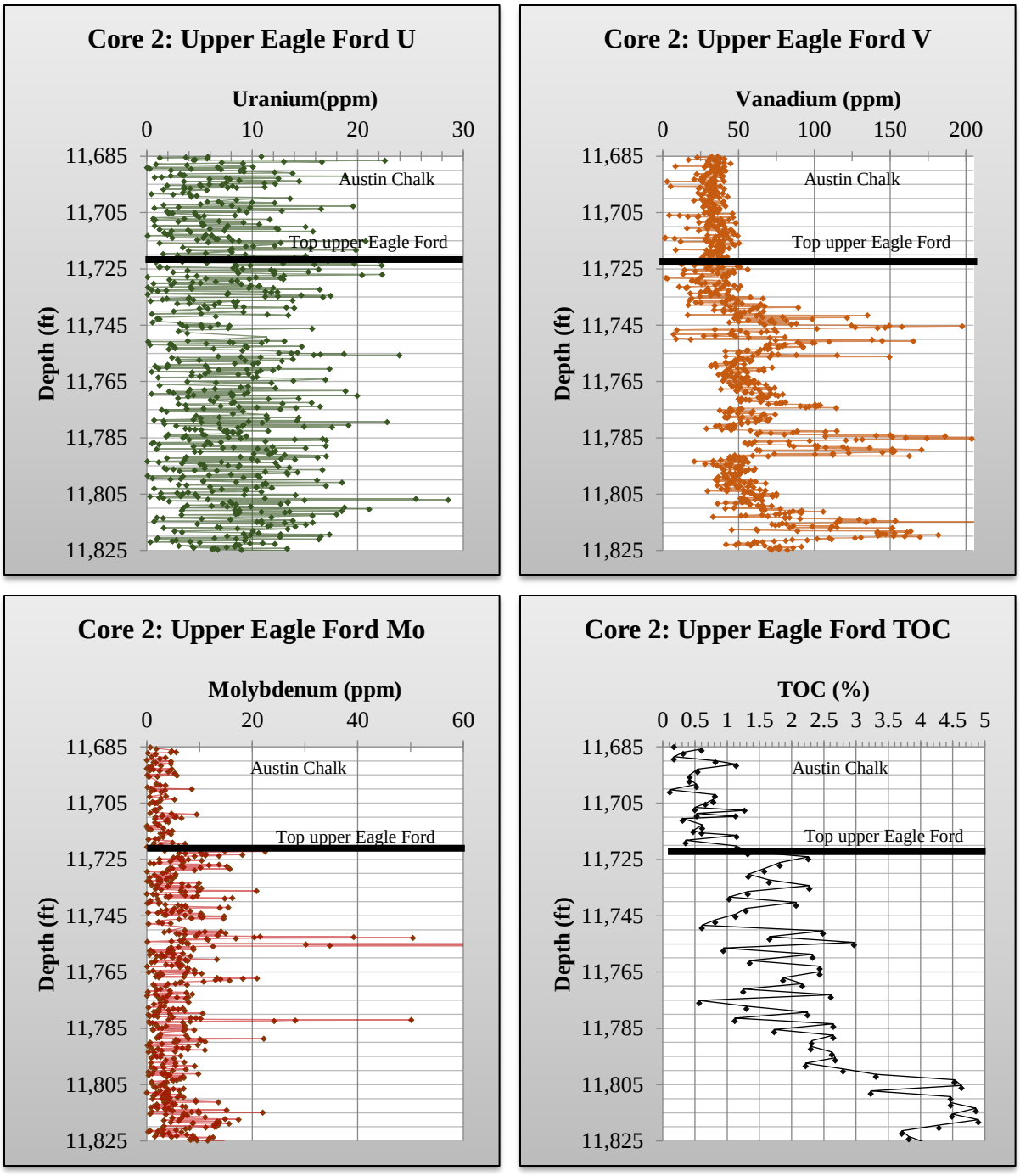

Figure 38: *Core2 XRF Uranium, Vanadium, Molybdenum, and TOC Graphs* with a two period running average trendline. Upper Eagle Ford top as identified in the core 2 description indicated by a bold black line. Within the upper Eagle Ford in this core there are three sections that are relatively enriched in vanadium. These are the lowermost upper Eagle Ford, the middle upper Eagle Ford, and near the top of the upper Eagle Ford. The highest enrichments of molybdenum occur near the top of the upper Eagle Ford. The uranium concentrations appear relatively random, but the lowermost portion of the upper Eagle Ford appears to have slightly higher values

much like that found in core 3. The TOC percentages show an upward decreasing trend with the highest value occurring at ~4.75% within the lowermost section.

Summary and Conclusions

This study of the depositional dynamics of the upper Eagle Ford focused on the lithological and sedimentological characteristics based on conventional core and thin section analyses. In addition, data from elemental analysis were used to further refine bottom water conditions and original influxes of organic material. The full Eagle Ford Formation records a rapid transgression and flooding phase across the underlying Buda Limestone succession. The majority of the uppermost lower Eagle Ford and lowermost upper Eagle Ford were deposited under highstand conditions. The middle to upper portion of the upper Eagle Ford records the regressive phase that was eventually succeeded by deposition of the Austin Chalk.

Lithological and Sedimentological Conclusions

Seven lithofacies and three primary lithologies that highlighted different depositional and geochemical processes were identified within the upper Eagle Ford. The 7 lithofacies listed below in decreasing order of contribution are:

1. Coarsely to Finely Laminated Wackestone/Packstone
2. Wavy Laminated Wackestone/Packstone
3. Bioturbated Wackestone/Packstone
4. Massive Packstone/Grainstone
5. Deformed Wackestone/Packstone
6. Massive Mudstone/Wackestone
7. Volcanic Ash

The 13 lithologies (sedimentary structure + limestone, shale, or Ash) are as follows:

1. Bioturbated Limestone
2. Bioturbated Shale
3. Deformed Limestone
4. Deformed Shale
5. Coarsely Laminated Limestone
6. Coarsely Laminated Shale
7. Finely Laminated Limestone
8. Finely Laminated Shale
9. Wavy Laminated Limestone
10. Wavy Laminated Shale
11. Massive Limestone
12. Massive Shale
13. Volcanic Ash

The Bioturbated Wackestone/Packstone lithofacies is interpreted as a relatively low energy environment within slightly more oxygenated waters that supported the existence of burrowing organisms. The Bioturbated Wackestone/Packstone lithofacies is the most abundant in Cores 4 and 3, and the least abundant in Core 1. This lithofacies shows an upward increase in occurrence in all four cores suggesting an upward increase in the degree of oxygenation related to an overall regressive period marking the transition to the overlying Austin Chalk. The Wavy Laminated Wackestone/Packstone lithofacies is interpreted as either a slightly higher energy environment that is near wave-base and more frequently affected by storm-wave base, or an environment subjected to stronger bottom water-currents. It is most abundant in the two most

proximal cores (4 and 1), and shows an upward increase in occurrence in all four cores. This is consistent with the model of an upward transition to the Austin Chalk as a genetically related depositional system. The Massive Mudstone/Wackestone is interpreted as either waning low-density mud-rich debris flow events, a reduction in the primary production and sedimentation of planktonic organisms, and/or homogenization from extensive but poorly preserved bioturbation. It is the most abundant in Core 4 and the least abundant in Core 1. The most continuous sections of this lithofacies occur above significant volcanic ash deposits. This suggests that, at least for these intervals, their formation is closely tied to the primary productivity and sedimentation of planktonic foraminifera. The Finely to Coarsely Laminated Wackestone/Packstone lithofacies is the most abundant lithofacies of the upper Eagle Ford in Karnes and Gonzales counties. It is interpreted as suspension sedimentation within a low energy marine environment below wave-base, and influenced by waning low density debris flows and weak bottom water currents. The laminations are reminiscent of seasonal varves and are likely caused by mass die-offs of foraminifera related to various cyclic climate changes and the organism's life and death cycle. These characters suggest a more distal setting relative to the Bioturbated Wackestone/Packstone lithofacies. Additionally, this lithofacies, specifically of the shale lithology, contains the highest percentages of TOC within all four cores. This suggests that the most organic rich interval within the upper Eagle Ford is likely correlative to the most continuously deposited sections of the Finely to Coarsely Laminated Shale. The Massive Packstone/Grainstone lithofacies is interpreted as event bed deposits that experienced varying degrees of recrystallization. These event beds likely originated as storm generated turbidity currents and debris flows from more proximal areas. These events transported carbonate sediment to more distal environments that resulted in vertically thin deposits with an overall higher carbonate percentage. However, some of these

sections appear to include the formation of small to large carbonate nodules that formed just below the sediment-water interface, while the sediment was still relatively soft. The nodule formation is interpreted to be the result of methane oxidation at the base of the zone of sulfate reduction ultimately related to anaerobic bacterial degradation of organic material in the underlying zone of methanogenesis. This lithofacies is most abundant in Cores 3 and 2 and least abundant in Core 4. The Volcanic Ash deposits formed as a result of fallout from subaerial volcanic eruptions; however, a few ash deposits exhibit highly to slightly scoured bases indicating that these ash deposit may have originated from a subaqueous eruption, or perhaps a subaerial eruption that triggered a subaqueous mass wasting event that left an irregular scar on which the resultant ash fallout was deposited. Additionally, although this lithofacies makes near equal contributions to in Cores 4, 3, and 2, it is slightly more abundant (by 2-6%) in the most westward proximal core (Core 4), and by far the least abundant in the most eastward proximal core (Core 1). This could be a reflection of each core's proximity to the Cretaceous western volcanic province mapped by Ewing (1987) (Figure 39 yellow triangles).

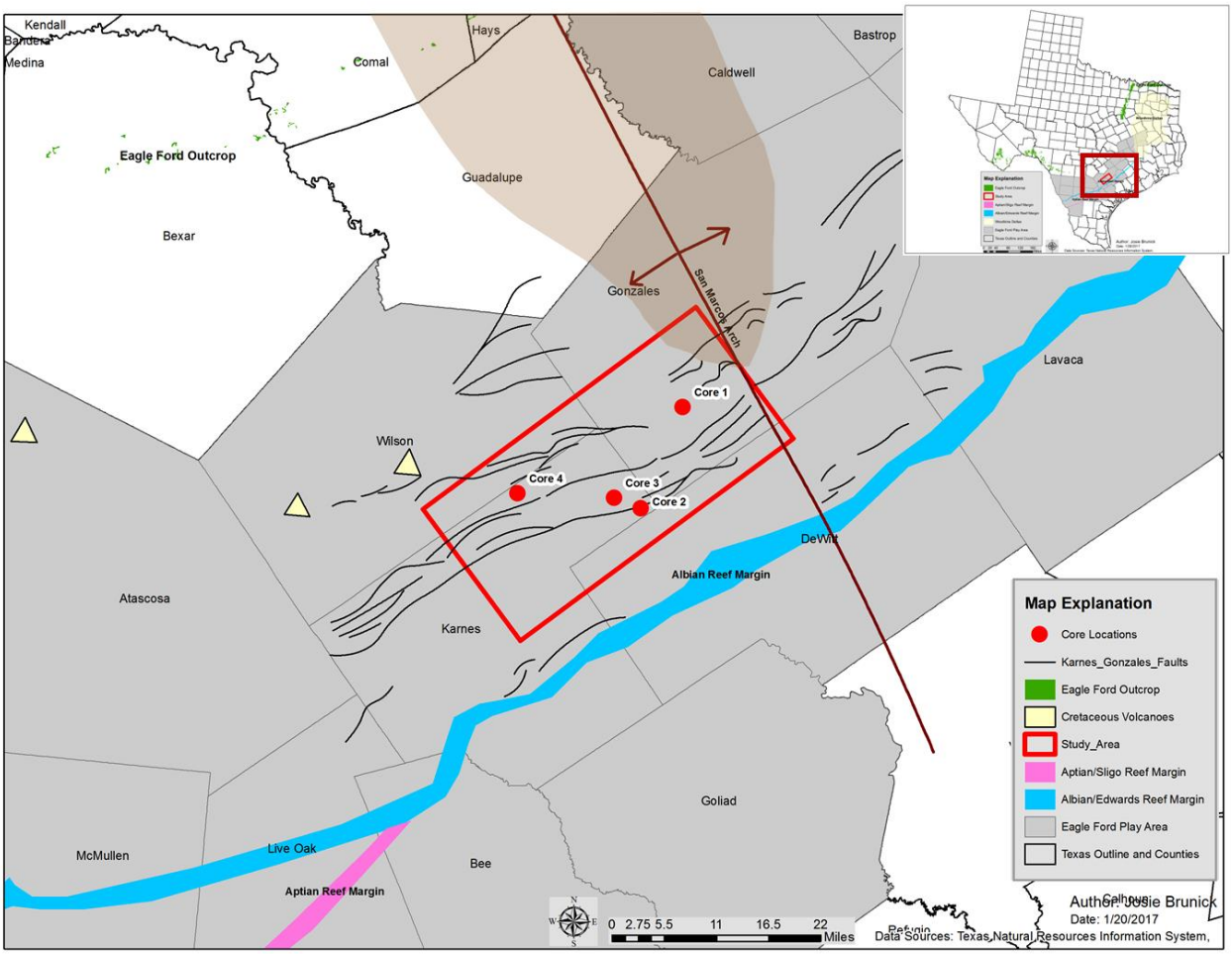

Figure 39: *Location of Cores 1-4* relative to the Cretaceous western volcanic province as mapped by Ewing (1987).

Geochemistry Conclusions

Analyzing thorium to uranium ratios and the distribution of nickel, copper, uranium, molybdenum, and vanadium within the upper Eagle Ford provided clues into paleoredox conditions, and the relative influxes of organic matter experienced at the time of deposition. The thorium to uranium ratios were fairly consistently below a value of 7 (most ranging between near 0 to 1) indicating that there was very little material deposited within the upper Eagle Ford that was reworked from terrigenous environments. The relative concentrations of nickel and copper

suggest that within Cores 1 and 4 the lowermost and uppermost portion of the upper Eagle Ford may have experienced a higher influx of organic material while experiencing sulfate reducing conditions relative to the middle portion of the upper Eagle Ford. These two intervals also contain higher TOC values. This indicates a strong relationship between increases in copper and nickel concentrations and TOC concentrations within the proximal locations of the upper Eagle Ford. Cores 2 and 3 appear to have three of these higher organic particle "pulses": one at the base of the upper Eagle Ford, one near the middle, and a smaller pulse at the top. The richest intervals of TOC are found in the lowermost portion of the upper Eagle Ford for both the distal cores. Increases in nickel and copper concentrations correspond to increases in TOC content, but this relationship is not as apparent as it is in the most proximal cores. The highly scattered nature of the uranium concentrations within all four cores suggest that throughout its depositional history the upper Eagle Ford was prone to relatively short lived oxygenated flushes of water that were able to remove and relocate adsorbed uranium ions. These "flushes" are likely related to the influence of gravity flow events. Molybdenum concentrations in all four cores suggest that the upper Eagle Ford experienced somewhat sporadic anoxic to euxinic conditions near the end of its deposition; however, slight increases in the molybdenum concentration is also evident near the base of the upper Eagle Ford in Cores 2, 3, and 1 that contain less scattering of values. This may indicate longer duration anoxic to near euxinic conditions, which could be a reflection of highstand conditions. Vanadium concentrations within the upper Eagle Ford suggest that anoxic conditions prevailed within the lower, middle, and upper portion within the most distal cores (3 and 2), within the lowermost portion of Core 1, and within the upper most portion of Core 4. The TOC percentages of all four cores reveal that the highest TOC enrichment of the upper Eagle Ford is located within the lowermost section of all cores, and higher enrichments occur in the

more distal locations. Core 2 contains the highest TOC percent (~4.75%) with Core 3 being a close second (4.5%). Core 4 contains the lowest maximum percentage of TOC (~3%).

What these data imply is that the upper Eagle Ford represents an overall shallowing upward sequence that accumulated under changing geochemical environments fluctuating between slightly euxinic to suboxic with the common influence of oxygenated waters brought in by more proximal gravity flow events. The upper Eagle Ford was subjected to stronger bottom water currents and wave action in proximal locations. In all core locations, the primary sedimentation was through suspension settling, but these sediments had minor influences of bottom water currents. Methanogenesis and methane oxidation likely played a primary role in the development of carbonate concretions, while debris flows and turbidity currents resulted in inversely graded and normally graded sedimentary units that vary in their degree of diagenetic recrystallization. These debris flows and turbidity currents also introduced burrowing organisms into deeper water and more anoxic settings where they would not normally live, but were able to survive for a short time creating small and relatively frequent intervals of bioturbation.

The highest TOC percentages are correlated with the longer intervals of the Coarsely to Finely Laminated Shale lithology. Variability of lithofacies within the upper Eagle Ford increases upward. The more consistent intervals of the Coarsely to Finely Laminated Shale lithology occur within the base of the upper Eagle Ford within all four cores. Based on these observations, the base of the upper Eagle Ford particularly in more distal locations contain the best chance for hydrocarbon production comparable to that of the lower Eagle Ford.

References

Adams, J., & Weaver, C. (1958). Thorium to Uranium Ratios as Indicators of Sedimentary Processes: Example of Concept of Geochemical Facies. *Bulletin of the American Association of Petroleum Geologists, 42*(2), 387-430.

Adams, R., & Carr, J. (2010). Regional Depositional Systems of the Woodbine, Eagle Ford, and Tuscaloosa of the U.S. Gulf Coast. *Gulf Coast Association of Geological Societies Transactions, 60*, 3-27.

Adams, R., & Carr, J. (2014). The Lower Woodbine Organic Shale of Burleson and Brazos Counties Texas: Anatomy of a New Old Play. *Gulf Coast Association of Geological Societies Transactions, 64*, 3-31.

Alexander, M. (2014). A New Look at Maverick Basin Basement Tectonics. *The Gulf Coast Association of Geological Societies Transactions, 64*, 33-40.

Arthur, M., Dean, W., Neff, E., Hay, B., King, J., & Jones, G. (1994). Varve Calibrated Records of Carbonate and Organic Carbon accumulation Over the Last 2000 Years in the Black Sea. *Global Biogeochemical Cycles, 8*(2), 195-217.

Berger, W. (1970). Planktonic Foraminifera: Selective Solution and the Lysocline. *Marine Geology, 8*, 111-138.

Berger, W. (1971). Sedimentation of Planktonic Foraminifera. *Marine Geology, 11*, 325-358.

Blakey, R. (2014). Paleogeography and Paleotectonics of the Western Interior Seaway, Jurassic-Cretaceous of North America. *Search and Discovery Article #30392*, 1-72.

Breyer, J., Denne, R., Funk, J., Kosanke, T., & Spaw, J. (2013). Stratigraphy and Sedimentary Facies of the Eagle Ford Shale (Cretaceous) between the Maverick Basin and the San Marcos Arch, Texas, USA. *Abstracts: Annual Meeting - American Association of Petroleum Geologists*, 1-23. Retrieved from http://0-search.proquest.com.library.uark.edu/docview/1553086311?accountid=8361

Brown, C., & Pierce, R. (1962). Palynologic Correlations in Cretaceous Eagle Ford Group, Northeast Texas. *Bulletin of the American Association of Petroleum Geologists, 46*(12), 2133-2147.

Cardneaux, A. P. (2012). *Mapping of the Oil Window in the Eagle Ford Shale Play of Southwest Texas Using Thermal Modeling and Log Overlay Analysis: Master's Thesis.* Louisiana State University Agricultural and Mechanical College.

Coleman, M., & Raiswell, R. (1993). Microbial Mineralization of Organic Matter: Mechanisms of Self-Organization and Inferred Rates of Precipitation of Diagenetic Minerals. *Philosophical Transactions of the Royal Society, 344A*, 69-87.

Coleman, M., & Raiswell, R. (1995). Source of Carbonate and Origin of Zonation in Pyritiferous Carbonate Concretions: Evaluation of a Dynamic Model. *American Journal of Science, 295*, 282-308.

Donovan, A., & Staerker, T. S. (2010). Sequence Stratigraphy of the Eagle Ford (Boquillas) Formation in the Subsurface of South Texas and Outcrops of West Texas. *Gulf Coast Association of Geological Societies Transactions, 60*, 861-899.

Driskill, B., Suurmeyer, N., Rilling-Hall, S., Govert, A., & Garbowlcz, A. (2012). Reservoir Description of the Subsurface Eagle Ford Formation, Maverick Basin Area, South Texas, USA. *Society of Petroleum Engineers, 74*, 2367-2390.

Dunham, R. (1962). Classification of Carbonate Rocks According to Depositional Texture. In W. Ham (Ed.), *Classification of Carbonate Rocks-A Symposium* (Vol. 1, pp. 108-121). American Association of Petroleum Geologists. doi:10.1306/M1357

EIA. (2016). *Maps: Exploration, Resources, Reserves, and Production*. Retrieved from U.S. Energy Administration: https://www.eia.gov/pub/oil_gas/natural_gas/analysis_publications/maps/maps.htm

Emerson, S. R., & Huested, S. S. (1991). Ocean Anoxia and the Concentration of Molybdenum and Vanadium in Seawater. *Marine Chemistry*, 177-196.

Ewing, T. (1987). The Frio River Line in South Texas-Transition from Cordilleran to Northern Gulf Tectonic Regimes. *Gulf Coast Association of Geological Societies Transactions, 37*, 87-94.

Föllmi, K., & Grimm, K. (1990, November). Doomed Pioneers: Gravity-flow Deposition and Bioturbation in Marine Oxygen-Deficient Environments. *Geology, 18*, 1069-1072.

Frébourg, G., Ruppel, S., Loucks, R., & Lambert, J. (2016, April). Depositional Controls on Sediment Body Architecture in the Eagle Ford/Boquillas System: Insights from Outcrops in West Texas, United States. *The American Association of Petroleum Geologists, 100*(4), 657-682.

Hallam, A., & Bradshaw, M. (1979). Bituminous Shales and Oolitic Ironstones as Indicators of Transgressions and Regressions. *The Geological Society, 136*, 157-164.

Hamblin, K. (1962). X-Ray Radiography in the Study of Structures in Homogeneous Sediments. *Journal of Sedimentary Petrology, 32*(2), 201-210.

Harbor, R. (2011). Facies Characterization and Stratigraphic Architecture of Organic-rich Mudrocks, Upper Cretaceous Eagle Ford Formation, South Texas. *M.S. Thesis, The University of Texas at Austin*, 1-184.

Helz, G., Bura-Nakiá, E., Mikac, N., & Ciglenecki, I. (2011). New Model for Molybdenum Behavior in Euxinic Waters. *Chemical Geology, 284*, 323-332.

Hentz, T., & Ruppel, S. (2011). Regional Stratigraphic and Rock Characteristics of Eagle Ford Shale in Its Play Area: Maverick Basin to East. *AAPG Search and Discovery Article #10325*.

Hill, R. (1887a). The Topography and Geology of the Cross Timbers and Surrounding Regions in Northern Texas. *American Journal of Science, 33*(3rd series), 291-303.

Hill, R. (1887b). The Texas Section of the American Cretaceous. *American Journal of Science, 34*(3rd series), 287-309.

Hiller, J. (2015, Nov 6). *Eagle Ford Operators Look Up to the Austin Chalk.* Retrieved from Houston Chronicle: http://www.houstonchronicle.com/business/article/Eagle-Ford-operators-look-up-to-the-Austin-Chalk-6616119.php

Hjulstrøm, F. (1976). Studies of the Morpyhological Activity of Rivers as Illustrated by the River Fyris. *Landforms and Geomorphology*, 274-287.

Huc, A. Y. (1988). Aspects of Depositional Processes of Organic Matter in Sedimentary Basins. *Organic Geochemistry, 13*, 263-272.

Irwin, H., Curtis, C., & Coleman, M. (1977). Isotopic Evidence for Source of Diagenetic Carbonates Formed During Burial of Organic-Rich Sediments. *Nature, 269*, 209-213.

Jackson, J., & McKenzie, D. (1983). The Geometrical Evolution of Normal Fault Systems. *Journal of Structural Geology, 5*, 471-482.

Klinkhammer, G. P., & Palmer, M. R. (1991). Uranium in the Oceans: Where it Goes and Why. *Geochimica et Cosmochimica Acta*, 1799-1806.

Komlos, J., Peacock, A., Kukkadapu, R., & Jaffe, P. (2008). Long-term Dynamics of Uranium Reduction/Reoxidation under Low Sulfate Conditions. *Geochimica et Cosmochimica Acta*, 3603-3615.

Kucera, M. (2007). Planktonic Foraminifera as Tracers of Past Oceanic Environments. In *Developments in Marine Geology* (Vol. 1, pp. 213-262). Elsevier. doi:10.1016/S1572-5480(07)01011-1

Lash, G., & Blood, D. (2004). Geochemical and Textural Evidence for Early (Shallow) Diagenetic Growth of Stratigraphically Confined Carbonate Concretions, Upper Devonian Rhinestreet Black Shale, Western New York. *Chemical Geology, 206*, 407-424.

Lehmann, C., Osleger, D., & Montanez, I. (2000). Sequence Stratigraphy of Lower Cretaceous (Barremian-Albian) Carbonate Platforms of Northeastern Mexico: Regional and Global Correlations. *Journal of Sedimentary Research, 70*(2), 373-391.

Lewis Energy Group. (2015). *The Eagle Ford Shale: a Prime Target for Natural Gas*. Retrieved 03 08, 2016, from Lewis Energy Group: http://www.lewisenergy.com/lewis-energy-natural-gas-exploration.html

Linnert, C., Mutterlose, J., & Mortimore, R. (2011). Calcareous Nannofossils from Eastbourne (Southeastern England) and the Paleoceanography of the Cenomanian-Turonian Boundary Interval. *Society for Sedimentary Geology, 26*, 298-313.

Loucks, R., & Ruppel, S. (2007). Mississippian Barnett Shale: Lithofacies and Depositional Setting of a Deep-Water Shale-Gas Succession in the Fort Worth Basin, Texas. *The American Association of Petroleum Geologists, 91*(4), 579-601.

Luning, S., & Kolonic, S. (2003). Uranium Spectral Gamma-Ray Response as a Proxy for Organic Richness in Black Shales: Applicability and Limitations. *Journal of Petroleum Geology,* 153-174.

Martin, R., Baihly, J., Malpani, R., Lindsay, G., & Atwood, K. (2011). Understanding Production from Eagle Ford-Austin Chalk System. *Society of Petroleum Engineers*, 1-28.

Prothero, D., & Schwab, F. (2014). *Sedimentary Geology* (3rd ed.). New York: W.H. Freeman and Company.

Railroad Commission of Texas. (2016, 03 01). *Eagle Ford Shale Information*. Retrieved from RRC: http://www.rrc.texas.gov/oil-gas/major-oil-gas-formations/eagle-ford-shale/

Raiswell, R. (1976). The Microbiological Formation of Carbonate Concretions in the Upper Lias of NE England. *Chemical Geology, 18*, 227-244.

Raiswell, R. (1987). Non-Steady State Microbiological Diagenesis and the Origin of Concretions and Nodular Limestones. *Geological Society of London Special Publication, 36*, 41-54.

Raiswell, R. (1988). Chemical Model for the Origin of Minor Limestone-Shale Cycles by Anaerobic Methane Oxidation. *Geology, 16*, 641-644.

Raiswell, R., & Fisher, Q. (2000). Mudrock-Hosted Carbonate Concretions: A Review of Growth Mechanisms and Their Influence on Chemical and Isotopic Composition. *Journal of the Geological Society London, 157*, 239-251.

Siegel, D., Chamberlain, S. , & Dossert, W. (1987). The Isotopic and Chemical Evolution of Mineralization in Septarian Concretions: Evidence for Episodic Paleohydrogeologic Methanogenesis. *Geological Society of America Bulletin, 99*, 385-394.

Stanley, S. (2009). *Earth system History 3rd Edition.* New york: W. H. Freeman and Company.

Texas Natural Resources Information System. (2007). *Geologic Database of Texas*. Retrieved from Texas Statewide Imagery and GIS Data: https://tnris.org/data-catalog/entry/geologic-database-of-texas/

Trabucho-Alexandre, J. (2015). More Gaps than Shale: Erosion of Mud and its Effect on Preserved Geochemical and Palaeobiological Signals. *Geological Society, London, Special Publications, 404*, 251-270.

Treadgold, Campbell, Mclain, Weinman, Sinclair, Nicklin, & Matador. (2011a, January). Eagle Ford Shale Prospecting with 3D Seismic Data within a Tectonic and Depositional System Framework. *The Leading Edge*, 48-53.

Treadgold, Peebles, Sinclair, & Nicklin. (2011b, December). Eagle Ford Shale Exploration; Integrated Regional Geology, Seismic and Microseismic Analysis. *Australian Society of Exploration Geophysicists, 155*, 28-32.

Tribovillard, N., Algeo, T., Lyons, T., & Riboulleau, A. (2006). Trace Metals as Paleoredox and Paleoproductivity Proxies: An Update. *Chemical Geology, 232*, 12-32.

Tribovillard, N., Riboulleau, A., Lyons, T., & Baudin, F. (2004). Enhanced Trapping of Molybdenum by Sulfurized Marine Organic Matter of MArine Origin in Mesozoic Limestones and Shales. *Chemical Geology*, 385-401.

US Census Bureau, Geography Division. (2011). *2011 Tiger/Line Shapefiles*. Retrieved from US Census Bureau: http://www.census.gov/cgi-bin/geo/shapefiles2011/layers.cgi

White, T., Gonzalez, L., Ludvigson, G., & Poulsen, C. (2001). Middle Cretaceous greenhouse hydrologic cycle of North America. *Geological Society of America*, *29*(4), 363-366.

Wignall, P. (1994). *Black Shales.* New York: Oxford University Press Inc.

Workman, S. (2013). Integrating Depositional Facies and Sequence Stratigraphy in Characterizing Unconventional Reservoirs: Eagle Ford Shale, South Texas. *Western Michigan University*, 1-152.

Appendices

Appendix A: Core 1 TOC Data

Core 1 TOC Data			
Depth (ft)	**TOC (%)**	**Cont. Depth (ft)**	**Cont. TOC (%)**
8814.75	0.55	8840.13	0.46
8815.42	0.13	8841.42	0.83
8816.08	0.56	8843.08	0.06
8817.42	0.76	8844.42	0.94
8818.42	2.10	8846.08	0.81
8819.08	1.12	8847.42	0.71
8820.42	1.16	8850.42	1.84
8822.08	2.44	8851.75	1.90
8823.42	2.35	8853.50	2.10
8825.08	2.45	8855.13	1.98
8826.42	1.00	8856.42	0.97
8828.08	1.28	8857.92	3.35
8829.42	2.08	8858.08	3.62
8831.08	0.82	8859.54	3.37
8832.42	1.96	8861.08	3.28
8834.08	2.80	8862.42	3.15
8835.42	3.14	8863.13	2.61
8837.08	1.54	8864.25	2.70
8838.42	1.51		

Appendix B: Core 2 TOC Data

Core 2 TOC Data					
Depth (ft)	**TOC (%)**	**Cont. Depth (ft)**	**Cont. TOC (%)**	**Cont. Depth (ft)**	**Cont. TOC (%)**
11685.08	0.17	11729.25	1.58	11786.42	1.73
11686.42	0.60	11731.25	1.33	11788.42	2.65
11687.50	0.32	11733.25	1.65	11790.42	2.31
11689.42	0.17	11735.42	2.28	11792.42	2.30
11690.50	0.82	11737.42	1.32	11794.42	2.63
11691.79	1.14	11739.25	1.03	11796.42	2.68
11694.00	0.54	11741.42	2.07	11798.42	2.22
11695.83	0.42	11743.42	1.29	11800.42	2.80
11697.42	0.41	11745.42	1.13	11802.25	3.31
11699.33	0.53	11747.42	0.82	11804.25	4.53
11701.25	0.11	11749.42	0.61	11806.25	4.64
11702.67	0.81	11751.42	2.49	11808.25	3.23
11704.67	0.79	11753.42	1.66	11810.25	4.47
11705.58	0.66	11755.42	2.97	11812.42	4.47
11707.50	0.50	11757.58	0.94	11814.42	4.86
11707.67	1.27	11759.92	2.33	11816.42	4.49
11709.67	0.53	11761.92	1.35	11818.42	4.90
11709.75	1.13	11763.92	2.44	11820.42	4.29
11711.25	0.31	11765.92	2.44	11822.42	3.71
11714.08	0.62	11768.08	1.87	11824.42	3.82
11715.33	0.47	11770.08	2.17		
11715.79	0.60	11772.08	1.25		
11717.08	1.15	11774.08	2.61		
11719.25	0.35	11776.08	0.57		
11721.25	1.14	11778.08	1.30		
11723.25	1.32	11780.42	2.25		
11724.92	2.26	11782.42	1.12		
11727.25	1.82	11784.42	2.65		

Appendix C: Core 3 TOC Data

Core 3 TOC Data					
Depth (ft)	**TOC (%)**	**Cont. Depth (ft.)**	**Cont. TOC (%)**	**Cont. Depth (ft.)**	**Cont. TOC (%)**
11191.08	0.43	11278.75	0.72	11330.58	1.71
11194.08	0.21	11281.25	0.99	11331.42	3.08
11196.75	0.27	11281.75	1.20	11333.58	2.64
11199.75	0.33	11284.25	0.95	11334.42	2.33
11202.75	0.48	11285.92	2.16	11335.08	2.88
11205.42	0.50	11290.08	1.72	11336.42	2.69
11208.42	0.51	11292.92	1.41	11337.58	2.63
11211.42	0.75	11294.92	0.60	11339.42	2.75
11215.08	0.46	11295.25	1.41	11341.25	3.29
11218.08	0.50	11298.08	2.37	11342.75	2.66
11221.08	1.03	11302.42	1.93	11344.42	2.92
11223.42	0.80	11303.42	2.24	11345.75	3.46
11226.42	0.79	11304.08	2.72	11347.25	3.06
11229.42	1.05	11305.58	1.68	11348.25	2.47
11230.08	1.47	11306.42	2.18	11352.25	2.91
11231.75	1.01	11307.58	0.66	11353.42	2.65
11234.75	1.22	11308.58	2.14	11354.08	2.87
11237.75	1.24	11310.58	1.67	11355.42	3.39
11241.25	1.45	11311.58	1.59	11357.58	3.56
11244.25	0.96	11312.58	2.91	11360.42	4.46
11247.25	0.62	11314.08	2.93	11363.42	3.91
11251.08	2.07	11315.58	2.70	11365.25	3.52
11254.08	0.87	11317.08	3.01	11370.42	2.90
11257.08	1.17	11317.42	1.56	11373.42	3.63
11262.92	1.80	11318.75	2.58	11374.92	3.19
11266.08	2.26	11320.42	2.62	11379.75	3.22
11267.75	1.91	11321.42	2.08	11393.75	2.92
11268.08	2.07	11322.58	2.77	11396.92	1.02
11271.08	0.96	11325.75	3.62	11399.92	3.71
11274.08	0.72	11326.25	2.61		
11278.25	1.65	11328.58	2.80		

Appendix D: Core 4 TOC Data

Core 4 TOC Data			
Depth (ft)	**TOC (%)**	**Cont. Depth (ft)**	**Cont. TOC (%)**
8415.58	0.24	8471.25	0.81
8418.58	0.21	8471.58	0.40
8418.92	0.36	8474.58	0.94
8419.42	0.08	8477.58	2.96
8419.75	0.23	8479.75	3.01
8421.58	1.04	8481.58	1.43
8423.75	0.30	8484.58	1.32
8425.58	0.15	8487.58	0.57
8427.75	1.15	8489.75	2.16
8435.58	0.26	8491.58	1.27
8440.58	0.37	8494.58	1.44
8445.58	0.37	8497.58	2.06
8450.58	0.35	8499.75	2.40
8455.58	0.80	8500.58	1.77
8460.58	0.47	8501.58	1.85
8465.58	0.45	8504.58	3.03
8468.42	0.62	8507.58	2.42
8469.42	0.40	8509.75	3.04
8469.92	0.73	8511.58	2.22

Appendix E: Core 1 XRF Data

Core 1 XRF Data						
Depth (ft)	**V (ppm)**	**Ni (ppm)**	**Th (ppm)**	**U (ppm)**	**Mo (ppm)**	**Cu (ppm)**
8752.42	49.42	14.67	2.37	17.79	4.14	10.55
8752.75	46.33	5.45	2.77	1.17	1.20	10.74
8752.92	18.82	33.73	5.46	16.19	4.09	21.29
8753.08	17.45	23.86	8.33	11.71	3.26	10.99
8753.42	36.05	18.59	2.46	6.46	1.77	11.20
8754.75	51.29	15.29	2.48	5.18	0.91	13.57
8755.42	39.59	12.28	2.62	7.28	1.48	12.09
8756.75	15.51	41.95	5.44	10.57	0.24	22.00
8758.75	15.30	18.43	3.92	0.37	1.04	12.89
8759.08	39.86	15.34	3.01	6.82	3.28	14.37
8759.75	39.20	7.99	2.85	9.96	3.74	13.40
8761.42	39.20	15.56	2.37	5.62	0.49	12.21
8763.42	42.22	18.54	3.10	17.18	2.34	13.60
8764.08	44.42	17.95	2.59	2.85	2.53	13.90
8764.42	44.00	17.54	2.24	3.08	1.29	13.65
8765.08	39.75	14.90	2.01	2.17	0.32	12.22
8766.08	45.91	13.90	2.24	2.90	4.89	14.22
8768.75	47.64	11.41	2.43	5.12	4.03	11.39
8769.42	46.11	15.21	2.26	7.88	4.51	8.71
8769.75	42.51	17.76	2.27	10.13	2.59	13.14
8770.08	54.89	19.50	2.44	9.24	2.02	14.56
8770.42	50.24	12.91	2.24	5.12	0.34	10.63
8773.08	42.91	12.47	2.13	5.02	0.36	15.91
8774.42	44.10	32.60	3.91	3.07	1.39	19.15
8775.08	42.11	16.31	2.29	2.81	0.98	10.44
8777.08	45.13	18.32	2.85	4.53	1.72	13.36
8778.42	40.36	19.33	2.44	6.51	0.47	11.62
8780.42	45.52	14.91	3.04	1.40	1.73	13.53
8781.42	49.16	11.33	2.28	15.96	0.81	10.61
8783.42	43.85	9.90	2.14	2.43	1.83	13.78
8784.08	20.75	27.19	4.01	11.66	0.92	16.36
8785.42	32.47	14.20	2.41	14.64	4.75	9.12
8785.75	44.90	13.88	2.32	8.03	2.76	12.33
8786.08	45.87	10.19	2.32	3.79	0.08	12.56

8786.75	41.54	12.82	2.68	10.51	1.68	18.26
8787.08	43.67	18.71	2.61	2.48	2.37	14.46
8787.42	50.26	9.17	2.42	4.65	1.74	12.96
8789.08	48.52	16.24	2.61	0.96	1.16	14.75
8789.42	49.49	15.96	2.44	5.87	0.65	14.19
8789.75	42.00	16.53	2.33	15.62	1.38	12.10
8790.08	39.37	12.04	2.69	9.41	0.56	14.40
8791.08	36.66	9.49	2.63	6.13	0.69	11.49
8791.42	39.59	7.76	2.73	10.69	2.82	16.39
8792.08	44.49	10.66	2.67	6.25	0.56	12.70
8792.75	45.39	11.89	2.53	8.92	2.06	12.80
8793.08	45.60	13.46	2.88	19.73	0.78	10.37
8793.42	38.66	14.84	2.62	7.04	2.09	11.28
8793.75	46.40	12.18	2.52	4.29	7.33	7.87
8794.08	41.63	17.76	2.56	2.28	2.30	10.12
8795.08	45.77	16.07	2.53	0.59	3.32	13.36
8795.75	40.30	14.96	3.08	11.38	0.14	8.78
8797.42	5.84	25.22	6.44	10.47	3.87	13.44
8797.75	42.64	18.95	2.68	10.13	0.21	11.99
8800.42	39.57	14.17	2.21	8.03	3.81	12.69
8801.08	38.98	24.36	3.28	9.38	2.85	14.21
8802.42	36.14	22.57	2.99	3.56	2.53	17.36
8802.75	40.51	21.94	2.72	4.31	0.83	11.27
8803.75	43.48	21.85	2.35	2.53	1.53	13.52
8804.42	36.37	11.99	2.41	4.28	1.68	7.99
8806.50	31.12	53.15	5.05	7.47	1.86	20.99
8807.42	42.53	20.05	2.56	5.96	5.76	9.53
8807.75	49.14	32.76	3.91	11.78	1.81	15.63
8808.08	50.64	13.37	2.39	9.44	7.63	12.28
8808.75	42.66	16.12	2.58	10.15	1.07	14.12
8811.75	44.79	13.74	2.17	4.79	0.29	12.22
8813.08	39.41	76.07	6.05	5.47	3.01	19.46
8813.42	42.85	30.09	3.73	7.85	2.81	13.39
8813.75	32.89	32.57	4.07	11.44	2.97	16.54
8814.75	42.67	34.34	3.86	4.11	5.08	20.39
8815.08	32.06	66.93	5.40	6.81	6.66	20.67
8816.08	67.88	28.94	3.46	6.04	3.79	17.38
8816.75	63.91	31.78	2.75	2.79	0.53	12.72
8818.42	14.47	85.76	4.99	4.63	12.64	37.34

8818.75	42.00	73.89	4.89	15.98	24.12	35.52
8819.08	53.62	24.60	2.42	3.95	3.92	17.52
8819.42	37.00	54.68	3.67	14.64	15.49	28.31
8819.67	29.94	31.59	3.26	18.60	8.59	18.79
8819.75	35.33	34.25	3.06	6.01	4.91	19.90
8820.08	52.05	26.99	2.44	2.01	1.60	17.94
8820.42	48.55	36.38	2.55	0.02	7.93	17.31
8820.75	56.15	16.71	2.33	2.89	0.79	13.58
8821.08	51.71	32.58	2.62	1.09	3.74	19.67
8821.42	23.48	72.98	4.90	7.56	17.53	32.67
8821.75	20.93	52.01	4.04	5.51	15.35	26.53
8822.08	33.23	60.49	4.11	14.46	11.47	30.72
8822.42	34.82	36.17	3.66	12.71	12.53	20.28
8822.96	32.30	53.50	3.25	2.72	7.44	31.48
8823.42	39.19	75.63	4.15	8.90	14.68	41.58
8823.75	46.01	47.92	3.47	5.20	10.45	27.18
8824.08	35.61	61.34	4.40	8.44	14.09	32.27
8824.42	52.49	20.80	2.71	14.20	7.16	18.45
8825.08	47.48	53.05	3.50	2.24	7.41	33.46
8825.42	55.63	39.68	2.63	4.76	7.71	24.88
8825.75	57.82	45.56	3.33	9.02	13.36	27.52
8826.08	49.80	80.15	5.10	2.92	28.70	38.11
8826.42	52.12	16.89	2.43	3.89	3.74	13.94
8826.75	50.55	44.71	2.73	6.06	15.92	23.26
8827.08	58.52	147.71	6.04	17.78	70.62	55.54
8827.42	46.57	19.37	2.22	8.46	7.32	16.15
8827.75	56.51	107.47	3.88	8.87	42.08	36.87
8828.08	52.75	19.31	2.22	5.97	10.01	15.01
8828.42	59.73	32.07	2.17	3.51	4.39	16.22
8828.63	69.37	64.67	3.65	10.44	23.54	27.38
8828.75	72.59	116.78	4.80	10.76	45.52	55.11
8829.08	61.41	43.15	2.61	3.80	10.19	23.24
8829.42	63.74	58.77	2.09	9.40	18.03	20.10
8830.08	56.31	98.81	3.82	9.78	62.70	44.15
8830.42	84.66	83.08	3.09	12.62	40.58	33.81
8831.42	96.38	55.55	3.02	8.86	22.27	23.38
8831.92	86.02	51.78	2.74	0.86	22.40	27.80
8832.08	95.10	51.80	2.67	9.93	21.50	23.21
8832.42	96.64	38.00	2.57	8.92	17.71	23.00

8832.75	95.03	58.77	2.85	8.92	25.01	23.00
8833.08	94.27	35.99	2.50	0.18	10.71	22.63
8833.42	97.26	61.69	2.28	6.28	15.35	27.51
8834.08	26.72	24.68	2.48	2.03	5.66	12.95
8834.75	71.48	64.98	2.98	6.43	30.78	32.12
8835.75	50.92	17.41	2.11	0.51	1.35	11.55
8836.08	177.98	26.16	1.96	4.40	7.30	9.80
8836.75	64.07	34.11	2.26	3.91	7.93	17.45
8837.08	59.84	25.42	1.90	2.88	2.46	21.00
8837.75	73.20	42.00	2.67	9.62	5.92	26.52
8837.96	102.79	34.84	2.24	7.75	4.73	22.09
8838.42	91.62	18.34	1.89	3.19	0.63	13.34
8839.04	91.04	31.36	2.14	9.76	6.44	18.93
8839.08	100.09	26.97	2.33	4.65	6.50	17.75
8840.13	63.71	10.13	1.76	0.91	0.83	12.62
8843.42	190.73	13.32	1.67	11.94	12.77	9.25
8844.08	120.06	38.45	2.16	8.19	19.39	15.86
8844.42	66.19	33.51	2.08	8.09	10.33	22.25
8844.75	79.60	53.38	2.49	4.71	32.41	25.14
8845.42	140.16	18.16	1.68	2.30	7.76	8.31
8846.08	50.76	25.14	2.86	9.79	9.05	20.39
8846.42	65.02	29.27	2.25	7.33	0.88	17.77
8846.75	43.72	51.17	5.69	10.04	2.72	35.60
8846.79	51.52	40.50	5.18	9.09	4.03	28.92
8847.08	46.24	39.95	4.69	14.33	2.30	23.48
8848.08	71.43	64.33	6.22	4.11	9.29	37.23
8849.08	57.68	47.28	4.15	11.37	3.35	24.08
8849.42	60.33	50.12	5.85	11.22	7.59	30.31
8849.75	59.41	26.09	3.94	12.72	5.38	19.04
8850.08	53.87	41.93	5.18	20.72	9.17	19.07
8850.42	59.96	41.03	6.27	8.32	5.16	23.80
8850.75	76.26	28.03	2.93	5.43	1.94	15.61
8851.08	100.53	36.59	5.03	6.11	4.94	24.15
8851.42	133.07	44.65	7.57	17.71	9.42	34.25
8851.75	121.62	43.74	7.66	16.28	9.16	29.36
8852.08	102.67	44.30	6.93	12.52	7.59	28.93
8852.42	131.43	44.57	7.17	13.07	1.87	31.17
8853.38	88.34	44.24	7.51	10.82	11.54	23.59
8853.50	87.73	38.75	6.58	10.89	6.66	28.01

8854.08	109.37	50.71	6.52	10.91	7.32	31.43
8854.42	118.91	44.77	6.98	12.65	2.56	30.53
8854.75	153.85	53.17	5.94	0.02	0.73	30.55
8855.13	96.65	37.17	6.06	9.42	0.31	28.61
8855.42	91.20	36.23	7.15	12.23	7.52	24.96
8855.75	86.41	40.20	6.16	10.68	1.25	25.48
8856.08	113.91	47.15	6.71	4.34	7.71	24.26
8856.75	75.21	50.56	4.94	13.13	10.79	30.78
8857.13	62.74	15.79	2.40	0.11	1.65	11.71
8857.42	64.70	30.85	4.93	18.93	6.52	23.43
8857.58	70.48	38.80	3.54	9.67	5.67	23.36
8857.75	87.72	27.14	3.51	6.97	5.55	21.75
8857.92	140.49	63.78	5.00	7.65	12.76	41.36
8858.08	161.69	60.03	5.31	16.16	18.54	38.82
8858.25	162.93	63.88	5.68	4.58	10.17	43.98
8858.42	156.32	69.35	6.02	15.95	20.93	44.69
8859.54	104.48	58.83	5.52	11.12	14.26	38.84
8859.58	107.67	54.54	6.19	5.39	7.98	38.81
8859.75	111.78	59.94	5.61	5.08	18.68	40.05
8859.92	118.29	53.66	6.12	10.66	11.63	33.56
8860.00	128.48	55.02	6.60	17.21	15.52	38.50
8860.08	109.60	56.81	5.73	3.69	7.04	38.38
8860.25	125.32	50.65	5.52	10.96	14.98	32.81
8860.42	114.26	55.05	5.13	8.53	9.18	38.42
8860.75	121.26	50.32	4.95	7.12	9.27	33.25
8860.92	139.85	55.52	5.09	10.93	15.30	41.03
8861.08	126.38	53.47	4.85	7.56	14.03	35.16
8861.42	119.49	47.15	4.65	16.74	16.28	33.89
8861.58	145.20	65.33	4.94	9.88	24.09	38.55
8861.75	122.54	60.18	4.65	6.42	13.85	37.97
8861.92	126.64	53.13	5.22	1.54	8.65	33.61
8862.08	134.87	51.85	5.09	20.24	16.32	35.65
8862.42	99.72	59.29	4.81	5.74	8.58	34.16
8862.58	100.04	55.20	5.25	9.96	6.37	33.52
8862.75	93.15	47.87	5.19	13.44	11.21	43.08
8862.92	85.42	42.23	4.68	6.21	6.44	29.04
8863.08	78.88	38.51	4.66	0.46	5.43	27.52
8863.25	120.04	46.80	4.50	10.57	10.33	24.29
8863.42	87.84	41.41	4.23	15.56	7.96	26.19

8863.58	92.75	43.06	4.11	8.90	1.16	27.61
8863.75	89.36	34.76	4.14	9.80	3.19	26.71
8863.92	87.85	39.30	4.32	6.44	8.03	25.48
8864.08	84.81	40.03	3.63	3.21	3.67	27.37
8864.58	97.84	41.51	3.92	4.51	8.72	26.65
8864.75	91.24	42.16	3.79	3.77	5.86	31.95
8864.92	100.74	42.56	3.45	5.70	5.90	25.91
8865.25	85.93	43.60	3.83	3.08	6.46	29.30

Appendix F: Core 2 XRF Data

Core 2 XRF Data						
Depth (ft)	**V (ppm)**	**Ni (ppm)**	**Th (ppm)**	**U (ppm)**	**Mo (ppm)**	**Cu (ppm)**
11685.25	32.48	13.61	2.12	5.80	0.69	7.51
11685.75	38.15	13.23	1.97	5.73	1.80	9.35
11686.58	35.30	17.54	3.06	22.60	4.75	3.23
11686.92	30.25	15.40	2.36	13.02	5.59	5.47
11687.08	35.44	18.52	2.50	16.63	4.55	4.16
11687.25	40.35	11.06	2.59	7.11	0.24	4.02
11688.92	27.67	7.02	2.34	6.72	3.55	5.28
11689.25	34.37	9.51	2.26	9.20	2.48	2.76
11689.75	32.60	14.06	1.87	7.05	0.04	2.97
11690.25	41.66	11.30	2.47	8.86	4.62	6.21
11690.75	31.21	17.09	2.24	12.13	1.75	8.42
11691.08	35.23	18.67	2.52	13.83	4.59	6.21
11691.75	38.89	36.37	3.61	3.38	2.72	11.77
11691.92	34.70	13.98	2.89	2.29	0.87	2.79
11692.25	27.90	13.85	2.56	18.83	0.32	2.89
11692.75	33.84	10.45	2.68	7.57	0.05	5.74
11692.92	26.57	14.63	2.53	12.50	4.77	5.54
11693.08	27.03	16.85	2.31	5.96	1.30	4.92
11693.25	20.81	9.51	2.50	7.89	0.71	5.48
11693.58	31.72	16.37	2.64	8.79	2.42	2.62
11693.92	40.36	23.93	2.74	14.46	4.08	1.75
11694.42	30.61	19.78	2.06	7.53	5.32	3.93
11694.58	32.12	13.17	2.51	11.15	5.34	2.73
11695.08	29.31	14.66	1.92	5.05	0.13	3.37

11695.25	32.02	13.91	2.61	7.14	5.75	3.39
11695.58	38.07	18.84	2.68	8.14	2.03	5.88
11695.75	5.25	28.05	3.63	5.16	0.42	5.85
11698.25	39.74	14.84	1.95	4.06	1.85	4.58
11698.58	33.72	14.63	1.91	2.52	2.55	3.95
11700.08	25.94	16.69	2.69	13.60	8.59	7.54
11700.58	27.78	10.89	2.51	8.52	3.46	3.62
11701.08	40.19	18.04	2.25	6.81	2.73	4.15
11702.75	41.48	13.29	2.34	19.57	0.53	3.56
11703.25	33.80	11.11	2.03	9.79	2.70	2.80
11703.75	35.05	10.83	2.31	16.55	5.26	5.52
11704.08	32.97	19.13	2.26	8.76	2.58	4.67
11704.58	34.38	9.99	2.28	1.90	1.12	4.68
11704.92	36.25	10.39	2.16	9.47	2.01	5.24
11705.08	27.62	12.08	2.07	4.56	1.57	3.20
11705.25	30.29	12.06	2.05	2.45	0.53	2.29
11707.75	36.00	16.76	2.60	0.65	1.85	6.90
11708.58	24.03	8.88	1.84	9.16	0.64	3.56
11708.75	48.23	6.24	1.96	5.24	4.70	2.24
11709.25	29.38	16.46	2.27	10.68	2.99	3.58
11709.58	37.11	20.05	2.04	5.28	2.89	3.93
11710.42	35.16	18.79	2.01	7.52	6.59	1.25
11710.58	16.05	24.75	1.88	12.32	1.56	3.54
11710.92	40.85	13.54	1.84	12.48	4.00	3.29
11711.42	23.99	17.58	2.53	7.37	3.68	6.00
11711.75	37.15	14.27	2.04	15.78	4.14	5.62
11711.92	46.64	17.73	2.01	4.16	1.55	2.17
11712.75	40.08	20.72	2.20	1.98	2.40	5.95
11712.92	39.93	21.91	2.26	5.59	2.12	5.76
11713.08	29.66	16.61	1.93	6.16	0.07	2.07
11713.92	1.95	47.54	3.98	5.36	3.17	13.02
11714.08	1.33	42.30	6.18	2.42	0.21	13.97
11714.42	28.22	26.83	2.65	6.73	0.80	1.73
11714.92	40.21	27.43	2.56	8.11	4.85	7.84
11715.25	29.10	43.08	4.20	20.77	4.12	12.66
11715.58	38.84	26.76	2.00	5.84	3.19	3.81
11715.75	32.92	23.53	3.09	12.70	2.60	7.55
11717.08	35.26	51.57	4.45	9.40	3.10	16.26
11717.58	40.66	23.66	2.27	15.55	2.22	4.76

11717.92	39.73	9.51	2.28	8.09	0.34	3.23
11719.08	31.73	14.89	2.17	8.06	4.92	2.87
11719.42	33.96	24.88	2.31	5.61	7.27	6.39
11719.92	33.29	24.64	2.45	9.36	2.66	2.04
11720.42	30.99	19.59	2.85	15.06	6.06	5.18
11720.92	37.39	17.48	1.81	7.77	6.17	3.37
11721.08	25.89	57.86	2.89	14.03	8.85	20.77
11721.25	37.05	40.56	2.69	10.19	6.01	11.42
11722.08	26.03	46.18	3.89	22.05	14.81	16.18
11722.25	4.71	95.50	5.40	17.17	22.45	31.38
11722.58	28.29	53.02	3.32	3.39	10.26	18.49
11722.75	37.10	18.46	1.84	0.88	6.14	10.68
11722.92	35.82	16.21	1.70	5.71	7.31	2.43
11723.08	27.22	42.97	3.54	12.94	11.22	13.68
11723.25	36.50	50.53	2.79	19.69	10.46	16.15
11723.42	12.53	89.55	5.19	15.89	18.14	35.21
11723.58	29.77	44.73	3.26	8.41	11.17	16.43
11723.75	21.12	38.51	3.11	22.27	13.71	11.76
11723.92	31.43	33.79	2.29	9.83	9.09	9.85
11724.08	49.18	14.97	1.81	8.54	5.90	4.95
11724.25	51.31	32.15	1.60	1.30	7.09	3.50
11724.42	39.51	30.27	2.78	1.16	5.08	10.25
11724.58	30.14	13.61	1.62	1.95	6.67	4.38
11724.75	28.91	32.49	2.64	8.21	6.60	7.89
11725.08	36.59	23.21	2.34	9.10	7.90	7.80
11725.25	56.13	18.07	2.22	16.30	6.50	7.88
11725.42	14.44	41.46	3.04	11.80	10.41	17.76
11725.75	32.92	17.57	2.19	8.57	4.51	7.48
11725.92	21.56	40.39	2.79	12.15	6.97	14.02
11726.08	46.62	17.14	1.88	15.34	2.42	4.58
11726.58	36.18	10.38	1.92	8.69	1.38	5.28
11726.92	13.48	49.74	3.51	12.09	13.73	15.78
11727.08	41.46	31.13	3.11	22.32	11.81	12.76
11727.25	40.24	54.05	3.57	20.43	6.53	16.99
11727.75	25.81	49.44	3.86	3.85	6.95	17.72
11727.92	39.40	19.03	1.79	0.09	10.20	3.35
11728.08	42.09	21.53	2.03	10.36	4.47	8.35
11728.25	2.23	32.16	3.29	12.67	4.87	11.34
11728.42	3.12	52.94	3.74	5.63	15.79	17.94

11728.58	23.78	22.59	2.30	9.74	4.44	8.35
11729.25	41.50	29.23	2.75	8.58	3.80	6.01
11729.42	19.46	43.53	2.99	8.05	0.08	17.42
11729.92	37.13	37.96	2.92	2.61	3.08	18.58
11730.25	43.39	16.29	1.65	0.66	5.46	6.45
11730.92	47.24	25.56	2.76	9.87	5.47	8.57
11731.25	40.24	29.71	2.77	10.63	4.55	12.04
11731.42	10.82	62.54	4.05	4.18	0.52	22.96
11731.58	16.52	37.35	3.08	0.12	2.21	14.94
11731.75	15.35	28.57	2.69	12.02	4.89	11.61
11731.92	29.81	22.13	2.39	9.68	3.82	10.95
11732.08	37.95	12.14	1.99	4.27	2.56	1.55
11732.42	49.65	33.11	2.66	16.40	3.76	10.94
11732.58	35.79	31.95	2.56	0.48	2.39	10.35
11732.75	43.53	29.11	2.43	1.87	0.12	5.73
11732.92	28.40	32.39	2.42	1.04	2.68	7.71
11733.08	30.91	34.47	2.73	11.25	0.76	12.86
11733.25	25.23	47.95	2.92	12.39	4.56	15.05
11733.42	34.49	31.93	2.52	11.79	9.93	13.15
11733.58	34.84	23.89	2.37	7.72	6.69	10.04
11734.08	31.91	31.46	2.80	0.08	0.97	13.02
11734.25	37.05	32.51	2.53	7.62	1.96	10.82
11734.42	31.93	29.73	3.06	14.65	7.91	7.69
11734.58	43.34	33.87	2.27	17.43	4.01	12.09
11734.75	24.58	55.53	3.93	12.46	9.50	21.45
11734.92	44.13	32.55	2.57	11.23	1.88	13.91
11735.08	57.97	28.46	2.91	16.72	6.67	12.69
11735.25	46.49	22.73	2.15	4.02	10.38	11.21
11735.58	66.12	37.52	2.58	1.92	1.69	12.21
11735.75	44.69	36.09	2.57	3.95	2.73	7.54
11736.08	49.25	17.20	1.74	4.43	6.50	6.57
11736.25	17.63	121.35	5.92	13.83	20.82	55.42
11736.42	49.53	48.41	2.82	0.37	9.80	16.10
11736.58	41.83	17.40	1.64	8.58	7.29	8.46
11736.75	39.38	16.09	1.75	8.26	6.55	5.75
11737.25	52.26	24.92	2.23	4.05	0.01	9.96
11737.42	48.05	19.04	2.07	2.88	1.18	5.07
11737.75	41.68	28.44	2.53	6.45	7.28	9.91
11737.92	16.85	39.39	3.71	6.42	9.60	17.16

11738.08	34.29	45.67	3.33	5.48	4.46	19.11
11738.25	67.27	32.40	2.07	8.43	3.73	7.44
11738.58	62.66	22.31	1.69	9.21	4.15	1.24
11738.75	89.52	32.51	2.38	13.24	16.25	11.97
11738.92	62.35	57.27	2.82	13.99	14.79	22.15
11739.08	59.55	30.91	2.09	5.01	2.09	8.81
11740.08	66.62	29.50	2.19	2.57	0.49	8.68
11740.42	54.04	19.63	2.03	9.16	2.47	5.98
11741.08	64.07	27.62	2.44	0.49	3.54	7.20
11741.25	48.21	38.09	3.62	11.44	5.95	12.07
11741.58	135.06	7.93	1.57	13.42	6.59	2.50
11741.92	51.60	17.84	1.57	6.56	7.47	2.98
11742.92	98.76	13.16	1.94	1.21	3.73	6.20
11744.08	43.96	18.25	2.31	0.54	2.07	2.75
11744.42	88.27	18.49	1.72	3.15	10.40	6.58
11744.58	66.49	8.71	1.49	6.75	3.27	1.63
11744.92	67.50	7.59	1.76	5.17	7.27	0.09
11745.08	124.62	3.99	1.48	3.42	10.11	2.64
11745.25	149.40	9.20	1.70	7.85	14.71	2.35
11745.75	127.12	13.83	1.76	6.03	8.44	4.92
11745.92	146.69	14.09	1.91	5.27	8.58	1.02
11746.08	141.67	13.64	1.69	7.75	14.57	3.65
11746.25	101.74	19.07	2.61	15.69	6.14	11.65
11747.25	68.75	11.88	2.05	3.01	2.22	5.84
11747.92	56.06	7.76	1.88	3.84	0.31	2.03
11750.42	74.53	23.53	2.95	11.38	4.24	9.89
11750.58	144.75	18.35	2.53	3.89	14.09	6.23
11750.75	165.48	7.74	1.61	13.06	11.04	2.35
11750.92	109.79	13.57	1.59	0.13	3.33	4.38
11751.08	89.12	18.60	1.75	7.89	9.96	7.71
11751.25	98.75	19.64	1.73	8.18	14.96	2.86
11751.42	100.19	17.33	1.68	10.90	5.63	2.37
11751.58	70.81	24.27	1.50	5.64	6.14	7.92
11751.75	90.93	17.49	1.48	2.21	7.21	4.68
11751.92	80.87	19.01	1.58	2.39	13.52	4.65
11752.08	80.15	29.81	1.96	0.31	13.39	10.77
11752.25	68.49	25.59	1.83	2.49	9.34	13.28
11752.42	79.14	29.54	1.96	9.36	21.50	11.63
11752.58	76.32	47.70	2.75	14.72	39.27	21.52

11752.92	92.60	90.68	2.92	9.53	50.47	32.93
11753.25	70.56	32.26	1.61	2.70	11.37	12.21
11753.42	67.32	28.06	1.73	6.36	6.91	10.59
11753.58	69.48	26.80	1.63	2.09	11.67	13.56
11754.08	55.33	14.37	1.59	9.06	4.69	4.79
11754.75	62.83	15.45	1.89	14.29	7.52	3.98
11754.92	49.71	16.70	1.84	12.55	7.92	3.13
11755.08	62.93	162.42	5.21	13.71	181.75	83.31
11755.25	72.07	42.70	2.17	18.70	30.21	16.87
11755.42	76.22	82.71	2.53	16.46	68.76	28.31
11755.58	88.17	61.46	1.70	15.85	34.73	14.22
11755.75	115.02	209.00	3.31	23.94	120.81	56.41
11756.08	41.64	11.36	1.80	6.78	6.05	3.98
11756.25	149.60	19.12	2.00	8.94	4.68	5.00
11756.42	70.60	32.61	2.11	10.80	8.83	16.45
11756.58	50.59	13.08	1.58	2.41	4.45	3.52
11757.08	56.15	38.90	2.22	13.86	8.86	17.11
11757.25	49.30	21.75	1.87	2.95	0.75	1.87
11757.42	47.84	10.12	1.87	4.98	4.93	6.94
11757.58	58.65	10.71	1.80	9.33	0.51	5.43
11757.75	47.43	43.72	2.41	12.83	4.51	15.69
11757.92	57.56	18.25	1.78	3.08	1.26	5.73
11758.42	45.28	60.69	3.61	10.53	6.88	21.99
11758.58	42.12	14.46	1.88	8.35	5.14	3.97
11758.92	53.81	30.83	2.26	10.10	0.54	12.78
11759.42	32.11	15.02	1.55	5.59	8.31	6.39
11759.58	32.04	16.04	1.59	0.80	3.42	0.68
11759.92	44.61	53.15	3.30	1.92	4.89	19.91
11760.08	72.33	45.43	2.87	12.51	6.24	17.12
11760.42	66.51	21.67	1.43	1.12	6.10	5.69
11760.58	53.36	57.51	3.18	17.33	13.32	14.50
11760.75	53.91	36.78	2.17	9.51	7.36	12.60
11760.92	42.74	36.82	2.20	6.82	1.60	11.67
11761.08	63.41	45.61	2.88	11.98	7.74	23.22
11761.25	66.75	23.87	2.03	10.79	1.60	7.80
11761.42	55.17	12.72	1.64	5.90	1.53	2.14
11761.58	41.16	16.20	1.41	0.47	0.87	3.52
11761.75	45.62	15.40	1.72	4.30	6.17	3.91
11761.92	55.76	27.50	2.07	10.42	5.81	7.35

11762.25	49.57	38.89	2.50	5.54	6.43	9.46
11762.42	39.57	60.07	3.39	9.66	3.67	26.37
11762.58	36.87	65.79	3.47	8.70	6.74	32.98
11762.92	48.84	25.69	1.86	4.27	6.37	3.16
11763.42	56.33	35.21	2.58	10.45	7.76	13.97
11763.75	51.64	54.05	3.00	10.08	7.84	22.44
11764.42	52.76	25.28	2.13	16.94	9.07	8.69
11764.75	39.86	32.25	2.18	13.91	7.75	8.59
11765.08	57.54	14.22	1.74	3.86	0.40	0.92
11765.42	43.94	56.85	3.31	6.58	9.14	22.78
11765.58	63.07	39.50	2.95	11.83	10.40	14.79
11766.75	46.23	14.75	2.07	9.62	7.05	5.33
11767.08	51.19	65.12	3.64	8.91	13.34	22.31
11767.42	60.95	54.96	3.46	12.22	18.23	25.13
11767.58	70.00	30.60	2.36	6.48	13.98	11.20
11767.92	71.00	28.30	2.17	4.11	13.03	11.23
11768.08	63.61	59.94	3.33	5.46	15.70	17.58
11768.42	48.90	25.51	2.00	18.87	10.78	6.55
11768.58	54.78	33.01	2.08	2.12	6.64	12.18
11768.75	55.01	31.27	2.57	3.94	6.28	12.06
11769.08	58.87	45.55	3.39	2.52	5.43	18.39
11769.25	71.16	49.96	4.31	7.98	4.03	20.96
11769.42	65.36	48.11	4.61	0.48	1.25	19.20
11769.58	79.16	46.84	4.68	9.25	7.66	20.73
11769.92	70.47	41.60	4.36	4.43	1.48	17.63
11770.08	76.22	40.26	4.63	19.95	3.69	17.27
11771.08	51.98	37.01	4.07	14.39	2.62	15.99
11771.25	50.04	26.58	3.20	11.53	1.95	14.19
11771.58	57.45	10.36	1.86	6.04	4.38	3.56
11772.08	51.63	20.02	2.46	6.34	0.25	9.89
11772.42	81.11	49.45	4.69	8.29	7.54	20.54
11772.58	78.88	50.24	5.44	15.64	4.47	26.03
11772.75	77.19	42.57	4.81	8.08	1.64	18.94
11772.92	74.87	48.36	4.86	12.88	8.68	26.09
11773.42	103.97	43.79	5.11	3.69	0.07	26.58
11773.75	90.90	60.95	4.84	7.02	2.06	26.97
11773.92	96.61	49.04	4.70	16.43	7.92	23.86
11774.08	100.87	49.73	4.89	8.76	5.73	26.63
11774.25	94.51	50.16	4.46	10.47	3.08	28.77

11774.42	114.61	54.99	4.68	14.16	7.43	27.08
11774.92	50.87	42.91	4.09	12.68	2.48	13.10
11775.58	59.58	18.16	2.53	9.12	3.63	5.82
11775.75	44.83	12.53	1.98	1.90	7.94	3.66
11776.42	49.69	47.80	4.46	8.16	1.35	25.39
11777.08	67.38	29.93	3.09	11.36	3.30	11.19
11777.25	65.27	36.33	3.60	4.70	2.71	17.21
11777.92	42.74	56.20	4.49	14.40	6.87	19.72
11778.08	61.12	40.22	3.08	5.10	5.02	11.12
11778.25	70.66	35.60	2.56	11.42	6.02	12.22
11778.58	64.10	37.49	3.15	4.44	4.16	10.01
11778.75	69.06	45.02	3.08	0.71	7.21	23.16
11778.92	61.93	23.87	3.09	14.24	2.34	6.00
11779.08	69.32	52.50	4.16	1.61	1.34	23.25
11779.25	56.09	55.61	5.45	9.67	1.76	24.56
11779.42	61.58	52.49	4.23	22.81	2.07	19.89
11779.75	56.35	31.45	3.25	10.95	10.65	10.07
11779.92	52.01	8.97	2.45	6.86	4.39	6.52
11780.08	51.99	18.83	1.94	1.67	0.33	5.77
11780.58	37.25	47.72	4.53	19.13	1.35	18.30
11780.75	47.76	51.51	4.91	2.80	0.56	23.46
11780.92	34.98	36.65	3.42	9.08	2.10	11.80
11781.08	43.27	22.57	3.07	14.92	4.90	14.47
11781.25	42.52	28.14	3.40	17.58	8.36	10.35
11781.42	44.04	26.23	2.84	8.63	9.33	5.58
11781.58	47.26	13.74	2.54	6.97	10.23	5.25
11781.92	45.57	24.18	2.29	4.09	4.14	9.13
11782.08	39.10	65.63	3.65	4.58	50.18	23.40
11782.25	45.30	66.31	3.41	5.15	28.17	17.76
11782.42	57.96	48.73	2.63	7.61	24.15	12.05
11782.58	114.87	38.26	5.24	11.52	8.27	21.94
11782.75	88.81	46.76	5.09	7.34	0.41	21.27
11782.92	107.38	50.54	5.57	8.86	6.88	20.06
11783.08	64.30	53.45	5.90	8.09	1.11	23.68
11783.25	86.11	47.67	6.02	8.23	0.66	24.62
11783.58	62.05	34.70	4.70	8.69	1.73	14.46
11784.08	150.20	56.41	7.11	5.56	7.25	24.61
11784.25	140.87	52.12	6.97	3.73	3.69	25.44
11784.42	186.27	63.09	7.68	9.46	7.12	32.84

11784.92	230.78	57.74	7.01	7.77	2.91	28.96
11785.25	174.14	66.15	7.44	8.92	1.15	27.17
11785.42	203.92	68.38	7.74	16.69	7.30	30.64
11785.58	131.80	51.54	6.96	14.05	9.03	25.06
11785.75	127.68	60.23	6.73	4.04	1.22	25.32
11785.92	120.92	53.25	5.73	17.02	7.02	21.85
11787.08	56.51	22.25	2.12	0.51	2.62	7.74
11787.42	56.18	24.76	3.25	1.18	2.43	11.13
11788.08	86.35	47.87	5.45	4.43	2.22	27.04
11788.25	119.08	45.83	5.51	11.93	2.41	24.55
11788.42	107.61	47.03	5.52	8.26	1.89	22.44
11788.58	136.60	49.69	6.10	7.23	7.89	23.61
11788.75	101.71	60.16	3.88	15.08	22.20	21.68
11788.92	121.93	53.41	5.53	10.52	10.09	21.06
11789.08	151.36	49.98	5.53	0.95	5.49	25.36
11789.25	170.76	47.52	5.61	11.36	10.33	22.87
11789.75	153.13	50.68	5.92	12.21	11.09	29.80
11789.92	151.17	47.87	5.16	4.57	5.21	25.38
11790.08	151.78	48.58	5.32	5.08	0.63	21.97
11790.92	100.54	55.00	5.10	11.62	9.70	23.75
11791.08	112.36	52.10	5.16	13.10	0.17	22.99
11791.58	69.53	40.85	5.81	17.03	7.92	19.01
11791.75	44.33	59.87	4.87	8.88	5.71	27.18
11792.08	53.32	30.43	3.17	16.20	6.75	15.09
11792.25	45.45	32.05	3.42	1.93	2.13	16.73
11792.42	54.44	34.62	3.68	9.98	7.78	18.54
11792.58	43.84	42.93	4.24	12.75	1.17	19.39
11792.75	47.42	45.55	4.19	14.07	11.03	22.01
11792.92	38.33	31.74	3.45	3.56	2.79	16.37
11793.25	33.46	40.47	4.09	10.48	5.39	17.38
11793.42	20.89	49.44	6.03	0.07	0.33	23.94
11793.58	53.49	44.63	5.72	7.10	1.44	25.06
11794.58	41.93	33.27	4.20	5.38	1.48	22.24
11794.75	52.38	37.88	4.09	8.80	6.47	21.11
11794.92	35.85	37.64	4.40	7.71	1.19	19.90
11795.08	50.27	33.50	4.08	5.50	1.90	17.03
11795.25	50.02	28.05	3.01	12.47	2.60	10.10
11795.58	38.65	46.36	4.96	13.51	0.86	22.57
11795.75	48.02	41.47	4.25	1.66	5.18	14.75

11796.42	40.52	44.05	3.85	16.67	3.63	15.48
11797.08	54.38	33.63	3.97	11.22	7.13	20.04
11797.25	51.40	43.02	4.30	14.29	0.81	21.44
11797.42	44.32	37.39	3.89	13.26	5.47	17.83
11797.92	41.53	35.58	3.96	13.37	3.04	17.34
11798.25	46.56	27.21	3.36	5.90	5.41	12.84
11798.42	46.39	32.19	3.50	10.52	9.13	12.43
11798.75	42.07	44.09	3.90	3.44	0.76	19.99
11798.92	36.80	30.31	3.66	10.71	3.21	17.88
11799.08	40.82	38.40	3.86	9.16	1.21	19.62
11799.42	42.88	16.72	2.30	0.55	1.58	10.52
11799.58	46.68	46.23	4.01	3.24	7.43	19.40
11800.08	50.93	41.95	4.09	16.16	4.91	22.28
11800.58	61.32	50.84	3.80	5.35	0.28	20.09
11800.75	44.65	43.40	3.27	8.49	3.48	13.90
11800.92	46.28	56.01	4.66	18.52	2.92	26.03
11801.25	68.01	57.43	5.58	11.24	9.80	22.37
11801.42	57.76	35.61	3.86	11.35	4.02	18.60
11801.58	42.61	38.26	4.00	10.99	4.33	18.54
11801.75	41.44	50.00	4.36	3.06	0.40	28.76
11802.08	48.69	48.49	5.01	16.99	6.90	23.79
11802.42	56.40	46.89	4.67	6.02	3.79	22.32
11802.58	59.85	47.83	4.90	10.40	7.06	21.46
11802.75	49.57	44.21	4.65	11.86	6.53	22.29
11802.92	42.63	42.15	4.47	11.88	6.31	24.24
11803.25	42.37	55.94	4.44	7.11	4.86	27.43
11803.42	64.15	56.66	4.32	9.49	5.71	21.91
11803.58	53.31	46.26	4.36	9.31	5.05	22.82
11804.08	42.27	46.43	4.39	6.21	0.97	23.67
11804.25	56.22	51.19	3.88	10.88	3.85	27.49
11804.42	58.41	42.70	3.62	3.91	3.26	19.18
11804.58	57.92	46.12	3.48	2.90	0.97	23.89
11805.25	60.49	36.25	3.04	9.25	2.62	20.01
11805.92	72.58	53.70	3.36	0.32	1.42	27.38
11806.08	62.98	43.10	3.08	4.86	1.74	16.81
11806.42	53.20	22.90	1.93	1.58	7.05	2.33
11806.58	51.31	39.84	3.60	11.20	5.08	17.00
11806.75	53.18	54.89	4.05	25.52	4.06	22.78
11807.08	55.81	47.48	3.90	28.59	6.18	23.33

11807.25	65.45	52.81	4.11	14.97	2.50	26.09
11807.58	53.66	45.18	4.22	2.12	4.15	26.48
11807.75	55.03	46.93	3.69	7.93	3.65	22.26
11807.92	52.24	41.80	3.97	13.36	0.01	19.01
11808.08	41.59	44.73	3.94	13.38	1.78	22.15
11808.25	48.28	44.42	4.37	8.08	4.17	24.94
11808.42	36.17	52.08	4.27	7.21	1.72	23.44
11808.58	57.81	45.21	3.81	12.71	6.34	24.29
11808.75	57.54	52.84	4.38	8.48	3.07	23.86
11809.08	62.92	50.43	3.45	3.81	1.34	23.90
11809.25	71.82	63.16	4.00	6.17	3.77	29.49
11809.42	66.61	52.93	4.36	9.87	6.96	28.51
11809.58	66.15	57.43	4.40	7.62	5.85	31.53
11809.75	65.12	54.56	4.61	18.75	4.39	25.42
11809.92	47.07	16.33	1.86	3.48	2.93	6.61
11810.42	66.99	47.97	4.40	21.09	3.09	26.35
11810.58	65.66	61.06	4.35	8.37	9.27	30.02
11810.75	67.23	44.42	3.60	8.79	4.14	24.22
11811.08	85.99	53.23	4.44	18.49	9.33	25.47
11811.25	105.88	63.89	5.02	13.56	13.60	26.57
11811.42	90.23	45.92	3.44	10.88	3.34	27.87
11811.58	83.66	51.23	3.87	13.10	3.65	25.75
11811.75	91.37	53.62	3.50	8.73	4.92	17.13
11811.92	80.69	53.77	4.54	8.54	5.37	25.62
11812.08	76.93	44.87	4.07	8.43	1.92	25.88
11812.25	74.56	50.01	4.03	18.01	5.01	23.04
11812.75	51.68	56.65	4.65	15.71	6.75	27.55
11813.25	80.74	46.05	3.52	11.83	4.20	21.05
11813.42	83.75	48.51	3.58	0.95	2.02	22.96
11813.58	80.82	45.75	3.70	1.55	3.41	24.93
11813.75	90.62	53.14	3.51	5.22	4.45	19.34
11814.08	129.61	76.37	4.42	7.93	15.17	37.28
11814.42	115.98	65.62	3.88	13.85	9.81	35.93
11814.58	153.53	66.65	4.05	10.87	0.94	30.45
11814.75	116.56	76.02	2.86	0.71	8.53	32.11
11814.92	205.98	113.13	4.28	10.45	22.00	50.96
11815.08	134.25	83.71	4.35	15.73	9.89	32.96
11815.25	114.62	59.79	4.39	13.08	7.06	26.31
11815.42	78.86	43.94	3.96	10.92	0.62	23.41

11815.58	81.72	54.10	4.06	4.80	3.64	25.17
11815.92	76.70	52.89	3.94	15.09	7.71	28.85
11816.42	111.80	44.38	3.19	11.49	6.82	24.63
11816.58	98.76	49.13	3.72	14.09	11.08	26.03
11816.75	114.94	49.16	3.49	6.71	4.87	22.16
11816.92	83.99	32.63	2.90	6.96	4.85	17.00
11817.08	151.68	66.71	4.52	1.62	6.52	36.08
11817.25	151.00	60.27	4.58	8.60	14.87	35.07
11817.42	110.68	39.29	3.60	13.37	17.43	18.97
11818.08	88.94	18.19	3.47	10.07	13.33	13.28
11818.25	163.65	76.56	4.88	2.64	13.79	39.72
11818.58	161.21	66.62	3.93	3.36	8.83	31.83
11818.92	152.88	56.72	4.07	10.62	15.64	28.14
11819.08	145.12	60.56	4.25	9.21	13.55	27.35
11819.25	147.08	63.57	4.21	12.71	12.81	28.38
11819.42	143.37	59.10	4.31	17.35	13.42	30.27
11819.58	181.87	66.60	4.25	9.85	13.47	38.84
11819.92	152.34	62.90	4.16	7.64	12.87	36.89
11820.08	159.61	83.71	4.90	16.51	13.16	48.24
11820.25	169.64	66.57	4.57	12.65	11.20	38.08
11820.42	130.78	50.60	4.39	9.38	8.18	30.08
11820.58	126.89	52.04	3.58	1.05	2.84	36.06
11820.75	109.91	49.72	4.11	6.41	7.40	28.60
11821.08	111.50	44.36	3.83	16.32	3.16	24.95
11821.25	85.59	41.57	3.57	0.94	5.58	28.61
11821.42	95.35	42.91	3.47	2.79	0.62	23.84
11821.58	81.18	35.15	3.56	9.30	2.15	21.93
11821.75	73.43	25.51	2.74	2.47	0.26	8.52
11821.92	60.58	16.03	2.16	4.12	6.61	8.74
11822.08	65.92	37.56	4.00	0.36	3.08	20.18
11822.25	62.50	35.83	4.04	5.04	4.21	25.95
11822.42	59.84	37.02	3.71	11.00	1.95	16.07
11822.75	56.23	51.00	6.09	12.17	7.57	29.46
11822.92	41.81	40.16	6.08	8.50	3.09	26.48
11823.08	48.21	50.60	6.57	8.49	8.76	25.99
11823.25	58.09	43.65	6.29	8.80	5.68	28.19
11823.42	67.47	37.50	5.10	3.06	1.56	27.71
11823.58	77.08	42.67	4.60	4.34	4.72	30.07
11823.75	91.53	59.02	5.13	8.36	12.59	25.75

11823.92	74.71	55.30	5.41	7.58	11.96	27.49
11824.08	86.04	52.94	5.61	4.47	9.25	28.25
11824.25	77.18	50.63	5.18	6.42	8.81	22.84
11824.42	70.71	45.56	5.75	13.31	8.19	30.57
11824.58	76.81	53.51	5.58	6.22	8.37	30.04
11824.75	71.96	51.62	5.71	6.72	9.53	32.75
11824.92	82.30	51.22	6.02	8.99	11.53	25.29

Appendix G: Core 3 XRF Data

Core 3 XRF Data						
Depth (ft)	**V (ppm)**	**Ni (ppm)**	**Th (ppm)**	**U (ppm)**	**Mo (ppm)**	**Cu (ppm)**
11134.42	31.95	18.35	2.62	8.38	0.49	13.01
11136.42	34.24	14.42	2.35	2.98	2.70	12.59
11136.75	8.88	50.33	5.76	4.74	6.18	24.84
11138.42	24.12	12.99	2.17	3.11	1.39	8.17
11139.08	42.63	9.88	3.00	8.04	1.63	13.48
11140.42	28.33	6.01	2.48	6.24	1.24	6.38
11141.08	28.26	23.44	3.02	21.64	4.09	9.56
11141.75	39.44	21.15	2.71	3.32	0.32	11.83
11142.42	21.36	18.46	3.42	2.90	0.61	6.49
11142.75	16.13	26.47	5.24	2.05	3.80	11.21
11143.08	44.41	19.42	3.64	6.19	1.73	7.97
11143.75	32.15	25.30	2.54	10.27	1.84	8.46
11145.75	41.49	85.33	5.53	10.68	3.22	28.19
11146.42	31.38	14.39	3.01	14.07	1.78	10.79
11147.08	37.73	10.23	2.32	8.59	3.91	7.26
11148.08	36.03	12.98	2.09	1.58	0.24	7.02
11149.75	30.97	9.32	2.25	2.84	3.50	5.68
11150.42	25.62	19.92	3.21	2.75	1.27	9.23
11152.42	55.01	9.47	2.22	6.47	1.23	7.10
11153.42	8.51	51.87	8.71	1.04	1.78	15.96
11154.42	37.72	19.40	2.43	10.22	1.43	11.29
11158.75	41.16	23.50	2.22	2.96	2.37	6.28
11159.42	33.37	19.52	2.16	16.33	3.46	6.35
11160.08	35.93	53.36	3.06	2.25	1.76	6.94
11161.08	33.03	26.69	2.38	0.18	0.87	11.25

11162.42	35.59	16.90	2.38	5.47	1.49	7.89
11164.42	33.04	8.19	2.62	1.50	3.78	6.43
11167.42	24.22	14.40	3.00	6.56	0.90	5.27
11168.42	26.17	9.57	2.79	5.75	5.42	7.08
11169.08	28.50	23.64	2.51	3.34	1.24	1.70
11169.42	23.69	10.52	2.47	5.23	0.80	3.71
11170.08	24.18	25.41	3.14	5.53	0.77	12.49
11170.42	6.81	43.79	4.73	9.52	1.94	17.53
11170.75	29.95	25.87	2.96	4.54	2.11	12.22
11175.75	35.09	11.63	2.51	5.23	0.55	10.29
11177.42	27.26	20.83	2.36	5.11	0.14	9.32
11178.42	25.35	47.44	6.49	2.60	2.61	31.18
11179.08	19.03	13.85	4.02	7.59	0.54	10.19
11180.42	26.00	12.81	3.63	5.37	0.48	10.64
11182.08	12.68	29.14	5.21	12.49	0.78	17.38
11183.42	19.69	27.16	4.26	4.69	2.06	17.48
11183.75	27.88	15.04	3.79	2.34	3.34	6.88
11184.08	32.34	27.57	3.84	5.11	3.56	13.01
11184.75	28.92	14.45	3.19	8.64	0.76	3.99
11186.08	19.73	21.56	4.68	9.45	1.12	12.19
11186.42	36.94	17.24	4.24	12.81	3.11	9.56
11188.75	11.75	14.00	3.87	7.44	0.44	13.90
11189.08	26.54	10.32	2.98	6.60	0.29	9.16
11189.42	27.41	17.94	3.41	4.76	4.09	4.05
11190.08	15.42	23.39	3.08	13.00	0.45	11.33
11191.08	30.12	16.31	3.99	6.52	0.47	14.24
11191.75	20.88	15.09	3.60	4.63	1.21	9.73
11192.08	30.60	23.01	4.00	18.83	4.12	11.41
11192.42	28.03	24.82	3.98	5.77	3.18	9.86
11192.75	17.14	30.43	4.96	5.38	4.30	14.58
11195.42	17.06	15.70	3.45	6.94	4.80	10.92
11195.75	8.78	34.61	6.24	6.78	5.97	19.58
11201.08	32.97	14.01	2.95	3.90	0.00	9.43
11201.42	20.61	19.44	3.56	1.26	0.03	17.86
11202.42	28.89	29.33	3.56	6.42	3.33	15.82
11202.75	27.88	23.43	3.85	8.92	0.19	12.22
11203.42	26.22	28.56	4.60	5.47	4.24	13.53
11204.08	21.60	19.96	3.41	6.85	2.90	9.41
11204.75	23.79	27.39	2.89	16.36	1.06	13.22

11205.58	19.00	29.08	3.60	2.03	3.22	9.97
11205.92	30.83	8.51	2.34	5.54	0.79	6.75
11206.92	26.37	15.90	3.63	7.71	5.10	7.23
11207.25	14.84	14.11	3.21	2.56	1.03	12.35
11207.75	36.49	19.32	3.24	9.10	1.53	10.08
11207.92	16.81	13.66	2.85	4.66	3.72	6.48
11208.75	28.15	10.46	2.83	7.66	0.60	7.82
11210.92	32.56	10.43	3.06	14.28	2.63	10.28
11211.08	28.22	20.50	3.03	2.45	0.54	6.54
11211.25	28.27	8.58	2.84	5.80	0.63	8.30
11211.42	23.23	34.13	3.68	5.28	2.73	14.34
11211.75	27.98	13.68	2.73	4.63	0.49	7.20
11212.75	31.17	19.24	2.80	11.18	2.93	11.95
11213.75	28.62	27.31	2.66	2.60	0.57	4.43
11213.92	26.09	17.69	3.17	9.18	3.11	7.71
11216.08	32.45	23.46	2.92	6.94	0.11	10.07
11216.58	19.53	15.22	3.23	1.71	0.32	7.79
11217.08	26.79	21.94	4.23	8.73	0.45	13.59
11218.58	17.59	34.27	4.23	0.22	2.47	11.66
11218.75	21.40	21.43	4.37	12.63	1.49	15.26
11219.25	33.89	20.71	2.78	6.04	1.22	7.59
11219.42	23.58	18.03	3.05	2.28	0.97	8.08
11219.92	20.63	28.50	4.06	17.61	6.60	16.29
11220.42	33.68	13.48	2.31	6.28	1.97	9.23
11220.58	32.29	24.03	2.26	5.24	1.49	5.41
11222.08	14.59	61.58	5.02	13.42	11.36	21.22
11222.58	30.01	24.10	2.93	6.98	3.34	13.07
11222.92	22.10	18.38	2.58	11.82	1.53	5.31
11223.25	36.52	26.94	3.08	11.72	7.32	16.30
11223.58	18.99	21.87	2.55	15.43	3.76	15.22
11223.92	16.84	32.72	3.07	9.38	7.57	13.91
11224.58	12.34	36.38	2.78	2.58	1.89	14.99
11225.75	13.19	32.39	2.90	10.28	0.41	10.73
11226.42	33.59	13.48	2.35	1.34	0.45	4.98
11226.58	27.18	18.67	2.43	0.49	0.34	8.73
11226.75	28.54	23.51	2.51	21.69	5.53	16.20
11227.08	31.70	19.74	2.48	6.52	4.46	3.48
11227.25	30.09	31.24	2.80	16.59	4.22	11.29
11227.42	10.09	45.52	3.43	15.30	9.53	18.26

11227.58	55.55	40.91	3.14	6.51	2.87	11.99
11227.75	30.74	16.68	2.48	9.23	7.68	12.92
11227.92	28.70	44.14	3.33	6.06	0.01	25.11
11228.25	21.79	41.52	3.36	16.16	7.48	19.26
11228.42	38.11	19.34	2.22	5.43	0.04	8.71
11228.58	29.12	15.44	2.23	5.87	3.46	11.08
11228.75	53.97	26.12	2.65	9.71	1.21	12.68
11228.92	28.16	28.43	2.25	1.51	1.63	8.65
11229.08	33.27	12.27	1.91	7.62	0.28	6.08
11229.42	29.70	24.92	2.69	8.05	0.74	10.84
11229.58	25.70	62.25	4.34	18.68	14.58	39.99
11229.75	33.42	39.70	2.56	12.43	1.65	15.79
11229.92	40.57	24.60	2.29	5.87	1.75	8.66
11230.08	41.26	53.44	3.68	9.96	5.32	19.47
11230.25	23.62	41.52	3.19	4.02	6.20	18.31
11230.58	37.58	15.93	2.09	2.60	3.29	9.26
11230.75	26.18	51.17	3.65	6.80	2.64	13.22
11231.08	28.92	43.51	3.77	9.79	8.23	27.34
11231.42	26.98	41.60	3.62	15.54	5.78	21.15
11231.58	27.11	38.22	3.79	5.20	1.69	23.84
11231.75	34.83	32.03	2.95	10.59	5.77	13.40
11232.42	36.21	12.24	2.26	3.54	1.15	11.33
11232.58	26.44	39.22	3.21	7.69	4.85	17.08
11234.08	47.41	15.35	2.63	6.89	3.06	5.06
11234.42	37.95	21.30	2.89	11.71	5.30	12.10
11234.58	6.39	48.10	3.54	10.62	5.22	27.63
11234.92	41.14	11.99	2.23	2.77	0.30	4.15
11235.25	16.81	23.35	3.02	10.66	8.11	15.54
11235.42	34.17	24.86	2.51	3.16	2.91	13.93
11235.92	23.28	39.34	4.03	12.02	8.79	23.83
11236.08	55.84	17.72	1.85	3.28	2.96	9.58
11236.25	22.58	50.36	4.11	16.70	12.65	25.02
11236.58	29.76	24.66	2.72	2.70	0.48	15.29
11237.08	9.75	26.96	3.35	4.66	4.59	14.72
11237.75	27.50	33.38	3.23	4.21	2.27	19.15
11237.92	12.52	45.33	4.52	6.87	1.63	28.15
11238.08	33.42	24.11	2.74	5.96	2.94	12.34
11238.25	36.52	24.36	2.57	8.24	1.12	9.84
11238.58	60.75	13.38	2.01	9.50	0.06	6.48

11238.75	37.38	41.54	3.95	5.79	3.89	20.31
11239.08	36.34	12.56	2.21	7.69	2.35	6.18
11239.42	35.61	35.19	3.49	5.53	7.24	17.83
11239.58	30.60	46.71	3.67	3.79	5.30	21.49
11239.92	35.09	13.03	2.55	12.20	6.09	3.93
11240.08	26.01	69.07	4.96	4.63	9.22	34.84
11240.25	23.78	56.37	4.07	4.90	7.28	30.24
11240.42	49.81	57.86	3.90	1.85	6.95	30.21
11240.58	43.04	40.23	3.52	4.66	13.75	24.08
11240.75	32.90	52.64	3.94	10.06	6.37	23.24
11240.92	34.03	20.75	2.54	8.15	1.87	14.75
11241.08	28.17	22.80	2.57	3.40	3.06	13.40
11241.25	32.41	12.92	2.29	8.66	2.25	9.73
11241.58	34.75	18.76	2.77	7.06	1.38	9.43
11241.75	24.62	26.03	2.51	10.44	4.23	8.28
11241.92	25.55	31.79	2.92	10.20	11.01	17.00
11242.08	27.29	47.22	3.60	6.23	13.68	20.82
11242.42	49.22	12.48	2.03	5.09	0.14	10.09
11242.92	52.27	25.20	2.40	5.04	6.08	10.12
11243.25	31.87	20.26	2.83	0.90	3.47	11.64
11243.75	61.16	39.67	2.41	1.94	6.01	29.80
11243.92	52.30	37.01	2.63	9.59	7.59	26.97
11244.08	59.01	21.38	1.93	2.49	1.41	8.32
11244.42	47.54	45.45	2.56	10.19	6.73	18.89
11244.58	47.27	53.84	3.03	2.22	9.35	29.75
11244.75	48.05	15.47	2.00	8.80	0.92	10.03
11245.25	55.92	12.59	1.93	13.28	1.51	11.05
11245.42	32.21	15.53	2.00	4.66	1.29	9.84
11245.92	42.61	24.28	2.80	5.56	4.85	21.74
11246.08	43.10	26.05	2.45	10.70	5.17	10.52
11246.42	39.39	13.00	2.23	0.53	2.48	5.45
11246.75	48.86	22.68	1.70	3.72	2.51	6.10
11246.92	24.01	62.36	3.79	7.54	8.76	39.88
11247.58	47.32	14.89	2.11	12.98	4.31	6.27
11248.25	42.45	6.49	1.83	10.09	0.75	10.72
11248.42	40.91	10.97	2.03	0.97	0.63	8.35
11248.92	35.47	13.85	1.95	4.09	1.89	9.42
11249.25	49.43	39.01	2.47	2.29	2.56	28.15
11249.42	58.19	58.15	3.55	9.37	14.13	28.27

11249.92	61.03	11.98	2.51	6.18	2.38	5.52
11250.08	59.15	10.89	2.52	11.59	0.14	10.50
11250.42	38.29	12.21	1.89	6.38	0.69	2.50
11250.58	48.82	17.18	2.02	9.19	0.17	4.51
11251.08	60.67	46.60	3.36	12.87	7.64	21.68
11251.25	42.39	11.86	1.72	6.61	1.91	4.64
11251.92	71.98	33.96	2.15	18.24	10.97	20.52
11252.08	77.44	39.92	3.59	6.45	13.15	23.79
11260.42	43.78	1.65	3.11	1.26	3.62	12.71
11260.75	117.20	4.76	1.53	1.59	2.86	8.52
11260.92	83.25	9.38	1.66	9.51	8.75	10.94
11261.08	126.58	11.40	1.53	11.13	4.47	11.78
11261.25	145.23	13.15	1.54	11.19	10.58	5.60
11261.42	47.50	4.31	2.42	7.32	4.63	13.16
11261.92	44.24	10.28	1.73	2.14	1.66	6.41
11262.08	52.97	8.36	1.91	4.02	2.82	6.61
11262.42	57.52	34.54	2.19	0.14	12.66	12.92
11262.75	59.69	48.36	2.42	2.26	22.07	23.18
11262.92	58.10	41.91	2.31	0.08	9.88	19.08
11263.08	46.54	43.14	2.48	5.18	20.59	21.37
11263.42	76.19	33.64	2.54	12.21	21.04	17.42
11263.75	53.51	37.33	2.62	6.07	18.80	14.65
11263.92	60.38	16.14	1.91	2.55	3.56	14.32
11264.08	55.95	20.03	2.11	4.24	10.35	10.13
11264.25	50.15	21.06	2.33	7.64	20.11	15.08
11264.42	55.44	31.23	2.23	4.13	15.62	14.65
11264.58	48.89	24.67	2.08	4.55	11.29	11.07
11264.75	57.95	21.63	2.34	3.80	10.69	12.94
11264.92	51.99	14.78	2.27	0.84	10.51	14.32
11265.25	61.11	32.15	2.15	3.97	10.20	14.82
11265.42	61.78	32.66	2.37	5.76	27.63	22.58
11265.58	59.35	37.13	2.44	0.02	16.56	16.10
11265.92	46.05	28.10	2.37	5.25	14.89	18.15
11266.08	37.01	59.52	3.29	9.92	23.65	25.20
11266.25	37.83	18.57	1.73	0.69	2.31	9.31
11266.42	58.04	15.93	1.73	10.03	4.28	6.73
11266.58	30.56	20.48	1.77	1.17	2.73	8.85
11267.08	57.45	22.33	2.31	0.29	12.87	9.42
11267.25	48.49	16.16	1.97	5.72	0.10	3.13

11267.42	25.56	46.14	3.22	4.74	21.64	32.39
11267.58	28.14	18.55	2.23	7.74	12.60	12.33
11267.75	44.75	66.12	2.82	4.73	27.54	22.62
11267.92	59.45	52.14	2.71	13.61	26.34	16.99
11268.08	41.37	98.79	2.92	14.45	46.63	24.41
11268.25	60.07	60.42	2.95	5.86	25.70	22.76
11268.42	39.50	40.69	3.18	8.87	14.39	20.86
11268.58	45.10	17.65	2.21	8.39	3.11	6.64
11268.75	43.21	5.95	1.72	11.62	0.02	7.06
11269.08	41.55	70.03	4.08	25.96	28.95	34.78
11269.25	46.64	38.92	2.75	4.50	7.18	14.87
11269.58	37.17	16.76	1.97	0.92	2.58	7.48
11269.75	35.88	11.39	1.83	6.54	3.01	5.59
11269.92	45.73	15.08	1.83	2.13	0.79	13.20
11270.08	41.10	31.48	2.60	2.05	2.48	24.54
11270.25	39.67	6.34	1.86	3.68	2.24	9.02
11270.58	31.77	14.13	1.94	10.95	3.02	5.89
11270.75	43.41	23.52	2.59	2.32	0.68	17.48
11270.92	30.45	64.13	3.48	9.61	5.59	25.89
11271.42	40.55	22.03	2.67	6.61	0.80	15.17
11272.08	33.74	12.98	2.03	5.79	3.11	6.80
11272.25	46.25	17.06	2.08	3.55	2.36	5.37
11272.58	49.24	20.31	2.20	1.03	0.22	7.68
11272.75	30.48	7.32	1.80	3.73	0.26	2.14
11273.25	45.84	13.47	2.23	10.25	2.96	13.52
11273.58	17.72	57.21	3.97	14.45	8.24	24.72
11273.75	39.91	15.28	2.02	5.83	0.38	7.10
11273.92	43.57	27.00	2.22	6.12	4.34	13.81
11274.42	50.14	17.66	2.20	11.16	2.49	9.94
11274.58	41.03	64.70	3.82	13.73	7.90	32.84
11274.92	43.12	80.12	4.21	15.47	15.76	35.20
11275.58	48.78	10.59	1.86	7.27	1.27	3.80
11275.75	40.92	43.80	2.89	19.73	8.47	24.48
11275.92	38.65	51.90	3.52	9.71	7.18	30.59
11276.08	53.01	48.52	3.13	17.91	10.52	22.18
11276.25	35.09	64.50	4.11	12.93	16.46	35.11
11276.42	52.92	72.60	3.63	2.66	7.10	29.69
11276.58	56.60	41.27	2.81	0.74	0.60	24.08
11276.75	58.38	16.25	2.17	7.78	6.20	7.15

11277.08	35.48	27.81	2.30	4.70	0.64	14.28
11277.25	43.31	44.62	3.03	9.08	8.41	20.43
11278.08	51.79	26.54	2.51	8.86	4.38	12.10
11278.25	51.99	27.84	2.83	7.99	6.00	14.49
11278.42	52.16	21.63	2.79	16.38	8.24	13.96
11278.75	50.79	22.42	2.31	4.25	5.59	18.13
11279.08	52.88	42.86	3.35	8.70	11.25	25.20
11279.25	48.55	101.11	5.19	0.90	33.56	49.40
11279.42	55.28	57.73	3.21	0.95	16.96	28.42
11279.58	41.93	60.32	3.82	4.46	16.66	32.85
11279.92	48.00	53.91	3.62	2.57	19.18	30.69
11280.08	40.76	55.82	3.04	15.97	13.00	27.94
11281.08	42.09	36.39	3.19	7.78	11.03	20.77
11281.25	52.64	12.15	1.69	1.15	2.77	2.25
11281.58	52.70	52.13	2.77	9.95	24.57	27.70
11281.92	62.26	80.05	4.17	14.69	25.42	33.40
11282.08	54.67	38.87	3.00	11.21	5.05	13.72
11282.25	56.36	32.38	2.60	9.20	9.29	12.20
11282.75	39.52	11.93	1.97	5.32	2.09	0.05
11282.92	51.63	70.80	4.73	9.80	13.12	41.67
11283.08	36.79	13.25	2.21	8.13	2.64	7.07
11283.42	39.73	19.56	1.86	9.02	1.54	5.52
11283.58	46.52	12.40	2.15	3.70	0.65	8.66
11283.75	44.89	49.78	3.42	11.18	9.76	35.87
11283.92	36.30	64.50	3.80	12.99	2.95	26.70
11284.42	51.89	11.36	2.40	7.87	3.55	7.33
11284.75	29.96	13.75	2.45	5.54	1.55	7.04
11285.25	52.37	32.54	3.26	11.06	1.10	11.09
11285.58	44.68	32.73	3.83	21.34	5.32	20.07
11285.75	43.75	36.69	3.85	7.85	2.91	22.84
11285.92	62.50	49.20	5.18	6.08	6.09	36.88
11286.08	58.84	53.77	4.85	13.40	5.83	24.44
11286.25	57.97	42.73	4.71	8.26	10.21	24.55
11286.42	62.51	38.99	5.50	16.32	8.72	28.20
11286.58	62.86	44.48	5.12	2.95	3.23	24.69
11286.75	49.16	41.59	4.77	9.61	1.00	25.72
11286.92	64.13	35.43	4.82	6.99	6.45	25.31
11287.08	58.95	38.01	4.04	8.35	0.84	23.44
11287.42	55.84	36.00	4.22	15.55	0.06	16.74

11287.58	59.11	33.71	4.33	12.24	2.57	22.17
11287.75	58.54	40.67	4.83	1.89	2.43	26.21
11287.92	50.22	43.88	4.52	0.30	0.96	21.68
11288.08	48.21	32.48	4.77	9.35	9.09	31.43
11288.25	66.17	35.66	4.63	17.17	3.77	19.43
11288.42	54.30	34.47	4.17	13.53	1.36	19.21
11288.58	55.34	29.47	4.18	10.70	3.46	16.59
11288.75	51.02	24.54	3.74	9.83	5.21	15.98
11288.92	63.52	35.24	3.49	6.67	4.98	17.82
11289.08	37.05	30.00	3.67	13.39	2.87	10.22
11289.25	50.31	27.59	3.91	15.17	0.17	14.75
11289.75	56.76	51.61	5.34	2.03	3.98	27.53
11289.92	79.96	27.88	4.94	13.31	7.81	24.28
11290.08	56.67	42.30	4.53	4.67	6.19	23.03
11290.25	73.48	39.39	5.49	3.09	2.62	26.98
11290.42	88.99	52.25	4.66	4.21	2.49	25.32
11290.75	80.41	46.27	5.35	3.06	5.44	26.64
11291.08	89.64	34.91	5.13	11.84	7.89	23.32
11291.25	85.05	42.96	5.33	15.59	6.57	29.15
11291.42	90.04	56.63	5.55	8.72	8.07	28.10
11291.58	87.82	42.60	5.40	17.06	4.26	27.96
11291.75	74.22	55.90	5.27	6.22	8.16	27.21
11291.92	106.86	47.05	5.63	7.76	5.25	33.46
11292.08	85.33	60.41	5.21	12.76	4.86	34.44
11292.25	82.31	36.26	4.01	1.85	1.73	23.84
11292.42	76.25	31.18	2.84	9.76	1.63	12.67
11292.58	40.05	49.54	5.44	5.65	3.37	31.44
11292.75	48.89	30.50	4.07	7.74	2.16	21.16
11292.92	41.95	21.66	3.41	5.90	1.14	12.26
11293.42	45.55	21.51	2.82	3.37	1.31	9.97
11293.58	44.02	18.51	1.99	3.94	1.71	6.46
11293.75	39.14	18.80	2.58	1.73	2.29	7.27
11293.92	50.60	12.93	2.92	0.84	3.82	11.74
11294.08	37.89	22.33	2.89	6.53	3.35	12.88
11294.25	35.33	10.89	2.11	3.15	1.11	4.17
11294.75	42.43	6.00	2.19	0.35	0.64	5.30
11294.92	40.73	5.72	2.35	0.99	0.95	5.60
11295.08	66.85	28.61	3.56	6.82	5.30	14.29
11295.58	43.82	25.82	2.90	2.30	6.85	4.41

11297.25	36.09	18.74	1.92	8.46	6.77	4.18
11297.42	53.18	73.55	6.09	6.79	14.08	37.76
11297.75	44.13	30.85	2.92	0.76	2.50	13.98
11297.92	90.94	87.78	8.23	11.88	8.68	45.17
11298.08	77.15	73.36	6.35	9.56	7.97	46.19
11298.25	35.51	50.91	4.97	31.29	6.72	27.09
11298.42	11.91	34.98	4.60	8.72	5.53	22.79
11299.08	41.54	17.33	2.59	2.22	1.43	13.36
11299.75	30.93	11.43	2.06	1.76	4.64	5.88
11299.92	46.78	64.92	7.79	12.42	4.11	33.25
11300.08	50.18	37.27	4.36	9.50	1.12	17.37
11300.92	39.13	15.13	1.98	7.19	1.40	8.20
11301.25	25.83	27.50	2.97	5.80	6.46	9.27
11301.75	47.61	35.12	5.85	7.87	7.21	21.95
11302.08	60.38	67.87	6.26	14.42	10.46	27.40
11302.25	60.65	57.29	5.62	13.22	6.82	21.55
11302.42	76.32	57.41	5.66	14.87	7.00	63.01
11302.58	77.94	35.96	6.08	3.28	1.55	21.01
11302.75	73.14	52.94	6.60	7.97	9.72	29.10
11302.92	54.45	38.62	6.11	13.22	13.67	19.86
11303.08	55.89	42.01	4.70	11.65	17.31	17.62
11303.25	137.06	58.83	8.49	17.77	16.23	32.84
11303.42	139.14	60.10	7.92	15.84	13.81	31.27
11303.58	176.29	60.20	8.24	10.15	12.86	30.20
11303.75	140.92	53.09	8.18	13.53	10.95	33.60
11303.92	147.20	71.65	8.52	11.91	11.11	34.61
11304.08	151.52	65.74	7.66	4.49	2.60	41.16
11304.25	155.87	65.20	8.55	5.26	10.04	29.33
11304.42	120.60	58.16	7.56	14.80	9.19	33.55
11304.58	137.22	51.97	7.98	7.97	9.90	31.39
11304.75	108.62	54.28	6.58	9.14	9.22	26.79
11304.92	90.15	37.96	7.04	2.30	1.33	26.51
11305.08	83.52	42.90	6.70	4.03	4.76	28.85
11305.25	78.92	46.28	6.74	14.42	5.96	30.72
11305.42	78.27	38.28	6.37	7.16	0.06	24.18
11305.58	56.71	37.65	5.31	9.52	4.09	21.68
11305.75	55.94	39.01	6.39	17.16	8.19	22.33
11306.08	52.67	31.61	4.62	11.79	2.48	18.30
11306.25	59.31	35.80	5.52	7.54	2.69	18.98

11306.42	58.93	39.01	6.20	8.39	7.04	21.71
11306.75	76.97	47.94	6.79	11.92	8.69	27.60
11306.92	108.14	55.25	5.58	2.54	12.66	33.04
11307.08	189.71	93.22	6.30	11.39	33.61	45.07
11307.25	75.95	33.18	5.21	12.92	3.13	14.42
11307.58	50.39	11.41	2.67	1.21	2.80	10.90
11307.92	50.38	14.76	3.21	1.20	1.53	8.34
11308.25	44.30	24.44	5.06	8.78	2.73	21.08
11308.42	112.84	46.34	6.34	12.11	10.58	33.09
11308.58	125.45	45.49	6.12	11.03	4.11	28.21
11308.75	132.40	48.33	6.69	19.91	9.44	30.58
11308.92	136.21	43.63	6.25	15.79	12.48	29.80
11309.25	68.95	34.07	6.12	19.76	6.08	20.51
11309.58	56.43	28.44	5.42	6.06	2.72	17.00
11309.75	82.86	40.94	4.63	7.42	13.43	19.50
11309.92	92.42	47.33	7.42	9.91	8.70	22.03
11310.08	88.67	35.67	6.19	14.06	8.26	19.66
11310.25	93.06	42.12	7.67	13.18	6.28	23.48
11310.42	81.61	41.70	6.96	9.01	3.10	14.26
11310.58	64.14	36.11	5.78	4.33	1.17	17.82
11310.92	46.17	40.07	5.67	13.84	0.00	18.50
11311.08	66.26	41.05	5.66	12.06	3.23	18.49
11311.25	66.04	31.10	5.25	11.21	3.14	17.30
11311.92	56.22	29.55	4.09	4.27	2.01	12.79
11312.08	57.69	47.30	4.62	10.10	4.84	19.91
11312.25	60.75	46.62	3.85	5.29	2.59	22.07
11312.42	50.79	49.55	4.57	8.73	11.05	30.30
11312.58	67.58	32.84	4.55	10.15	1.31	18.50
11312.75	58.02	43.63	4.25	2.02	3.36	23.70
11312.92	49.83	36.15	4.55	7.93	7.00	20.78
11313.08	52.30	36.45	4.92	5.95	1.34	23.45
11313.25	34.14	41.22	4.41	5.10	0.74	22.06
11313.75	62.85	53.45	4.80	21.47	10.45	25.82
11313.92	45.56	30.99	4.12	2.62	2.94	21.60
11314.25	21.33	36.43	4.96	19.06	4.81	24.21
11314.42	40.96	38.99	4.73	13.80	9.88	29.23
11314.75	33.54	44.86	4.85	6.17	2.92	27.99
11314.92	50.24	44.03	5.17	12.95	1.59	32.60
11315.08	40.16	47.31	4.94	4.96	2.31	30.10

11315.42	29.87	43.76	4.99	6.47	3.43	23.84
11315.75	32.47	35.43	3.88	9.37	3.15	19.47
11315.92	24.58	52.23	4.68	9.90	4.01	20.14
11316.08	61.81	46.17	5.53	10.67	10.30	24.61
11316.25	41.27	48.62	5.15	13.25	13.86	29.99
11316.42	55.79	47.86	4.55	6.82	6.49	28.47
11316.75	63.17	45.74	5.19	5.83	7.48	28.82
11316.92	44.25	33.07	3.76	5.61	3.79	20.48
11317.08	45.37	31.99	3.50	5.03	2.12	20.00
11317.42	43.12	35.98	3.88	4.14	1.37	17.43
11317.58	44.04	35.91	3.78	3.85	0.16	19.84
11317.92	47.68	36.29	4.45	1.19	2.52	23.45
11318.08	43.23	35.81	4.18	1.82	4.88	20.33
11319.25	65.31	39.27	4.26	8.94	4.80	27.50
11319.42	51.38	38.35	3.22	7.47	0.84	21.78
11319.58	56.51	37.62	3.93	12.20	2.86	26.28
11319.75	47.23	47.61	3.79	16.11	6.33	25.74
11319.92	44.98	39.10	4.12	9.23	8.14	20.43
11320.08	40.35	43.19	3.57	10.23	0.73	20.80
11320.25	36.25	39.04	3.94	7.93	3.28	21.83
11320.42	38.75	44.17	4.41	8.55	3.55	26.69
11320.58	44.90	46.43	4.36	4.07	4.17	26.56
11320.75	31.99	48.29	4.44	14.99	5.09	23.91
11321.08	31.61	49.84	4.89	1.87	2.89	27.99
11321.25	35.24	37.28	4.70	0.39	0.63	30.26
11321.42	21.70	47.27	4.20	1.06	2.15	14.83
11321.58	38.99	33.84	4.06	7.57	1.80	28.37
11321.92	43.22	38.51	4.05	15.02	3.67	21.57
11322.08	33.88	42.13	3.89	8.98	3.22	25.88
11322.25	39.24	38.36	4.23	17.18	1.88	24.01
11322.58	39.09	35.89	4.26	8.37	7.10	26.48
11322.92	34.65	38.93	4.12	0.65	0.32	17.19
11323.08	36.03	24.52	4.19	2.38	3.01	20.75
11323.25	34.46	28.78	4.57	6.77	3.41	20.37
11323.42	42.56	37.87	4.51	14.72	8.69	24.49
11323.58	27.66	38.38	4.21	23.43	7.99	27.63
11323.75	35.21	39.38	4.53	9.82	5.98	28.82
11323.92	40.22	33.84	4.32	15.88	2.73	18.07
11324.08	34.71	38.31	4.33	18.38	0.34	18.92

11324.25	42.67	36.95	4.12	12.08	0.60	22.85
11324.58	34.01	39.28	4.17	5.55	1.38	22.74
11324.75	29.22	37.54	4.20	8.06	4.86	20.07
11324.92	33.82	45.72	4.30	5.13	4.95	24.38
11325.08	39.39	39.35	4.42	12.94	1.01	21.60
11325.25	40.49	28.02	4.59	11.46	3.68	23.72
11325.42	34.20	34.74	5.00	10.11	1.26	36.30
11325.58	30.16	47.25	6.06	11.69	5.68	34.07
11325.75	43.25	49.78	5.42	12.74	4.48	32.18
11326.08	32.14	47.43	4.36	6.60	4.23	26.68
11326.25	36.23	39.39	4.18	3.31	5.44	18.90
11326.58	44.79	54.94	5.40	9.71	7.99	42.53
11326.92	46.60	21.19	2.60	6.42	0.35	13.03
11327.08	51.59	20.62	2.78	4.44	2.99	9.19
11327.25	41.38	24.97	2.81	2.98	1.49	14.53
11327.75	28.59	36.49	4.55	7.13	5.62	17.44
11327.92	18.41	40.93	5.12	7.42	4.74	22.08
11328.08	21.75	39.19	4.97	0.35	0.23	15.79
11328.25	33.33	35.57	5.02	11.64	3.11	22.14
11328.58	28.56	40.37	5.38	4.32	8.32	30.52
11329.08	41.00	18.82	2.38	10.52	3.32	8.24
11329.25	27.10	29.29	3.97	8.44	4.94	16.03
11329.42	33.08	32.10	4.49	9.73	3.24	22.85
11329.58	27.92	39.20	5.73	1.57	3.62	30.43
11329.75	43.67	40.82	5.01	11.60	3.26	20.65
11329.92	34.40	44.15	5.62	13.39	7.68	26.31
11330.25	34.48	25.32	2.65	1.38	3.34	11.84
11330.42	32.82	32.08	3.53	6.08	4.63	18.49
11330.58	40.45	25.71	3.91	7.56	2.79	18.69
11330.75	34.36	33.34	4.84	1.60	0.92	29.07
11331.08	44.30	45.68	5.72	11.87	1.94	28.79
11331.25	43.25	46.89	5.57	6.51	0.25	29.76
11331.42	46.37	47.57	5.09	5.18	6.93	29.47
11331.58	50.75	40.53	4.15	0.81	4.42	18.04
11331.75	47.09	28.59	2.95	5.42	4.57	16.89
11332.58	47.83	40.87	3.69	0.66	4.47	11.97
11332.75	52.58	30.11	3.08	7.37	3.94	16.34
11332.92	57.19	44.61	3.93	13.42	10.40	21.53
11333.08	71.53	60.57	4.54	6.09	15.29	31.86

11333.25	88.44	56.65	5.19	5.36	4.08	29.11
11333.75	31.98	35.96	4.80	16.63	4.36	24.91
11334.25	27.62	30.78	4.47	6.45	3.52	26.99
11334.58	34.45	36.39	4.63	9.39	0.38	17.76
11334.92	20.35	52.68	5.17	9.37	5.18	31.33
11335.08	49.10	44.37	4.30	8.83	7.00	20.54
11335.25	40.72	42.94	4.02	14.35	2.01	26.50
11335.42	30.53	38.96	4.11	9.91	4.19	27.91
11335.75	42.27	37.30	3.85	4.71	2.61	22.00
11336.25	23.43	37.53	4.79	6.69	1.57	23.95
11336.42	20.37	45.41	4.99	6.01	5.39	34.03
11336.58	20.39	28.00	4.73	8.77	5.73	29.36
11336.75	41.70	38.07	3.63	12.50	5.82	26.19
11337.42	45.64	34.47	3.72	7.11	2.57	24.31
11337.92	36.15	40.99	3.89	6.67	0.48	21.40
11338.08	34.88	41.21	4.50	7.61	3.73	24.80
11338.25	41.55	39.68	4.60	17.61	1.39	21.30
11338.75	46.77	40.57	4.18	1.70	2.73	28.76
11338.92	33.27	39.82	4.02	8.10	4.25	26.95
11339.08	51.63	49.50	4.24	3.91	6.69	25.85
11339.25	42.66	46.94	5.02	6.64	1.35	24.00
11339.42	37.36	43.86	4.91	12.35	2.22	25.83
11339.58	23.79	46.98	5.12	14.25	7.53	24.14
11339.75	35.69	32.35	4.12	20.82	0.96	18.43
11339.92	35.24	39.38	4.43	6.24	2.46	28.62
11340.08	41.22	39.20	4.44	1.00	4.90	34.04
11340.25	36.98	41.94	4.73	4.11	8.93	25.41
11340.42	29.04	47.78	4.72	4.49	6.02	21.99
11340.58	31.82	46.92	4.59	6.99	4.24	34.30
11340.75	39.27	40.39	4.72	9.50	7.67	25.51
11340.92	42.40	44.21	4.76	5.36	7.16	29.46
11341.08	54.29	50.31	4.80	15.67	2.37	33.37
11341.42	43.33	49.14	4.56	17.38	5.58	26.34
11341.58	31.83	48.01	5.08	8.49	0.21	26.69
11341.92	32.96	37.50	4.60	9.04	4.58	28.97
11342.08	32.06	41.58	5.22	11.92	3.72	25.03
11342.42	49.67	37.40	4.62	15.92	4.33	24.39
11342.58	38.27	47.13	4.24	9.70	9.00	31.34
11343.08	40.12	35.25	3.62	12.62	4.87	17.86

11343.42	63.36	46.15	4.22	9.09	2.56	26.77
11343.58	40.54	48.60	4.38	11.93	0.12	28.93
11344.08	45.23	44.98	4.76	8.94	5.23	27.56
11344.25	34.65	44.22	4.71	8.11	2.89	26.59
11344.42	41.90	48.43	4.30	9.06	0.39	17.02
11344.75	41.81	36.13	4.15	4.40	2.00	24.66
11344.92	46.42	50.75	4.83	1.92	3.45	31.62
11345.08	44.15	46.02	4.53	1.08	0.87	27.02
11345.25	44.57	45.55	5.18	5.39	1.99	24.55
11345.42	47.06	48.68	4.87	4.69	4.97	42.97
11345.58	46.12	29.19	3.97	9.12	2.41	18.83
11345.75	38.03	51.25	5.00	0.15	2.56	32.86
11346.42	38.95	44.41	4.28	5.41	5.70	25.11
11346.58	51.72	35.68	3.22	6.91	2.15	30.67
11346.75	38.26	24.52	2.21	1.87	8.72	13.73
11346.92	78.79	41.53	3.96	4.21	1.96	25.21
11347.08	61.33	42.76	3.83	3.47	6.78	25.59
11347.58	63.81	43.57	5.15	14.60	9.99	31.52
11347.75	69.40	40.52	4.21	17.70	5.92	31.33
11347.92	66.62	44.07	4.30	7.56	8.77	26.87
11348.08	75.55	51.43	4.39	19.83	4.95	32.86
11348.25	75.81	29.03	3.64	11.26	7.08	20.61
11348.42	82.47	48.39	4.50	6.66	5.44	31.90
11349.25	59.90	47.37	5.42	13.32	4.29	29.78
11349.58	45.21	36.76	4.64	1.72	1.48	35.57
11349.75	58.75	41.68	5.33	9.35	0.89	25.20
11349.92	56.38	54.25	5.04	4.64	3.05	30.35
11350.08	58.59	50.24	4.71	12.34	4.85	32.39
11350.25	72.07	52.00	3.95	4.08	8.59	27.69
11350.42	62.99	47.44	4.54	8.05	6.61	21.01
11350.58	56.40	41.27	3.72	14.61	5.01	18.26
11350.75	52.02	41.15	4.15	9.28	4.88	27.20
11350.92	64.96	41.50	3.55	7.11	3.49	18.65
11351.25	61.87	41.30	3.91	4.88	3.57	23.79
11351.58	99.88	68.02	4.56	12.78	11.65	30.32
11351.75	84.52	53.47	4.64	7.10	5.91	33.18
11352.08	67.52	45.00	5.12	5.34	4.48	29.56
11352.25	51.92	42.11	4.35	5.78	0.55	27.40
11352.42	42.65	31.16	4.48	1.17	0.40	23.60

11352.58	43.95	33.97	4.63	5.72	6.64	24.91
11352.75	43.71	33.19	3.78	0.03	1.57	21.10
11352.92	52.33	41.11	4.58	8.92	8.59	23.66
11353.08	61.03	36.65	3.47	13.52	5.39	17.88
11353.42	59.12	59.24	4.55	16.25	10.50	31.59
11353.58	72.96	59.82	4.63	8.58	6.29	26.59
11353.75	44.48	44.36	4.03	6.81	0.89	28.49
11353.92	60.03	39.46	4.61	16.39	7.51	20.92
11354.08	72.30	38.46	4.44	12.03	4.53	27.23
11354.25	61.06	34.49	4.61	14.61	8.59	27.64
11354.42	60.15	45.36	4.78	15.37	8.85	34.50
11354.58	59.61	48.69	4.65	4.35	0.52	24.04
11354.75	71.58	32.49	4.71	7.19	5.36	22.70
11354.92	70.00	27.99	5.42	5.00	4.83	25.45
11355.08	106.97	39.12	5.15	8.70	5.78	28.01
11355.25	110.74	57.62	5.90	13.73	16.07	32.09
11357.08	121.12	57.55	4.77	8.96	16.30	32.03
11357.25	124.86	53.74	4.69	11.79	12.25	31.84
11357.42	132.89	52.16	4.82	6.26	16.47	37.08
11357.58	168.64	62.57	5.31	1.87	13.93	31.71
11357.75	157.18	56.06	6.48	5.56	17.47	36.71
11357.92	76.64	35.81	3.79	16.37	11.09	28.38
11358.42	70.22	44.81	5.42	2.41	13.25	25.11
11358.92	91.39	47.80	6.48	9.74	15.61	37.56
11359.08	92.97	52.62	4.70	12.04	10.57	33.16
11359.25	98.81	40.94	6.52	9.33	14.72	33.84
11359.42	96.77	66.64	5.85	8.29	14.08	36.41
11359.58	89.51	56.66	6.00	4.93	11.83	37.08
11359.75	88.62	48.32	5.75	3.19	14.19	38.49
11359.92	92.95	43.26	5.69	6.80	12.93	35.31
11360.08	100.21	52.58	5.45	11.89	12.56	36.94
11360.25	106.05	51.38	5.38	4.63	11.83	34.11
11360.42	104.01	46.81	5.96	6.18	11.24	36.10
11360.58	95.54	44.99	5.10	4.76	14.65	34.09
11360.75	101.06	49.38	5.64	15.01	12.23	31.64
11360.92	113.97	56.60	5.78	0.79	16.25	34.10
11361.08	96.08	51.74	5.59	10.39	13.37	31.79
11361.25	111.38	49.38	5.60	7.01	17.96	27.70
11361.42	123.62	52.16	5.12	9.73	10.18	29.78

11361.58	124.43	42.93	5.03	15.51	15.31	25.08
11361.75	133.83	59.12	5.38	16.53	17.27	39.72
11361.92	120.23	54.76	5.34	14.56	12.60	36.39
11362.08	123.69	56.97	5.12	8.00	12.85	34.87
11362.25	123.88	50.27	5.00	9.34	15.82	38.58
11362.42	139.70	51.46	4.55	17.02	13.88	35.78
11362.58	119.99	43.47	4.65	13.52	9.44	24.91
11362.75	124.81	56.08	4.81	2.04	13.02	34.35
11362.92	116.27	59.86	4.94	1.25	11.43	36.74
11363.08	128.57	61.37	5.21	2.85	18.51	40.88
11363.25	122.82	62.20	4.88	5.95	14.56	46.42
11363.42	125.60	71.03	4.69	5.98	16.08	35.97
11363.58	143.47	63.16	5.28	7.67	17.76	35.29
11363.75	126.14	50.68	4.76	12.52	15.48	25.89
11363.92	148.09	69.06	5.26	9.25	18.29	31.71
11364.08	136.66	47.76	5.12	13.05	13.14	29.83
11364.25	138.19	49.30	4.58	10.43	16.05	37.36
11364.42	156.53	63.89	5.16	11.20	18.18	38.21
11364.58	131.15	58.63	5.19	15.70	15.77	30.45
11364.75	120.28	43.81	4.66	1.09	11.99	29.42
11364.92	121.67	55.76	5.15	16.14	14.37	35.40
11365.08	109.83	54.77	4.91	3.99	8.68	32.03
11365.42	86.18	47.96	5.36	7.24	7.68	35.38
11365.58	74.06	52.29	5.23	7.05	6.16	34.18
11365.92	74.31	27.75	4.35	4.85	7.13	27.77
11366.08	52.13	29.78	4.37	15.04	5.05	19.20
11366.25	59.96	26.46	4.09	10.34	0.93	15.48
11366.42	56.69	34.47	4.43	8.86	4.73	24.02
11366.75	60.79	23.88	4.36	8.36	3.19	22.66
11366.92	56.14	28.76	4.60	17.89	3.30	23.38
11367.08	52.14	37.00	4.10	12.16	8.00	25.97
11367.25	65.54	39.08	4.44	7.04	5.12	30.85
11367.42	71.95	47.81	3.88	0.27	8.72	28.21
11367.58	105.14	54.49	4.35	8.37	9.26	28.70
11367.92	80.02	41.78	4.42	4.23	2.38	24.81
11368.25	68.00	41.80	3.99	5.44	1.55	24.07
11368.42	81.28	37.05	3.81	9.06	4.70	22.44
11368.58	70.53	32.90	4.02	9.32	1.73	25.61
11368.75	57.85	37.63	3.91	11.69	7.59	25.06

11369.08	78.11	42.41	3.72	16.42	2.33	27.55
11369.25	74.19	27.81	3.66	2.37	3.20	27.23
11369.58	87.81	26.42	3.69	11.78	7.13	17.69
11369.75	80.66	30.49	3.86	11.57	6.75	21.10
11369.92	121.05	47.72	4.27	5.05	8.03	26.65
11370.08	109.84	49.38	4.41	9.56	10.00	30.33
11370.25	98.06	41.12	4.00	12.09	13.29	37.33
11370.42	93.91	42.72	3.81	9.81	14.18	31.64
11370.58	109.38	39.01	4.44	24.13	14.87	25.88
11370.75	128.70	51.21	4.77	17.98	5.63	33.57
11371.25	118.24	48.01	4.49	9.34	10.28	22.43
11371.42	111.68	46.23	4.69	7.57	11.72	29.77
11371.58	147.59	55.95	4.64	9.09	7.25	32.24
11371.75	120.80	58.55	4.94	9.38	10.66	35.02
11371.92	101.91	45.79	4.12	9.64	10.33	41.59
11372.08	109.23	49.09	5.58	4.52	7.69	33.70
11372.25	125.24	57.79	5.52	15.28	14.02	34.33
11372.42	103.55	44.36	5.23	17.07	16.11	37.91
11372.58	104.42	52.27	5.60	1.79	16.03	41.27
11372.75	104.27	48.15	6.18	13.39	13.63	35.19
11372.92	103.22	42.19	4.89	10.44	15.50	36.29
11373.08	75.66	45.84	3.78	18.06	9.53	31.72
11373.25	147.84	49.05	5.33	11.08	6.67	34.73
11373.42	145.92	54.35	5.53	5.95	16.77	37.86
11373.75	67.03	30.62	4.96	13.53	6.94	28.06
11373.92	66.09	34.94	5.47	3.02	6.31	27.19
11374.08	57.27	37.28	4.66	10.46	6.90	23.88
11374.25	88.50	24.96	4.69	3.02	10.10	27.62
11374.42	84.42	42.67	5.50	9.73	18.16	33.93
11374.75	93.96	43.88	5.84	6.22	14.75	28.15
11374.92	113.50	36.71	5.79	16.75	12.03	26.32
11375.08	108.73	46.42	5.36	12.58	13.00	34.78
11375.25	96.67	55.92	5.40	8.72	15.88	33.74
11375.42	109.65	60.06	5.61	9.96	13.40	28.89
11375.58	121.82	54.75	6.78	10.63	13.60	27.32
11375.75	120.81	55.27	5.53	8.37	15.61	26.39
11375.92	107.91	53.57	5.65	7.90	13.56	28.43
11376.08	121.15	41.45	5.59	8.87	13.59	23.42
11376.25	118.94	47.77	5.38	15.69	17.12	26.21

11376.42	104.65	49.34	5.17	8.18	6.17	30.47
11376.58	116.44	56.28	5.17	1.84	15.02	27.31
11376.75	108.86	46.09	4.45	6.22	12.74	26.72
11376.92	114.58	49.82	4.80	6.01	14.45	31.51
11377.25	118.55	50.90	4.96	5.48	11.92	22.55
11377.42	112.87	49.33	3.42	13.71	13.14	26.72
11377.58	121.39	59.25	4.83	12.99	14.90	30.80
11377.75	124.33	57.94	4.95	18.01	18.74	32.76
11377.92	118.22	50.42	4.70	8.91	14.67	29.11
11378.08	114.37	57.43	5.13	4.50	13.50	33.54
11378.25	125.55	54.13	5.00	10.08	12.81	29.88
11378.42	140.94	60.03	4.66	12.40	11.96	34.38
11378.58	106.05	51.03	3.88	7.17	6.00	36.81
11378.75	121.53	55.42	5.45	9.16	9.99	30.37
11378.92	93.46	32.32	5.55	7.19	11.89	17.62
11379.08	82.00	46.83	5.74	5.92	11.11	23.13
11379.25	96.13	56.36	5.12	21.35	12.78	25.08
11379.42	106.90	61.66	5.67	12.22	15.92	39.93
11379.58	114.93	62.53	5.59	18.20	16.58	30.10
11379.75	127.51	54.16	5.06	7.13	19.92	31.50
11379.92	138.67	52.28	5.35	5.68	12.47	35.61
11380.08	125.98	58.96	4.88	16.31	14.83	33.18
11380.25	129.34	50.82	5.38	16.10	11.35	37.46
11380.42	127.65	59.27	5.24	12.76	17.18	37.62
11380.58	122.28	58.43	5.09	1.70	14.48	28.68
11380.75	134.58	61.23	5.44	13.46	16.43	43.69
11380.92	120.01	64.84	5.45	17.68	18.32	35.23
11381.08	137.45	49.37	4.88	10.94	9.89	26.07
11381.25	193.11	56.11	4.78	7.88	15.55	28.37
11381.42	115.76	55.86	4.51	11.71	14.33	29.46
11381.75	94.00	49.07	4.57	3.69	10.17	34.18
11381.92	75.72	40.05	4.97	23.98	7.81	32.31
11382.08	77.97	30.82	4.43	4.15	4.07	24.45
11382.25	58.41	42.33	4.92	15.34	17.03	26.91
11382.42	81.96	50.56	4.20	3.39	6.99	29.40
11382.58	80.27	38.75	4.97	6.83	8.84	25.69
11382.75	72.43	40.77	4.24	1.52	4.10	31.62
11382.92	84.82	40.37	4.20	6.65	6.87	33.57
11383.08	69.67	36.87	4.28	11.59	10.28	22.57

11383.25	87.59	34.49	4.14	0.74	3.87	22.31
11383.42	79.72	48.95	4.53	12.64	14.70	24.89
11383.58	73.31	45.48	4.55	5.13	5.34	23.77
11383.75	58.04	41.48	4.50	3.70	1.12	18.88
11383.92	82.49	39.17	4.06	12.24	7.41	26.52
11384.08	70.27	39.84	5.22	7.45	8.23	23.05
11384.25	70.27	38.12	3.85	7.29	5.49	19.05
11384.42	66.69	50.86	3.91	2.91	2.30	24.50
11384.58	74.08	42.01	2.88	9.19	9.19	42.54
11384.75	76.55	46.34	4.37	9.09	9.62	24.33
11384.92	74.85	37.50	4.02	13.45	7.60	21.76
11385.08	83.37	45.53	4.11	11.93	6.41	29.98
11385.25	70.98	42.74	4.30	17.87	6.71	25.44
11385.42	63.81	43.92	4.01	7.46	3.20	29.09
11385.58	67.65	42.87	4.69	16.26	11.41	24.64
11385.75	56.02	42.93	3.86	10.68	6.65	26.19
11385.92	63.16	45.64	4.32	9.92	9.15	25.83
11386.08	62.06	37.64	4.03	7.73	7.51	27.66
11386.25	64.50	36.65	4.44	14.07	4.36	20.79
11386.42	46.88	83.64	3.89	24.60	1.97	912.94
11386.58	42.07	24.16	3.81	5.07	4.42	14.87
11386.75	21.02	14.81	4.07	13.57	1.49	15.78
11386.92	40.94	15.53	3.51	8.79	2.56	14.28
11387.08	37.52	22.34	4.00	5.61	3.56	14.90
11387.25	32.42	18.23	3.93	18.05	2.77	17.71
11387.42	23.45	19.31	4.12	1.68	3.74	14.48
11387.92	33.69	16.20	3.63	3.69	3.01	8.19
11388.08	43.13	18.11	3.22	17.20	1.02	13.81
11388.42	33.54	10.60	2.93	13.98	4.77	14.46
11389.08	45.77	23.79	2.93	7.80	0.46	12.58
11389.25	40.84	45.64	3.65	14.95	5.82	26.02
11389.42	41.29	50.03	4.15	6.02	11.97	22.84
11389.58	53.95	66.39	3.80	13.98	10.89	22.90
11389.75	36.09	34.40	3.73	8.39	6.72	17.88
11389.92	61.78	68.02	4.09	17.50	21.60	25.57
11390.08	66.98	67.50	3.36	13.58	12.80	20.67
11390.42	89.52	46.52	4.11	4.18	14.81	25.96
11390.58	85.99	53.14	4.39	6.55	9.76	33.22
11390.75	82.84	53.12	4.25	12.46	12.92	23.79

11390.92	93.30	47.13	4.85	10.75	10.10	25.38
11391.08	85.19	48.51	5.13	4.45	9.57	29.46
11391.25	77.14	50.02	5.67	5.89	10.39	30.60
11391.42	69.80	47.76	5.34	6.63	9.68	33.08
11391.58	82.41	45.08	5.12	19.98	6.41	26.84
11391.75	72.34	38.28	5.81	15.88	9.94	23.09
11391.92	53.36	38.19	5.63	2.37	8.00	22.44
11392.08	37.69	36.63	5.32	4.45	7.20	17.75
11392.42	42.45	27.92	4.53	8.15	4.31	19.92
11392.58	35.87	26.83	5.03	17.15	3.04	13.95
11392.75	45.10	25.58	5.21	7.10	0.04	19.36
11392.92	30.21	31.85	5.16	7.88	4.91	15.40
11393.08	44.94	42.51	5.12	1.96	4.79	17.16
11393.42	41.76	32.93	5.32	6.92	0.69	18.99
11393.58	48.00	37.49	5.11	2.35	1.58	22.10
11393.75	71.70	44.02	4.66	5.38	2.83	50.92
11393.92	63.30	30.77	5.97	19.16	4.67	23.98
11394.25	42.06	39.97	4.82	6.45	5.62	20.07
11394.42	36.29	42.04	5.84	13.24	7.97	21.42
11394.58	34.88	36.43	5.77	9.92	7.55	27.48
11394.75	74.54	39.81	5.48	3.78	6.65	25.08
11395.58	81.32	32.76	3.25	7.50	11.10	15.49
11395.75	133.93	56.93	5.01	10.93	12.60	36.10
11395.92	75.91	37.72	3.90	8.06	4.57	27.92
11396.08	51.89	50.82	3.84	11.02	8.62	24.52
11396.25	49.60	22.26	3.55	15.70	2.35	14.87
11396.58	30.78	21.58	2.86	11.12	5.35	12.32
11396.75	52.99	35.11	3.90	1.52	1.36	17.34
11396.92	40.02	16.16	2.38	11.50	6.82	9.83
11397.08	45.17	25.22	2.28	0.52	1.19	3.78
11397.25	37.76	9.83	2.43	8.24	8.41	13.58
11397.58	61.59	27.30	3.92	0.84	4.58	20.55
11397.75	75.42	32.53	4.29	10.13	12.96	19.87
11398.08	58.77	23.08	3.22	3.82	1.93	12.64
11398.25	48.20	37.91	3.88	4.86	5.37	20.09
11398.42	74.71	30.27	3.70	15.94	5.91	12.03
11398.58	71.59	40.44	4.12	15.46	3.27	17.23
11398.75	79.63	72.23	5.98	17.64	12.20	27.73
11398.92	63.02	29.44	3.79	12.15	5.51	18.75

11399.08	62.71	25.42	4.38	2.17	2.68	18.14
11399.25	41.01	53.70	6.07	3.37	9.08	20.88
11399.58	40.08	30.46	3.58	10.24	1.76	18.77
11399.75	171.73	46.30	7.17	11.94	35.65	22.57
11399.92	164.88	69.32	7.25	13.54	48.94	33.12
11276.58	56.60	41.27	2.81	0.74	0.60	24.08
11376.25	118.94	47.77	5.38	15.69	17.12	26.21

Appendix H: Core 4 XRF Data

Core 4 XRF Data						
Depth (ft)	**V (ppm)**	**Ni (ppm)**	**Th (ppm)**	**U (ppm)**	**Mo (ppm)**	**Cu (ppm)**
8415.58	44.38	4.91	2.18	2.78	1.98	15.16
8415.75	47.15	8.04	1.93	7.64	6.28	17.43
8416.92	39.58	11.49	2.28	4.00	3.23	18.11
8417.25	19.05	6.66	4.34	14.63	2.32	14.02
8417.75	46.66	12.71	2.75	1.16	3.04	14.14
8417.92	47.82	12.62	2.63	3.13	0.27	14.80
8418.08	38.14	23.45	3.57	8.49	1.68	18.31
8418.75	30.73	20.29	3.65	13.56	0.17	14.00
8418.92	6.67	51.36	8.49	21.56	7.56	19.88
8419.25	36.00	8.57	2.37	16.57	3.49	14.81
8420.75	34.89	33.37	5.16	10.66	0.30	17.47
8421.25	29.70	18.48	3.39	17.88	7.60	15.12
8421.92	44.01	44.28	6.39	16.76	5.70	20.89
8422.75	31.46	18.32	3.04	12.35	1.81	15.86
8422.92	39.27	10.05	2.85	13.09	0.03	13.22
8423.25	28.64	18.08	2.39	11.17	1.59	16.15
8423.42	29.41	40.99	4.64	11.11	6.16	18.99
8423.92	31.06	49.95	5.65	9.82	4.63	23.88
8424.42	43.44	15.93	2.26	5.62	2.37	17.56
8424.58	40.63	19.54	2.24	9.02	0.72	18.32
8425.92	43.18	10.17	2.29	15.75	5.27	15.34
8426.75	36.66	6.52	1.81	0.13	0.13	15.66
8428.75	40.33	33.36	3.03	9.05	0.94	19.01
8429.92	24.41	18.87	3.28	0.66	4.92	18.30
8430.25	34.23	16.39	2.32	6.05	0.22	18.45

8431.42	36.78	18.25	2.34	0.33	0.19	19.75
8432.08	35.14	20.64	2.36	3.80	1.22	12.90
8433.08	38.86	19.39	2.71	7.98	3.46	16.86
8433.58	22.68	24.15	4.52	12.50	4.21	18.08
8433.92	37.44	11.82	2.86	9.46	0.98	13.83
8434.08	29.92	13.11	3.14	5.83	1.53	18.97
8434.42	31.15	18.58	3.16	8.16	1.09	17.54
8434.58	30.25	16.57	2.82	8.23	0.52	20.63
8435.58	30.71	8.16	2.89	13.96	3.25	14.92
8436.08	35.55	21.38	3.22	7.58	3.77	17.26
8436.42	39.04	19.18	2.54	2.03	2.22	17.10
8436.58	41.76	28.59	2.48	5.67	6.15	18.33
8437.08	30.52	20.96	3.16	6.23	6.38	19.80
8437.42	31.83	12.37	2.65	5.39	0.05	16.43
8437.75	33.64	14.77	2.94	1.87	2.93	17.20
8437.92	37.88	11.56	2.76	4.74	0.92	15.55
8438.58	34.44	14.03	3.15	10.32	0.27	15.59
8439.42	36.39	16.37	2.87	2.21	1.14	21.21
8440.42	35.44	29.05	2.59	2.07	1.89	20.56
8441.25	48.74	17.29	2.46	19.08	0.29	15.79
8441.92	39.75	22.13	3.10	11.92	4.84	15.81
8442.08	36.40	29.39	2.75	6.06	0.01	20.81
8442.25	35.16	25.70	3.30	3.14	0.17	18.76
8442.42	36.17	30.78	3.13	0.94	3.43	19.54
8442.58	37.98	17.38	2.72	2.82	0.44	17.35
8442.92	37.92	10.86	2.76	7.03	7.63	18.87
8443.08	31.39	18.96	3.15	22.20	6.30	17.12
8444.58	35.06	12.22	2.33	4.26	0.93	15.83
8445.42	29.89	23.23	2.95	8.21	0.09	17.04
8446.08	39.97	13.38	2.61	8.95	3.83	15.53
8446.25	34.05	21.60	2.48	15.27	0.05	19.64
8447.42	35.80	22.76	2.58	9.20	0.48	19.87
8448.25	45.71	22.38	2.12	4.66	0.60	15.95
8449.08	44.67	12.83	2.62	11.34	0.34	16.21
8449.25	38.20	23.21	2.66	4.30	0.12	20.32
8449.92	36.44	15.78	2.61	1.26	1.35	15.58
8451.42	37.29	17.45	2.96	10.67	1.04	17.27
8451.58	31.64	18.54	2.55	0.60	2.53	15.25
8452.25	38.46	16.60	2.99	8.99	2.10	15.41

8452.58	33.66	8.58	3.21	2.19	2.24	16.42
8454.08	25.99	20.35	3.50	3.63	1.51	18.24
8454.42	34.43	16.22	3.03	12.43	0.09	18.44
8454.92	32.83	22.47	2.82	8.11	2.24	19.46
8455.08	37.64	10.52	2.90	4.88	2.81	16.61
8457.25	46.75	5.99	2.38	4.47	0.59	15.63
8457.75	47.94	23.97	2.56	0.29	0.21	21.76
8460.08	31.11	24.37	3.38	0.97	0.04	21.97
8460.58	35.74	21.76	3.22	7.16	1.36	18.19
8460.75	35.75	17.79	3.60	1.13	2.00	19.46
8461.25	25.78	28.90	3.75	5.56	1.85	22.06
8462.08	45.33	18.42	2.22	3.43	0.50	16.68
8462.58	45.04	12.25	3.26	9.88	0.75	16.13
8462.75	30.26	9.58	3.17	9.72	0.38	18.04
8463.75	46.81	14.81	2.55	1.07	1.20	17.34
8463.92	52.83	23.27	3.25	12.39	2.99	21.64
8464.75	47.62	19.93	2.98	0.94	1.55	15.37
8465.08	38.99	19.08	3.06	4.97	0.25	19.25
8465.58	31.87	17.94	2.97	5.91	2.30	17.01
8466.92	44.25	17.81	3.15	7.97	3.14	19.37
8467.25	9.00	20.85	3.78	1.01	2.84	20.83
8467.75	28.99	26.69	3.72	11.76	1.50	21.63
8468.75	44.40	16.96	3.18	0.35	0.58	15.67
8469.58	42.44	20.93	2.88	10.08	1.50	17.44
8469.75	54.52	16.06	3.04	2.69	1.81	16.74
8469.92	28.40	20.52	3.43	7.92	0.43	17.56
8472.25	94.86	50.51	2.82	6.55	5.40	21.63
8472.42	56.07	13.95	1.87	11.14	0.61	15.88
8472.92	57.24	20.34	1.67	5.31	0.52	16.99
8473.08	60.86	13.50	1.74	8.47	3.33	17.79
8473.58	52.81	9.14	1.70	11.04	0.54	17.16
8473.75	41.80	33.19	2.41	12.62	4.80	20.32
8473.92	59.46	78.22	2.88	10.13	7.52	32.17
8474.08	55.37	13.41	1.82	6.97	3.98	15.81
8474.58	55.99	19.70	1.91	14.53	2.75	19.65
8475.25	44.21	30.67	2.15	5.36	2.66	20.55
8475.42	54.74	27.15	1.88	3.70	2.70	18.53
8475.58	49.29	31.78	2.32	9.71	4.63	19.53
8475.75	38.96	41.24	2.65	9.00	10.55	23.10

8475.92	50.80	15.48	1.68	4.54	3.44	15.45
8476.08	11.81	99.43	5.28	9.99	58.85	60.22
8476.42	54.56	21.26	1.93	7.58	2.00	17.94
8476.58	59.69	12.96	1.94	1.67	1.64	17.77
8476.75	60.72	17.79	1.99	7.86	2.81	19.22
8477.08	70.23	37.18	2.10	10.66	8.31	22.81
8477.25	33.32	34.65	1.98	10.71	8.66	20.87
8477.42	36.07	72.86	3.91	5.46	24.12	38.52
8477.58	75.32	12.34	1.84	6.13	2.58	16.13
8477.92	60.81	19.76	2.14	5.74	7.38	20.37
8478.08	58.07	26.51	1.97	1.32	4.24	18.00
8478.58	52.51	15.20	1.78	4.84	1.50	18.19
8479.25	56.97	19.40	1.81	7.64	1.49	17.98
8479.58	52.32	14.28	1.77	1.69	2.08	17.53
8479.75	56.46	34.08	2.32	9.24	3.47	18.99
8479.92	45.76	57.62	3.09	5.93	14.89	26.32
8480.25	39.61	74.34	3.63	1.87	20.41	44.19
8480.42	67.14	35.47	2.07	13.31	9.88	22.16
8480.58	72.14	35.06	1.90	11.72	10.48	23.44
8480.75	64.18	21.02	1.79	1.78	0.13	18.56
8480.92	64.76	92.03	3.64	6.35	20.14	41.34
8481.25	65.24	17.60	1.65	6.87	1.74	16.16
8481.42	44.70	47.06	2.69	1.33	11.25	27.44
8481.75	67.46	12.82	1.85	3.79	2.64	17.72
8482.25	70.37	16.26	1.45	2.08	0.04	15.85
8482.42	107.39	70.63	3.22	6.77	16.02	41.84
8482.58	74.23	29.67	1.99	6.83	8.80	18.89
8482.75	150.92	89.93	3.76	3.73	28.37	48.85
8483.08	67.89	51.99	3.02	13.59	14.30	33.51
8483.25	65.70	13.85	1.91	9.66	0.69	17.08
8483.42	55.09	50.55	2.90	2.96	7.05	35.96
8483.58	46.21	51.69	2.84	7.17	9.71	31.69
8484.08	44.73	23.94	2.51	9.26	5.28	21.43
8485.58	29.20	30.05	3.29	12.80	5.72	22.19
8485.75	44.48	29.31	2.73	4.09	2.75	21.33
8486.08	42.40	41.75	3.36	16.19	1.21	24.21
8486.58	52.43	32.21	2.54	2.69	1.39	20.93
8486.75	46.12	33.93	2.91	6.38	4.82	21.18
8486.92	46.44	41.39	3.19	9.23	8.88	24.91

8487.08	68.07	32.49	2.26	4.48	2.25	20.15
8487.25	66.81	44.85	4.33	8.93	23.35	29.35
8487.42	43.26	12.23	1.86	13.22	1.68	19.11
8488.25	155.51	125.73	6.36	6.69	52.89	62.69
8488.58	76.72	35.15	2.60	9.92	12.38	25.12
8488.75	73.58	43.98	2.80	4.96	19.05	26.15
8488.92	87.78	56.32	3.29	13.00	23.24	30.80
8489.08	70.73	37.29	2.35	8.99	11.66	21.24
8489.25	82.56	27.42	2.41	2.88	9.73	21.50
8489.42	71.09	48.18	3.14	7.24	21.71	27.84
8489.58	54.60	19.03	1.87	0.75	0.03	17.44
8489.75	77.57	39.42	2.66	4.09	17.97	24.32
8489.92	82.81	39.80	4.50	5.97	6.46	27.77
8490.08	93.14	108.10	3.84	15.69	42.54	41.35
8490.25	76.65	52.85	2.89	8.64	14.08	25.66
8490.42	60.78	19.93	1.62	0.95	1.38	17.43
8490.75	89.27	64.53	2.78	1.06	16.31	28.18
8490.92	92.67	43.74	2.91	1.04	16.88	22.92
8491.42	83.21	34.15	2.33	5.00	10.61	21.36
8491.58	99.09	42.92	3.16	4.91	10.37	24.22
8491.75	108.17	59.46	3.05	2.96	10.22	32.18
8491.92	83.55	41.48	4.19	2.37	6.59	26.42
8492.08	67.30	50.48	4.21	6.69	2.07	30.47
8492.25	53.55	44.10	4.72	9.62	7.14	30.60
8492.42	50.98	38.63	4.45	16.70	6.73	26.57
8492.58	50.81	36.27	4.37	9.73	5.01	28.75
8492.75	52.80	40.23	4.15	8.27	4.12	27.10
8492.92	61.96	31.04	4.16	9.77	2.90	24.26
8493.08	55.99	41.67	4.38	3.09	0.20	30.88
8493.42	68.82	26.17	3.84	17.47	3.33	24.59
8493.58	75.12	35.82	3.73	8.65	2.86	26.50
8493.75	50.62	24.55	3.42	5.56	5.14	24.58
8494.42	57.90	39.94	2.98	4.89	1.98	24.11
8494.75	47.83	31.04	4.54	3.22	2.12	25.13
8495.08	64.94	41.96	5.14	0.06	2.41	30.70
8495.42	66.82	34.48	4.99	7.36	1.81	27.22
8495.58	90.67	48.12	5.98	12.50	11.40	32.99
8495.75	70.98	51.19	5.35	4.75	10.35	33.52
8495.92	87.04	63.35	6.18	6.37	8.50	35.22

8496.25	71.53	53.85	5.69	8.60	5.98	36.07
8496.42	81.10	63.07	5.81	3.74	7.41	39.15
8496.58	66.45	52.73	4.20	5.51	10.76	39.98
8496.75	61.59	21.27	2.30	3.49	2.21	19.53
8496.92	50.86	37.40	3.53	5.56	1.84	24.19
8497.25	39.64	9.08	1.78	3.36	1.06	15.86
8497.42	40.44	8.26	1.95	4.64	1.84	17.32
8497.92	49.05	48.90	3.55	3.28	6.62	26.09
8498.25	46.80	30.28	2.80	3.21	2.64	22.84
8498.42	58.71	29.40	2.50	1.63	1.06	22.39
8498.58	63.80	39.18	3.33	1.36	4.08	27.05
8498.92	33.87	43.31	5.13	11.63	3.92	27.83
8499.08	53.16	46.68	4.45	15.62	11.50	29.39
8499.25	38.25	34.10	4.49	7.20	6.16	24.40
8499.58	94.60	59.68	6.38	26.19	18.25	30.00
8499.75	112.56	56.39	7.36	6.07	9.56	38.41
8499.92	110.82	49.25	6.88	15.47	6.97	30.26
8500.08	52.24	21.14	4.29	9.61	6.54	19.25
8500.25	42.48	34.91	4.38	6.38	3.37	23.60
8500.42	40.31	34.45	4.46	12.40	1.00	23.17
8500.58	19.14	34.83	5.23	9.78	4.39	25.73
8500.75	37.83	35.95	5.36	20.38	12.46	26.43
8500.92	37.79	46.63	5.12	13.20	1.73	31.12
8501.08	18.29	38.87	5.01	21.57	2.19	27.72
8501.25	44.05	40.62	3.74	8.99	2.65	26.28
8501.42	37.34	38.40	4.44	6.62	4.56	26.61
8501.58	17.51	36.57	4.43	3.09	2.39	24.26
8501.92	38.53	48.64	4.65	12.43	4.37	29.07
8502.08	31.02	44.36	4.75	15.65	0.36	28.15
8502.25	33.57	49.63	4.98	12.47	3.33	33.55
8502.42	42.17	43.61	4.74	16.86	2.94	27.72
8502.58	29.68	41.31	4.90	14.31	2.08	26.44
8502.75	15.80	38.90	4.76	8.65	0.24	26.32
8502.92	30.78	39.29	4.95	13.43	2.12	30.68
8503.25	30.46	36.46	5.20	14.68	7.22	30.24
8503.42	21.88	41.40	5.16	6.38	3.07	26.60
8503.58	5.71	41.93	5.76	9.94	2.51	27.78
8503.92	40.36	48.76	4.87	7.20	3.00	31.93
8504.25	13.44	54.41	5.20	13.23	2.40	34.47

8504.42	50.55	38.50	3.73	18.75	7.18	30.02
8504.58	23.42	24.73	3.85	10.61	0.67	23.22
8504.75	37.11	36.69	4.66	9.13	4.18	27.42
8504.92	48.59	27.34	3.02	12.53	3.53	18.00
8505.25	35.21	40.92	3.94	13.68	6.29	25.96
8505.58	18.77	36.23	4.70	5.84	2.80	23.15
8505.75	23.74	36.18	4.77	11.50	7.19	27.38
8506.08	29.23	49.34	5.05	10.48	5.97	29.50
8506.25	35.86	32.96	3.87	5.72	1.62	27.32
8506.42	36.30	33.39	4.86	3.58	20.45	23.28
8506.58	26.34	40.16	4.10	15.28	2.36	29.61
8506.75	32.06	46.18	4.60	7.79	6.68	30.22
8507.08	30.45	56.58	4.98	12.71	4.38	37.23
8507.25	42.65	44.52	5.06	16.31	3.91	31.94
8507.42	43.98	41.86	4.12	10.36	2.37	30.06
8507.58	33.88	40.07	4.46	6.05	7.93	28.44
8507.75	31.30	49.38	5.35	15.76	5.74	33.76
8507.92	27.94	42.91	4.32	0.24	1.29	27.88
8508.42	33.04	53.74	5.49	6.54	0.06	33.99
8508.75	22.31	47.21	4.56	11.98	1.00	29.94
8509.08	44.82	39.37	4.41	5.53	6.28	29.76
8509.25	31.29	49.47	3.94	2.19	4.54	31.01
8509.92	20.19	51.93	5.69	11.32	4.41	35.86
8510.42	44.17	46.02	4.69	8.01	4.92	29.80
8510.58	38.68	47.44	5.29	10.13	2.18	35.60
8510.75	33.98	50.19	4.74	12.35	8.05	35.02
8510.92	33.15	51.17	4.89	6.22	5.03	30.80
8511.08	46.88	49.45	4.96	6.65	4.73	31.96
8511.42	40.92	47.02	5.93	3.73	1.53	35.03
8511.58	36.04	45.75	4.70	8.50	3.64	30.34
8511.75	48.26	44.21	4.35	8.14	6.00	27.76
8511.92	51.62	45.64	4.72	13.51	9.95	30.61
8512.08	50.67	24.96	3.61	5.39	3.79	24.12
8512.25	30.70	24.48	3.21	7.30	1.23	24.43
8512.58	37.87	34.99	4.15	6.56	2.79	25.43
8513.08	15.33	27.81	4.38	13.48	3.83	22.57